Geo L

JOURNAL OF PETROLOGY

VOLUME 2 · NUMBER 2

JUNE 1961

OXFORD · AT THE CLARENDON PRESS

JOURNAL OF PETROLOGY

Editors

T. F. W. BARTH (Oslo); C. E. TILLEY (Cambridge)
L. R. WAGER (Oxford); H. S. YODER (Washington)

Managing Editors

G. M. BROWN (Oxford); S. R. NOCKOLDS (Cambridge)

Honorary Advisory Board

C. R. BURRI (Zürich)
C. W. CORRENS (Göttingen)
H. VON ECKERMANN (Stockholm)
P. ESKOLA (Helsinki)
L. HAWKES (London)
J. E. HAWLEY (Kingston, Ont.)
H. H. HESS (Princeton)
D. S. KORZHINSKY (Moscow)
H. KUNO (Tokyo)
W. T. PECORA (Washington)
E. RAGUIN (Paris)
H. H. READ (London)
A. RITTMANN (Catania)
F. J. TURNER (Berkeley, Calif.)

It is the aim of the editors to provide, in the *Journal of Petrology*, a place for the publication of original researches in the whole range of subjects which fall within a liberal definition of petrology. The subjects will thus include the physics and chemistry of rocks, their mineralogy and textures, and certain aspects of petrology which involve the dating of rocks by natural radioactivity. Quantitative studies of rock-forming minerals, experimental physical chemistry relevant to petrology, and parts of isotope geology, will appropriately find a place. Regional studies, unless they lead to results fundamental to the science of petrology, will not usually be considered suitable to the journal.

The journal is being published at first in 400-page volumes consisting of three numbers per year, in February, June, and October. The subscription price for three consecutive numbers is 80*s*. ($12 in the U.S.A. and Canada), post free. Single numbers cost 30*s*. net. Orders may be placed with any bookseller or sent direct to the publishers.

OXFORD UNIVERSITY PRESS

AMEN HOUSE · LONDON · E.C.4

A Study of Phase Equilibria in a Metamorphic Iron Formation

by SVANTE HAKAN KRANCK[1]

Dept. of Geology and Geophysics, Massachusetts Institute of Technology, Cambridge 39, Mass., U.S.A.

ABSTRACT

The paper is based on a study of mineral assemblages in metamorphic iron formations in northern Quebec. Thirty-four mineral analyses have been performed, using photometric methods of silicate analysis.

Three facies of iron formation are represented, namely, quartz–specularite iron formation, quartz–magnetite iron formation, and quartz–silicate iron formation. The silicate iron formation is made up mainly of quartz, ferrohypersthene, ferroaugite, cummingtonite, and calcite. Arfvedsonite and aegirine–hedenbergite occur in magnetite-rich rocks.

The analysed coexisting minerals are from the silicate iron formation and from overlying mafic rocks of igneous origin. The analysed assemblages include ferrohypersthene–ferroaugite–cummingtonite, ferrohypersthene–ferroaugite, cummingtonite–ferroaugite, diopside–hornblende, anthophyllite–hornblende, hypersthene–diopside–hornblende–garnet, and olivine–hypersthene–chlorite.

The analyses show that (1) the minerals are nearly in equilibrium as shown by parallel tie lines, (2) cummingtonite generally has a higher MgO/FeO ratio than coexisting ferrohypersthene, (3) the phase higher in calcium has the higher MgO/FeO ratio, (4) the solubility gap between ferrohypersthene and ferroaugite is 43 mole per cent.

The stability relationships of pyroxenes and amphiboles are discussed in view of the new data. It is shown that FeO–CaO–SiO_2 systems often behave differently from MgO–CaO–SiO_2 systems. Hedenbergite is probably not stable in the presence of excess CO_2 in the area.

The low variance of the ferrohypersthene–ferroaugite–cummingtonite–calcite–quartz assemblage indicates that the rocks were closed to H_2O and CO_2. The behaviour of the volatile components is discussed in view of this fact.

The source of the silicate minerals is assumed to be hydrous iron silicates and carbonates. A model of the sequence of chemical reactions taking place in carbonate–silicate iron formations during metamorphism is suggested.

1. INTRODUCTION

In this paper are presented the results of a study of the phase equilibria among silicate minerals in iron formations in the Mount Reed area of northern Quebec. The study is based on chemical analyses of coexisting minerals, principally ferrohypersthene, ferroaugite, cummingtonite, and hornblende. Some general inferences have been drawn as to the stability relationships in the system FeO–MgO–CaO–SiO_2–CO_2–H_2O during metamorphism, and as to the role played by the volatile components in determining the mineral assemblages.

The writer spent three summers in the Mount Reed area with the Quebec Cartier Mining Company. The chemical analyses were carried out at the Department of Geology of Massachusetts Institute of Technology, using the rapid silicate analysis methods developed by Shapiro & Brannock (1956) of the United

[1] *Present address*: Bolidens Gruvaktiebolag, Boliden, Sweden.

[Journal of Petrology, Vol. 2, Part 2, pp. 137–184, 1961]

States Geological Survey. The project was supported by a grant from the National Science Foundation.

Very little information is available in the literature on the phase equilibria among naturally occurring iron-rich silicates. The phase chemistry of hydrous iron silicates has been discussed briefly by Yoder (1957). Experimental studies of the FeO–SiO_2–H_2O system have been carried out by Flaschen & Osborn (1957) and by Smith (1957). Few chemical data on minerals and mineral assemblages have been published in connexion with field descriptions of iron formations and most data on the mineralogy of high-grade silicate iron formations are from Manitoba and Sweden. In the eastern part of the Mesabi Range the iron formations have been contact metamorphosed by the Duluth gabbro with the development of pyroxene and grunerite. The mineralogy of these rocks has been described in papers by Grout & Broderick (1919), Grout (1919), Richarz (1927), and others. In Sweden the so-called eulysites probably are of similar origin to the silicate iron formations here described. Eulysites are dealt with in papers by Palmgren (1916), von Eckermann (1922), Carstens (1924), Geijer (1925), Lindroth (1926), and Tilley (1936).

The Mount Reed silicate iron formations differ from the eulysites and the metamorphic iron formations of the Mesabi Range in the absence of fayalite and the abundance of ferrohypersthene and calcite. The mineral assemblages include the association ferrohypersthene–ferroaugite–cummingtonite–calcite–quartz. This assemblage is interesting both because of the association hypersthene–calcite, so far unknown in geological literature (Ramberg, 1952*b*, p. 154), and because the low variance of the assemblage indicates that the rocks in the course of the regional metamorphism were closed to the volatile components H_2O and CO_2.

2. THE GEOLOGICAL SETTING OF THE MOUNT REED AREA

The Mount Reed area is at the southern end of the Quebec–Labrador Iron Range where the Kaniapiskau group of the Labrador trough becomes affected by the complex folding and high-grade metamorphism of the Grenville province. Most of the area is underlain by biotite granite gneiss and migmatite gneiss which form the base of the stratigraphic sequence in the area. The iron formation and an underlying dolomitic marble horizon outcrop in long sinuous bodies mainly in isoclinal synclines that have been re-folded along transverse fold axes. An upper sequence of gneiss, mainly garnet–biotite gneiss, is exposed farther north. The regional geology has been described in more detail elsewhere (Kranck, 1959; Duffell & Roach, 1959).

The stratigraphic thickness of the iron formation is of the order of 200 ft. It has been subdivided into three facies, quartz–specularite iron formation, quartz–magnetite iron formation, and quartz–silicate iron formation. Transitional facies between specularite and magnetite iron formation on the one hand, and magnetite and silicate iron formation on the other hand, are common.

The quartz–specularite iron formation is best developed at Jeannine Lake where an open pit mine is under development (1959). The formation consists almost entirely of quartz and specularite. The rock is in part massive, in part well foliated. Where the foliation has been distorted into drag folds, large segregations of solid, coarse-grained specularite have formed along the fold crests. The only minor constituents are magnetite, finely disseminated throughout the rock, and in places clusters of actinolite, diopside, and calcite.

The quartz–magnetite iron formation is similar to the specularite iron formation except that the oxide is in the form of magnetite. Transitional rock types with specularite intermixed with magnetite also are common. The magnetite iron formation as a rule is finer grained. Where no specularite is present, layers of silicates are commonly found intermixed with the oxide layers, producing brownish stains on the weathered surface.

The silicate iron formation shows a greater variety in composition and lithology. Here and there the facies includes layers of ferrodolomite and should more properly be classified as carbonate–silicate iron formation. However, since there is good evidence that a major part of the silicates is derived from carbonates, no attempt has been made to differentiate the carbonate and the silicate facies. The main mineral constituents of the silicate iron formation are quartz, ferrohypersthene, grunerite–cummingtonite, ferroaugite, calcite, and, locally, magnetite. Iron silicates mixed with magnetite are usually high in manganese and sodium. They include such minerals as arfvedsonite and aegirine–hedenbergite.

The silicate rock is usually well banded, the banding being produced by varying proportions of the different mineral constituents and presumably directly reflecting the original bedding. The banding is most obvious on the weathered surface, where quartz-rich resistant layers stand up over rusty, brown-weathered, carbonate–silicate-rich beds.

The texture of the silicate rocks consists of a granular, medium-grained, xenoblastic mixture of the different constituents. Cummingtonite sometimes appears to be replacing ferrohypersthene. Otherwise no replacement textures are evident that would indicate disequilibrium in the rock.

3. THE CHEMICAL ANALYSES

Chemical analyses have been performed of silicate minerals from two separate areas located about thirty miles apart, a southern area around Blough Lake and Athol Lake at longitude 68° 00′ W. latitude 51° 55′ N., and a northern area around Hobdad Lake at longitude 67° 30′ W. latitude 52° 20′ N. The mineral assemblages found in both areas are very similar, so that the degree of metamorphism is probably about the same in the two.

The analyses were made by photometric methods, as first described for use in silicate analyses by Shapiro & Brannock (1956). The deviation between duplicate analyses seldom exceeds 3 per cent, and is generally much less. The main sources of error lie either in the preparation of the solutions or in the presence

of inhomogeneities in the samples. The reproducibility of measurements in a single solution is generally extremely good in all the procedures used.

The main difficulties were encountered in the analysis of small amounts of aluminium in the presence of large amounts of iron. Iron interferes in the photometric test for aluminium under these conditions. The analyses for aluminium are therefore not as reliable as the other analyses. Because H_2O has not been determined, the amphibole and chlorite analyses do not add up to 100 per cent. A more detailed discussion about the analytical methods used is to be found in a laboratory report of the Department of Geology, Massachusetts Institute of Technology.

Thirty-four complete mineral analyses and several partial analyses were carried out in the course of the present study. The results of the analyses with descriptions of the source rocks are listed in Appendices A–C. Most of the analyses represent coexisting ferrohypersthene, ferroaugite, and cummingtonite from silicate iron formation. A few analyses were also made of more magnesium-rich pyroxenes and amphiboles from metamorphosed mafic rocks of igneous origin occurring in the same areas, in order to gain some idea about the stability relationships among the more magnesium-rich end members of the pyroxene and amphibole solid solution series. The optical characteristics of the analysed minerals will be published in a separate paper.

4. SIGNIFICANCE OF THE CHEMICAL ANALYSES

The chemical analyses were carried out to determine how the different elements distribute themselves between the different phases. The most significant components in the analysed minerals are FeO, MgO, CaO, and SiO_2. From the analyses one can draw some conclusions as to how the FeO–MgO–CaO–SiO_2 system looks at the temperature and pressure conditions present in the Mount Reed area at the time of the metamorphism.

Fig. 1 represents a plot of the FeO–MgO–CaO ratios of the different minerals together with the tie lines of the different mineral assemblages. All minerals plotted are in equilibrium with excess silica. Five phases are represented in the diagram, namely, hypersthene, diopside–augite, cummingtonite–grunerite, anthophyllite, and actinolite–hornblende. Other components such as Al_2O_3, Na_2O, and H_2O also affect the stability relationships of the minerals represented, so that the relationship between chemical bulk composition and mineral associations cannot be represented completely on this diagram. However, some significant features of the phase chemistry of the minerals can be demonstrated. The following points should be noted:

1. The minerals appear to be in approximate equilibrium, as shown by the fact that the tie lines between the different mineral pairs are nearly parallel. The only exceptions are the hypersthene–ferroaugite pairs of B1-6 and B1-21. It is possible that in some cases the FeO/MgO ratios still reflect the compositions of the carbonates from which the hypersthenes and ferroaugites formed.

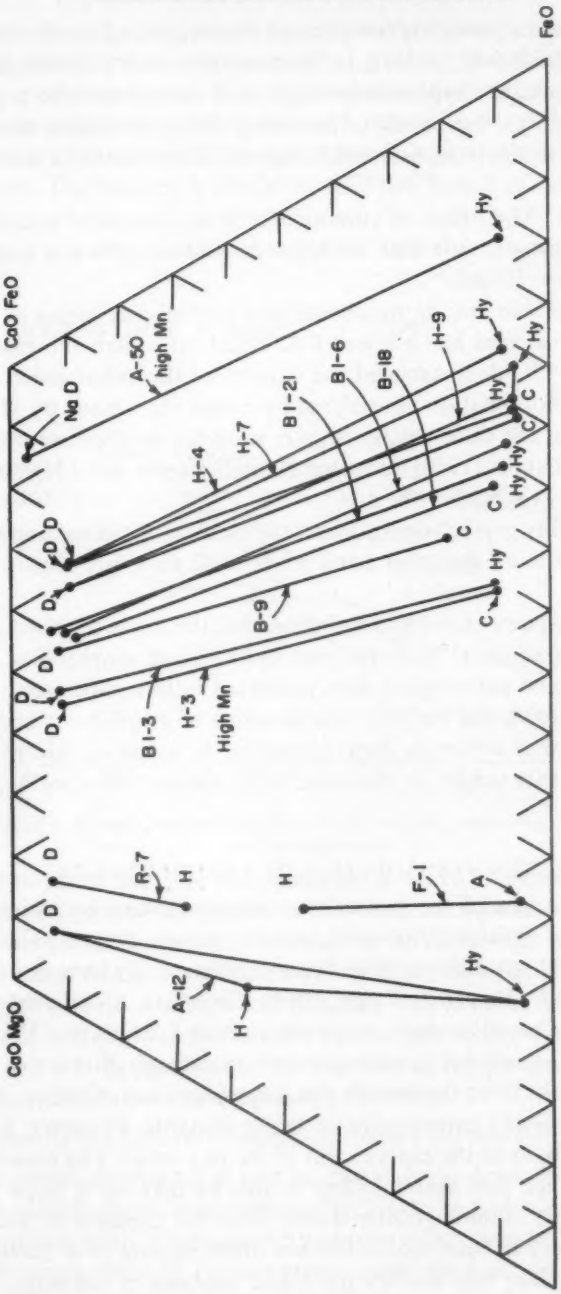

FIG. 1. Diagram showing FeO/MgO/CaO ratios in analysed silicates of the Mount Reed area. *A*, anthophyllite; *C*, cummingtonite; *D*, diopside–ferroaugite; *H*, Ca-amphiboles; *Hy* hypersthene.

2. Cummingtonite is slightly more magnesium-rich than the hypersthene with which it is in equilibrium, at least in the more iron-rich assemblages. Towards the magnesium side, the hypersthene–augite and cummingtonite–augite tie lines appear to become almost parallel, indicating that a coexisting cummingtonite and hypersthene in this compositional range may have about the same FeO/MgO ratio.

The lower FeO/MgO ratio in cummingtonite as compared with hypersthene agrees with the general rule that the high-temperature phase is higher in magnesium (Ramberg, 1952*a*).

3. The general rule among pyroxenes and amphiboles seems to be that the phase higher in calcium has a lower FeO/MgO ratio than the phase lower in calcium. Hess (1951) demonstrated the validity of this relationship for igneous pyroxenes and a compilation of analysed pyroxene pairs made by Muir & Tilley (1958) shows that the same relationship is valid for magnesium-rich metamorphic pyroxenes. Eskola (1950) finds that cummingtonite has a higher FeO/MgO ratio than the coexisting hornblende.

4. The miscibility gap between calcium pyroxene on one hand and hypersthene and cummingtonite on the other hand is about 42 mole per cent in the Mount Reed area.

5. The mineral pairs of F-1 and R-7 show that the range of miscibility of CaO and FeO/MgO is about 11 mole per cent in low alkali amphiboles.

The chemical and petrological data presented in this paper contribute some useful clues regarding the stability relationships of amphiboles and pyroxenes and the factors that influence their formation in metamorphic rocks. In the following pages this subject is discussed with special reference to the Mount Reed area rocks.

5. CUMMINGTONITE AND ANTHOPHYLLITE

The stability ranges of the monoclinic cummingtonite–grunerite series and the orthorhombic anthophyllite series are still poorly defined. Unfortunately, the attempts to delimit their stability fields experimentally have not proved successful (Boyd, 1959; Bowen & Tuttle, 1949). Therefore, all inferences as to the stability fields are based on field occurrences. Both Sundius (1933) and Rabbitt (1948) conclude that neither cummingtonite nor anthophyllite forms a complete solid solution series from the iron to the magnesium end member, iron anthophyllite and magnesian cummingtonite being unstable. However, there is still considerable doubt as to the exact extent of the two series. The problem is complicated by the fact that anthophyllite is able to take up a large amount of aluminium whereas cummingtonite is not. Thus the presence of aluminium as well as the presence of magnesium favours anthophyllite over cummingtonite. This fact may explain why the few published analyses of coexisting cummingtonites and anthophyllites show a great range in MgO/FeO ratios (Rabbitt, 1948; Kranck, 1959). An overlap in the cummingtonite and anthophyllite

stability fields may also be caused by temperature and pressure effects. High temperature might favour cummingtonite, pushing the field of coexistence towards the magnesium side. Fig. 2 shows how the compositions of anthophyllite and cummingtonite may be related to temperature. As a rule, when two ferromagnesian phases coexist, the one richer in iron is generally the low-temperature phase. The diagram is similar to the hypothetical diagram presented by Boyd (1959).

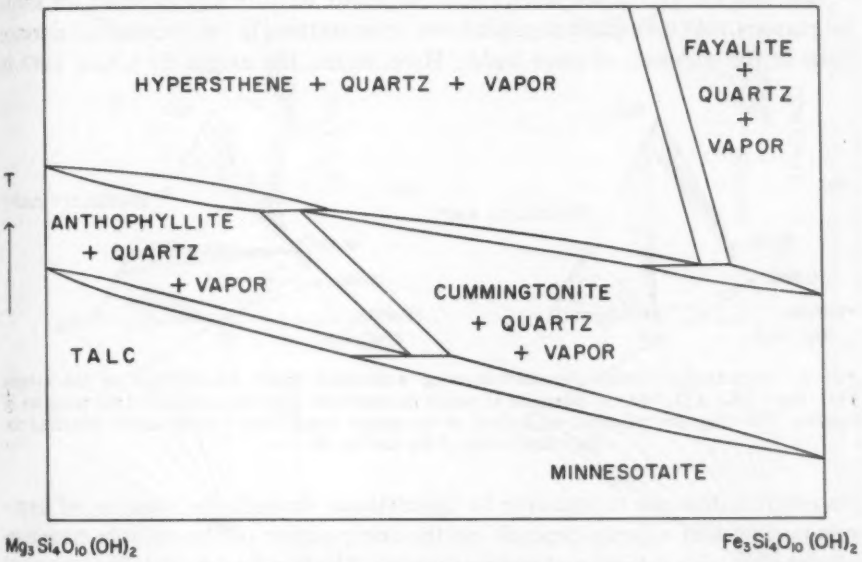

FIG. 2. Hypothetical phase diagram showing possible stability relationships of cummingtonite and anthophyllite.

It should be noted that the temperatures at which minnesotaite changes to cummingtonite and cummingtonite to hypersthene depend on the activity of H_2O in the rocks. In the presence of siderite, the cummingtonite and minnesotaite, at the temperature of the reaction, would not be in equilibrium with pure water but with a mixture of H_2O and CO_2, and maybe other compounds. Therefore, since the activity of water would be less than unity the reactions would take place at lower temperatures. The reaction taking place at the decomposition of minnesotaite could be expressed as follows:

$$\text{Minnesotaite} + \text{siderite} \rightarrow \text{cummingtonite} + \text{carbon dioxide} + \text{water} \quad (1)$$

To what extent siderite takes part in this reaction depends on the CO_2/H_2O ratio in the volatile phase in equilibrium with siderite and minnesotaite. Fig. 3*a* assumes that over most siderite/cummingtonite ratios, siderite will remain stable after the decomposition of cummingtonite, and the reaction can be expressed approximately as below with only a small amount of siderite taking part:

$$\text{Minnesotaite} \rightarrow \text{cummingtonite} + \text{water} + \text{quartz} \quad (2)$$

On the other hand, Fig. 3*b* assumes that the volatile phase in equilibrium with siderite and minnesotaite is very high in CO_2, so that siderite, in the course of the reaction of minnesotaite to form cummingtonite, will disappear or decrease greatly in amount. Then the reaction is best expressed as in reaction (1).

A rock composed only of minnesotaite and quartz can be in equilibrium with varying activities of H_2O, so that its temperature of decomposition may vary from place to place in an environment where CO_2 gas is present.

Likewise the decomposition of cummingtonite to form hypersthene, for similar reasons, may take place at much lower temperatures in the presence of siderite than in the presence of pure water. Here, again, the extent by which FeO is

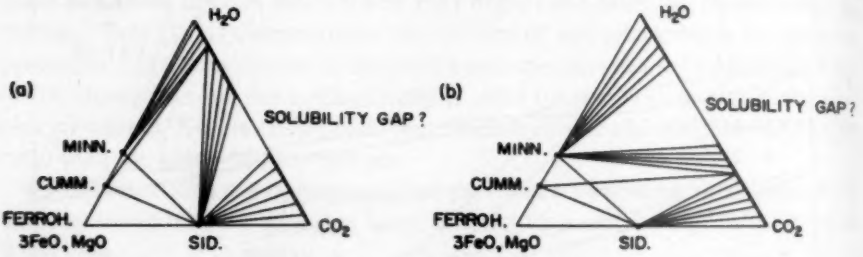

FIG. 3. Hypothetical phase diagrams showing alternative phase relationships in the system FeO–MgO–SiO_2–CO_2–H_2O at the point at which minnesotaite becomes unstable in the presence of siderite. The diagrams represent projections of the phases in equilibrium with quartz assuming the FeO/MgO ratio of the rock to be 3 to 1.

transferred from cummingtonite to hypersthene through the reaction of cummingtonite with siderite depends on the composition of the volatile phase in equilibrium with siderite and cummingtonite. The fact that the association cummingtonite–hypersthene–quartz is so common in the Mount Reed area, and the association hypersthene–siderite–quartz is unknown to the writer, indicates that for most bulk compositions, cummingtonite does not become unstable through this reaction, i.e. the volatile phase is high in CO_2. The decomposition of siderite therefore can be expressed essentially as the reaction below with little minnesotaite taking part:

$$\text{Siderite} + \text{quartz} \rightarrow \text{hypersthene} + \text{carbon dioxide} \qquad (3)$$

The probable changes in the stability relationships in the range of temperatures within which siderite and cummingtonite become unstable are shown in Fig. 4.

In the Mount Reed area cummingtonite is thought to have formed partly from minnesotaite as a product of normal progressive metamorphism, and partly from hypersthene by reaction with water. To what extent the latter reaction has taken place in the area is not quite clear. In some places, particularly at Jeannine Lake and at Hobdad Lake, cummingtonite occurs as large clusters and acicular rosettes. These mineral clusters may be of hydrothermal origin, having formed

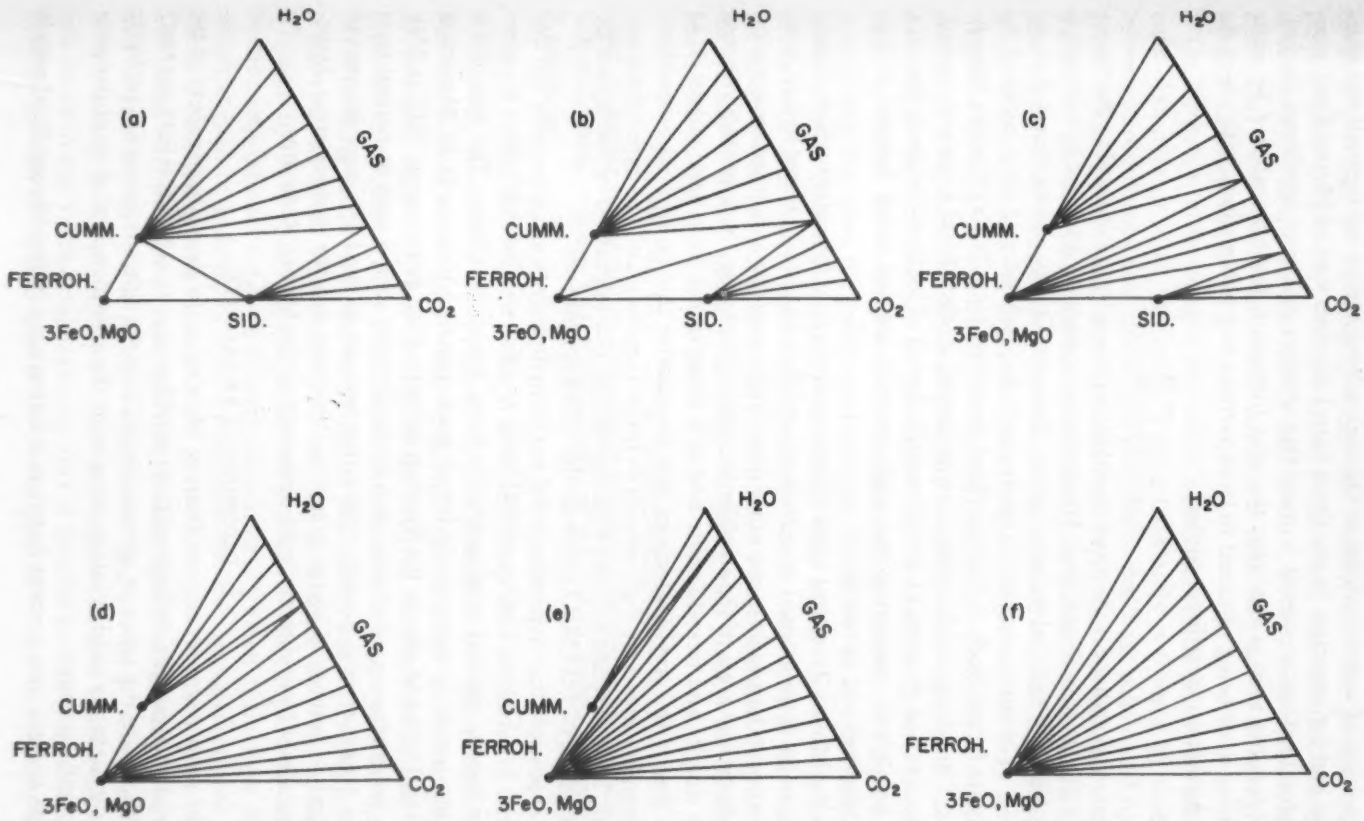

FIG. 4. Hypothetical phase diagrams showing possible changes in stability relationships with progressive metamorphism in the system FeO–MgO–SiO_2–CO_2–H_2O at the interval during which cummingtonite and siderite become unstable. The diagrams are of a similar nature to those in Fig. 3.

by addition of water or steam to the rock subsequent to the regional metamorphism and deformation. In the Black Dan Lake area west of Mount Reed, cummingtonite alone is present in most thin sections and hand specimens studied. It is possible that in this area the iron formation has been altered by water diffusing in or being squeezed in from surrounding paragneisses with which the iron formation is in direct contact.

6. HYPERSTHENE

Ferrohypersthene is the most abundant ferromagnesian mineral in the Mount Reed silicate iron formations. Hypersthene is generally thought to represent a high degree of regional metamorphism. However, it may also represent dry conditions. It is most common in norites and charnockites and other rocks of the granulite facies. Such rocks have been described from India, Uganda, Scandinavia, Canada, and other places where deeply eroded shield areas are exposed. Large areas of these rocks are commonly devoid of hydrous minerals like mica and amphibole, indicating that such minerals are not stable because of high temperatures and pressures.

In the Mount Reed area hypersthene occurs in iron formation which initially contained a large amount of carbonate and thus was low in water to start with. The surrounding gneisses are muscovite–biotite gneisses and other rocks typical of migmatized areas of the amphibolite facies. The hypersthene probably formed from siderite and ferrodolomite and to a lesser extent from cummingtonite, as described in the previous section. It is conceivable that in iron-rich assemblages the temperatures were high enough to invert cummingtonite to hypersthene and steam, but this seems unlikely since cummingtonite appears to be stable over the same range of FeO/MgO ratios as the ferrohypersthenes.

It is possible that hypersthene did not form directly from carbonates, but that siderite first reacted with quartz to form fayalite, and then at higher temperatures fayalite reacted with quartz to form ferrohypersthene. The association fayalite–quartz is common in lower grade metamorphic rocks in Minnesota (Grout, 1919) and also in the Swedish eulysites (von Eckermann, 1922, p. 274). This assemblage is, of course, also in equilibrium with a melt at normal pressures. However, it is possible that either because of the fairly high magnesium content or because of higher pressures than were present in these areas, hypersthene could form directly from carbonate in the Mount Reed area.

7. DIOPSIDE–FERROAUGITE

The most common calcium-bearing silicates in the area are members of the diopside–ferroaugite–hedenbergite series. All proportions between FeO and MgO are known in the series in igneous rocks, and the calcium pyroxenes probably form a complete solid solution series with the acmite radical at most temperatures and pressures.

The highest iron content found in a ferroaugite in the Mount Reed area is

63 mole per cent of $FeCaSi_2O_6$. Only the sodium and manganese-bearing aegirine–hedenbergite of A-50 has a higher iron content. High iron hedenbergites of metamorphic origin are also rare in the literature. In the Mount Reed area the assemblage ferrohypersthene–calcite appears to take the place of ferroaugite in extreme iron-rich rocks.

The formation of ferroaugite represents a problem which the writer has not quite been able to solve. Although it almost certainly is formed by reaction between ferrodolomite and quartz, the problem is that both calcite and hypersthene typically are present, together with ferroaugite and one may ask why, at the time of dissociation of dolomite, the calcium in its entirety did not go into calcite and the ferromagnesian components into hypersthene. All three minerals could be expected to form simultaneously from dolomite only within a limited range of FeO/MgO ratios; that is, within the four-component field at which the activity of CO_2, temperature, and pressure would be just right both for the dolomite at that composition to decompose and for calcite, hypersthene, and augite to coexist. Such a state would be represented by a line on a *PT* field which may or may not cross the geothermal gradient. However, as hypersthenes and ferroaugites of different compositions coexist with calcite, this cannot be the whole truth. It is conceivable that ferroaugite forms metastably at the time of the reaction and becomes stable only when some of the liberated CO_2 has left the system. It is also possible that two reactions take place. First, dolomite reacts with quartz as shown below:

$$(Fe,Mg)Ca(CO_3)_2+2SiO_2 \rightarrow (Fe,Mg)CaSi_2O_6+2CO_2$$

Later, at higher temperatures, ferroaugite becomes unstable in the presence of CO_2 and reacts with any CO_2 that has not left the system, forming calcite and hypersthene:

$$(Fe,Mg)CaSi_2O_6+CO_2 \rightarrow (Fe,Mg)SiO_3+CaCO_3+SiO_2$$

However, in any case there appears to be a change in the stable assemblage that forms from dolomite at high FeO/MgO ratios, since no ferroaugite or hedenbergite apparently has formed in the extreme iron-rich rocks and only hypersthene–calcite appears. It is possible that the non-existence of hedenbergite has something to do with the instability of the compound $FeCa(CO_3)_2$. This compound has never been synthesized and has never been observed in nature (Goldsmith, 1959). However, even if siderite and calcite were the parent minerals in this compositional range, ferroaugite should have formed at the time of the decomposition of siderite, or later by reaction between ferrohypersthene and calcite if hedenbergite was stable.

It seems as if we have to conclude that hedenbergite and ferroaugite of high iron content are not stable at the temperatures and partial pressures of CO_2 present during the metamorphism. These facts support a phase relationship such as is shown in Fig. 5. The complicating factors of ankerite not being stable and the possible stability of fayalite–quartz have been ignored for the sake of simplicity.

If the diagram is qualitatively correct, the assemblage ferroaugite–ferrohypersthene–calcite forms directly and reversibly within one compositional range, through two reactions or metastably in more magnesium-rich rocks.

The above ideas about the origin of the ferrohypersthene–ferroaugite–calcite assemblage are supported by thermochemical data. The *PT* curves calculated by Weeks (1956) for the reactions

$$MgCa(CO_3)_2+2SiO_2 \rightarrow MgCaSi_2O_6+2CO_2 \quad \text{and}$$
$$MgCa(CO_3)_2+SiO_2 \rightarrow MgSiO_3+CaCO_3+CO_2$$

are very close together and cross each other at 440° C. and 1,300 atm. pressure of

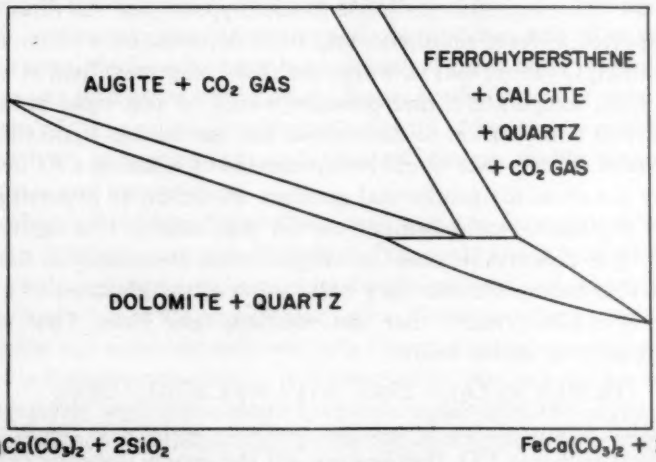

FIG. 5. Hypothetical phase diagram showing the phases that can be expected to form by reaction between dolomite and quartz at different MgO/FeO ratios in a dry environment.

CO_2. Ferrodolomite presumably would decompose to calcite and hypersthene up to much higher temperatures and pressures. FeO favours hypersthene over diopside as shown by the fact that hypersthene has a higher FeO/MgO ratio than the coexisting diopside.

8. ACTINOLITE

In the Mount Reed iron formations actinolite occurs principally in the oxide iron formations with or without diopside. Actinolite–diopside rock is also found as an alteration product of dolomite in the dolomite formation underlying the iron formation.

The stability relationships of the actinolite series are complicated by the fact that actinolite is just one end member of the complex hornblende group. The presence of such components as aluminium, ferric iron, and sodium may have a large influence on the stability. Three of the four calcium amphiboles analysed contain a major amount of aluminium. It is not the purpose of this paper

to present a complete discussion of the stability of hornblende. It will only be discussed to the extent that it affects the mineral assemblages present in the MgO–FeO–CaO system. However, as an introduction, the following general observations on hornblende should be mentioned. High pressure appears to favour the inclusion of NaAl, the glaucophane molecule, into the structure. High temperature favours aluminium particularly in the four-coordinated positions (Harry, 1950); the presence of aluminium should stabilize ferrous amphiboles (Ramberg, 1952).

The main problem of interest to this discussion is how the Fe/Mg ratio affects the stability of the actinolite structure. As was mentioned earlier, iron-rich actinolite has not been observed in the Mount Reed area. Apparently, the assemblage cummingtonite–ferroaugite takes its place. Whether ferrous actinolite is stable at some lower temperatures is not quite clear. Ferrous actinolite analyses from the literature are rare, although this may be due to scarcity of rocks of suitable bulk composition for formation of ferroactinolite rather than to complete instability of the structure. The association cummingtonite–green amphibole is common in lower grade rocks, suggesting that the actinolite field extends farther to the iron side at lower temperatures. This assumption agrees with the general rule that the iron end members become unstable at lower temperatures than the magnesium-rich varieties. It is also interesting to note that, although the association cummingtonite–ferroaugite is common, the association anthophyllite–diopside has never been reported. Thus, on the magnesium side, the ferromagnesian amphibole dissociates before the calcic amphibole, whereas towards the iron side this relationship is reversed. The associations cummingtonite–actinolite–augite and cummingtonite–anthophyllite–actinolite are also common, so that qualitatively we can deduce phase diagrams such as are shown in Figs. 6 and 9.

Fig. 9 is valid only for a certain temperature, pressure, and activity of H_2O. Fig. 6 illustrates how the mineral assemblages may be affected by the activity of water. If a system open to water, or a system with excess water, is assumed, the activity is related to temperature, so that the diagram can be turned upside-down and be used as a temperature–composition diagram.

The lower temperature boundary of actinolite is probably controlled by the dissociation temperature of dolomite–ankerite, since most actinolite occurs as an alteration product of carbonates. The point where the dissociation curve cuts the field boundary of actinolite–calcite should therefore represent the maximum amount of iron present in naturally occurring actinolite. Kunitz (1930) has reported a few very iron-rich actinolites, but the writer has been unable to find a description of their source. Conceivably ferroactinolite may form during retrogressive metamorphism as an alteration product of ferroaugite. In any case it cannot be said at present that the ferroactinolites are unstable as such, as the lack of such minerals in the field may reflect the lack of rocks of a suitable bulk composition for the formation of these minerals.

Iron-rich aluminous calcium–amphibole is more common. A plot compiled by Sundius (1946) of the aluminium content against the FeO/MgO ratio in common hornblendes shows that iron-rich hornblendes are usually high in aluminium. Ramberg (1952) has shown that, because of the larger electronegativity of iron as compared with magnesium, it is easier for aluminium to substitute for silicon in high-iron amphiboles.

The low-grade metamorphic iron formations of the Lake Superior district commonly contain a blue-green amphibole associated with cummingtonite.

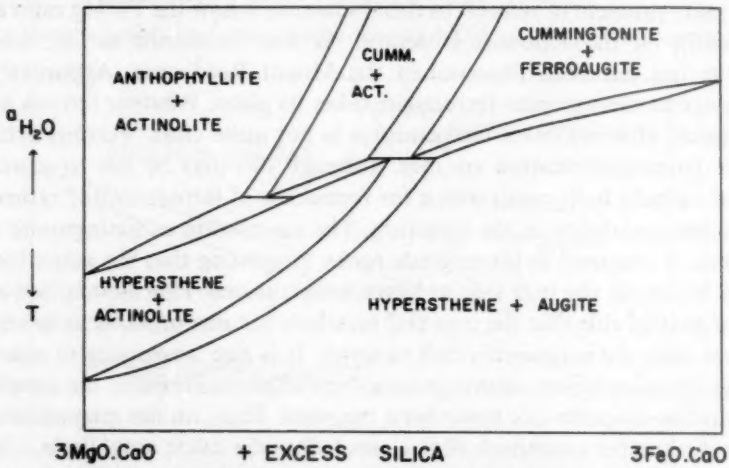

FIG. 6. Hypothetical phase diagram showing how the stability relationships in the system 3MgO.CaO—3FeO, CaO plus excess silica may change with the activity of water.

(Richarz, 1930; James, 1956). The amphibole has been analysed by Richarz. The analysis is reproduced below, together with those of three somewhat similar amphiboles also occurring in iron formations, the last one from Fire Lake. This amphibole, characterized by a high ferric iron content and a low alkali content, apparently is quite typical for iron formations, probably forming in beds containing shaly fractions.

Blue-green amphiboles from iron formations

	Eastern Mesabi (*Richarz, 1930*)	*Gillinge* (*Palmgren, 1916*)	*Western Australia* (*Miles, 1943*)	*Fire Lake*
SiO_2	48·76	37·35	n.d.	47·2
Al_2O_3	11·15	12·75	n.d.	8·9
Fe_2O_3	7·92	7·18	8·7	6·0
FeO	21·72	18·73	25·0	9·3
MnO	trace	1·42	n.d.	0·15
MgO	0·38	4·94	n.d.	13·3
CaO	6·16	11·46	n.d.	11·6
Na_2O	1·67	0·96	0·1	1·0
K_2O	0·58	2·87	0·1	0·90
H_2O	1·89	1·22	n.d.	n.d.

9. THE EFFECT OF MANGANESE, SODIUM, AND ALUMINIUM

Manganese, sodium, and aluminium are the main components which may affect the stability relationships of the minerals in the iron formation in addition to those already discussed. Aluminium is present in the upper part of the iron formation where it grades into the overlying gneisses, in garnet, aluminous hornblende, and biotite. Manganese and sodium show a peculiar sympathetic relationship, and layers enriched in one are usually enriched in the other as well. The elements are abundant in rocks transitional between the oxide and the silicate facies.

Aluminium

Aluminium-bearing assemblages have not been extensively studied in this work, partly in order to avoid more complicating factors, and partly because of the difficulties encountered in analysing iron-rich minerals for aluminium by rapid silicate analysis methods. The only garnet analysed was from specimen A-12, a diopside–hypersthene–hornblende–garnet skarn from north of Blough Lake. It is an almandite–pyrope with a surprisingly high magnesium content. The rock is from a suite of peculiar mafic rocks occurring commonly in a zone immediately above the iron formation north of Blough Lake. From somewhat superficial evidence the rocks have been classed as meta-eclogite and are described in Appendix A. The only other aluminous rock, whose mineralogy has been studied in detail, is the peculiar olivine–hypersthene–chlorite–spinel–cordierite rock from Hobdad Lake (H-1). The association hypersthene–chlorite is interesting, as it shows that chlorite, generally thought of as a hydrothermal mineral, can exist at a lower water-pressure than anthophyllite. This assemblage, and the earlier-mentioned garnet-bearing rock, seems to delimit fairly closely the Mg/Fe ratios of hypersthene coexisting with garnet and with cordierite. As noted above, the high magnesium content of the garnet is surprising and may indicate a high pressure at the time of the regional metamorphism in the area.

The garnet which occurs locally in the silicate iron formation presumably is common almandite. More work is needed to establish tie lines between augite, hypersthene, and almandite.

Manganese

The study of the manganese content of the ferromagnesian minerals was of special interest since it was expected to show whether manganese could possibly have an effect on the mineral assemblages present. Many cummingtonites analysed from the so-called eulysites in Sweden, which probably represent meta-iron formations similar to the ones studied by the writer, have a high manganese content. A separate name, dannemorite, has been applied to these manganese-rich cummingtonites. Therefore, it seemed possible that the cummingtonite content might be dependent on the manganese content. The present study has

shown, however, that manganese distributes itself between the different ferromagnesian amphiboles and pyroxenes roughly in the same proportions as iron. Thus none of the phases appears to be saturated with manganese. The table below illustrates this fact. The relationship does not hold for the magnesium-rich mineral assemblages.

Mn/Fe × *100 in the silicates of the iron formation*

	Ferrohypersthene	*Ferroaugite*	*Cummingtonite*
B1-3	1·14	1·12	—
B1-6	3·06	3·12	—
B1-21	0·38	0·33	—
A-50	7·50	9·18	—
B-9	—	2·00	1·68
B-18	—	0·85	0·71
H-3	—	16·9	16·9
H-4	1·28	1·25	—
H-7	3·79	3·63	3·62
H-9	4·14	3·71	3·53

It is noteworthy that all the mineral assemblages analysed which show a high manganese content are also high in magnetite. Again, the association acmite–rhodonite is known from Mount Reed in specularite iron formation. This shows that manganese is precipitated mainly in the oxide facies of the iron formation. No work has been done on the chemical composition of the opaque minerals, so it is not known how much manganese is taken up by them.

Why manganese-rich layers of the iron formation are generally also rich in sodium is not very well understood, but it probably has something to do with the fact that the precipitation of both manganese and sodium is favoured by an oxidizing environment. Sodium would need ferric iron to be included in the structure of pyroxene.

Sodium

Sodium-iron silicates are common in the Mount Reed–Blough Lake area. Pure acmite is present in a narrow zone at Mount Reed. Aegirine–augite associated with ferrohypersthene, cummingtonite, and magnetite has been found at Blough Lake. Arfvedsonite, associated with hypersthene and magnetite, is common in the iron formation zone between Silicates Lake and Athol Lake.

The analyses made of sodium-iron silicates in the area are too few to make it possible to state anything definite about the Na_2O–FeO–MgO system, but it is likely that this system with an excess of ferric iron behaves very much the same way as the corresponding CaO–MgO–FeO system. At the iron end of the system the association cummingtonite–acmite seems preferably to form. In more magnesium-rich rocks arfvedsonite and magnesio–riebeckite are stable together with hypersthene, in the same way as actinolite in the corresponding CaO system.

In contrast to calcium, sodium probably is derived directly from silicates. Acmite is known to be precipitated out under surface conditions (Milton & Eugster, 1959) and is probably stable, at least in a dry environment, under all metamorphic conditions.

10. THE ROLE OF THE VOLATILE COMPONENTS IN METAMORPHISM

The role of volatiles in metamorphism has been much discussed in recent geological literature and the subject is still very controversial.

The classical view has been that water is generally present in excess so that it can be ignored as a factor determining the stability fields of different minerals (Turner & Verhoogen, 1951). This view was challenged by Yoder in 1952, who shows that many variations in the mineral composition of metamorphic rocks, generally attributed to changes in metamorphic grade, can just as well be caused by a variation in the water content in the rocks (Yoder, 1952, 1955). Thompson (1959) and Fyfe, Turner & Verhoogen (1958) maintain that petrological evidence does not support Yoder's assumption that rocks are closed to water. Rather, water seems to be able to move fairly freely within the rock, so that the activity of water at each point in the rock is determined by such external factors as the permeability of the rock towards diffusing material, the amount of water in surrounding areas, temperature and pressure gradients, and so on.

Both in the case of the open system concept and in the case of the classical view that the system contains an excess of water, water can be disregarded as a component in applying Gibbs's phase rule since the activity of water is independent of the bulk composition. If the system is open to this component, the activity of water has to be dealt with as a degree of freedom in the same way as temperature and pressure. Thus, for a certain isograd defined by a reaction involving water, not only temperature and pressure have to be taken into account but also the activity of water. If the system has an excess of water, the activity of this component always is close to unity (standard state defined as the pure phase at the pressure and temperature in question) provided no other volatile components are present. In any case, water does not have to be included in a graphical representation of such a system if it is assumed that all the phases shown are in equilibrium with the volatile phase. On the other hand, if the system is closed and there may or may not be free water present, the mineral composition depends on the amount of water present in the system, and water cannot be neglected in a graphical representation. The activity in such a system is fixed by the minerals which are in equilibrium at such a bulk composition. The activity in such a system changes abruptly at points in the rock where changes in bulk composition produce changes in mineral composition.

In the following section we shall see which of the three concepts best agrees with the mineral assemblages in the Mount Reed area.

11. THE ROLE OF THE VOLATILES IN THE MOUNT REED IRON FORMATIONS

Gibbs's phase rule states that

$$\text{Variance} = n+2-\phi.$$

The variance of a system equals the number of independently variable components, less the number of phases, plus two. By variance is meant the number of intensive variables which can be altered independently without bringing about the disappearance of a phase or the formation of a new one (Thompson, 1959).

If there are five phases present, e.g. cummingtonite, ferroaugite, ferrohypersthene, quartz, and calcite composed of six components, FeO, MgO, CaO, SiO_2, CO_2, and H_2O, the variance is $6+2-5 = 3$. Therefore, in order to define the state of the system, the temperature, pressure, and the activity of one component would have to be defined. The fact that the activity of one (and only one) component can be varied independently of temperature and pressure in the assemblage makes it possible that the activity of one component is externally controlled. Any change in bulk composition in such an assemblage in time or in space produces a change in the activities wherefore the primary condition for diffusional transfer of material, an activity gradient in the rock, may exist.

On the other hand, it is possible that the rock had initially a bulk composition such that it happened to fall in a five-phase field. This is particularly likely when ferromagnesian minerals are involved because of the extensive solid solution between FeO and MgO.

If diffusion has taken place, there should be a continuous activity gradient in the rock over the distance the component has travelled. Accordingly, if long-distance diffusion has taken place, the activity of the component within a limited area should show little variation. If there are large local activity gradients it is not likely that material has travelled far.

If the size of the system is chosen so that it extends only over a small portion of such an activity gradient, the activity of the mobile component should be almost constant.

The mineral assemblages in a rock where the activity gradients of one component have been evened out as a result of diffusion, can be represented graphically without considering the mobile component as a component. Thus, a phase diagram representing a section of the FeO–MgO–CaO–SiO_2–CO_2 system can be plotted and it can be assumed that the diagram is valid for a certain temperature, pressure, and activity of H_2O. Alternatively, the system can be assumed to be open to CO_2 and a diagram representing a section of the FeO–MgO–CaO–SiO_2–H_2O system with the activity of CO_2 fixed can be plotted. Sections of such diagrams are shown in Figs. 8 and 9, together with a section of the FeO–MgO–CaO–CO_2 system with the activity of O_2 fixed (Fig. 7). The possibility of the system being open to H_2O, CO_2, and O_2 will be discussed with the help of these diagrams.

The relationship shown in Fig. 7 is definitely not favoured by field evidence. Magnetite is not common in association with the iron-rich silicates, ferrohypersthene, and cummingtonite. The silicates associated with quartz–magnetite iron

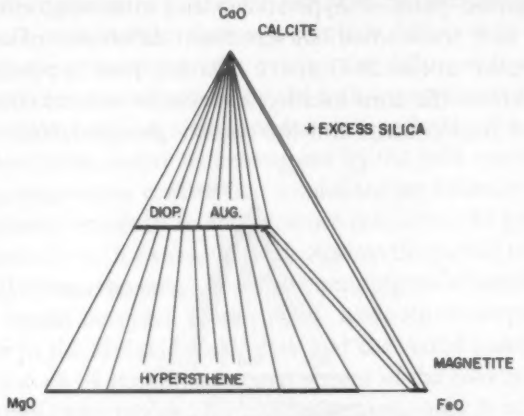

FIG. 7. Hypothetical phase diagram showing a projection of the system FeO–MgO–CaO–SiO_2–CO_2 for a fixed temperature, pressure, and activity of oxygen. The diagram shows phases in equilibrium with quartz.

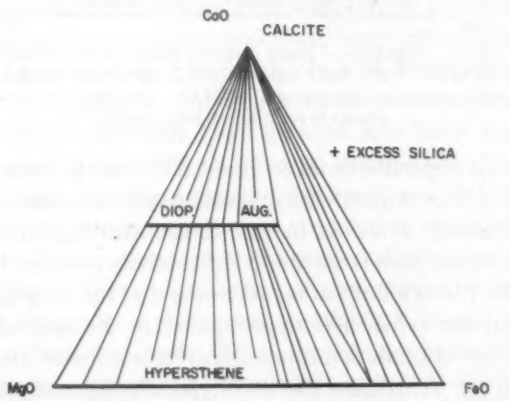

FIG. 8. Hypothetical phase-diagram showing a projection of the system FeO–MgO–CaO–SiO_2 for a fixed temperature, pressure, and activity of CO_2. The diagram shows phases in equilibrium with quartz.

formation are such magnesium-rich minerals as actinolite and diopside and also manganese-rich hypersthene and cummingtonite. The limited mobility of oxygen during the regional metamorphism is illustrated also by the association magnetite–specularite in the oxide iron formations and by the presence of graphite in some of the magnetite-free calcite-bearing silicate iron formations.

If the system was open to H_2O, the composition of cummingtonite should fall

within one range of MgO/FeO ratios, the composition of hypersthene within another, and the hypersthene and cummingtonite should coexist only within a limited range of compositions as shown in Fig. 9.

The two analysed pairs of hypersthene and cummingtonite from Hobdad Lake, H-7 and H-9, show small but significant differences of composition. The samples were taken about 20 ft apart. The analysed hypersthene–ferroaugite assemblage H-4 from the same locality, a specimen without cummingtonite, has a slightly higher iron content and the cummingtonite–ferroaugite assemblage,

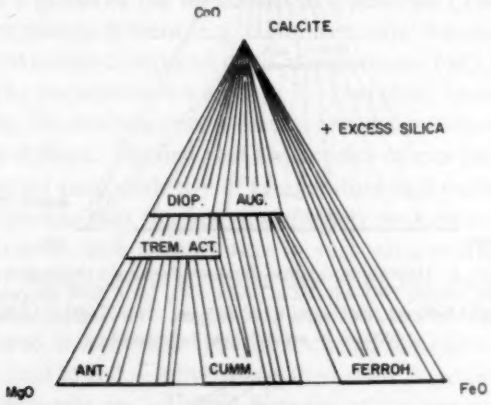

FIG. 9. Hypothetical phase diagram showing a projection of the system FeO–MgO–CaO–SiO_2–CO_2 for a fixed temperature, pressure, and activity of H_2O. The diagram shows phases in equilibrium with quartz.

a specimen without hypersthene taken about 100 ft away, has a lower magnesium content. All these four mineral assemblages could have been in equilibrium at about the same activity of water, in accordance with Fig. 9.

In the southern area there is a definite H_2O activity gradient between the Athol Lake area and the Blough Lake area, assuming that the *PT* conditions in the two areas were about the same. The hypersthenes in the specimens from Blough Lake, which do not contain cummingtonite, have a lower iron content (mostly about 36 weight per cent) than the two hypersthenes analysed for iron in the Athol Lake area, which are associated with cummingtonite. The fact that several other analysed hypersthenes not associated with ferroaugite also contain about 40 per cent FeO, indicates that hypersthene coexisting with cummingtonite commonly contains about 40 per cent FeO, not because this is the only composition at which hypersthene and cummingtonite are stable together because of an externally controlled activity of water, but because the bulk composition of the silicate iron formation favours a hypersthene of this composition.

In this connexion it should be noted that in the case of multivariant mineral assemblages which include one or more phases capable of extensive substitution of one component for another, it is very difficult to prove that the rock has been

completely closed. In such an assemblage, the activities of the different components and the bulk composition are variable, and it may be difficult to say whether the bulk composition or an externally controlled water pressure determined the mineral compositions. Also the fact that the assemblages appear to be related to the bulk composition does not preclude diffusion in and out of the system, provided the activity gradient driving the diffusion is of local nature. Such activity gradients are influenced by the bulk compositions of the rocks in the immediate neighbourhood, and therefore are probably not much different from the activities of the system as determined by the bulk composition.

However, it is reasonably certain that long-distance diffusion such as would be driven by regional temperature and pressure gradients, the gravity field, &c., has not taken place. In such a case, the odds against the partial pressure of water happening to fall within the range in which cummingtonite and hypersthene are stable together would be much larger. Also, it would seem peculiar that the activity of water in the Hobdad Lake area and the Athol Lake area would be quite similar as shown by the similar compositions of the coexisting hypersthene and cummingtonite, whereas the Blough Lake area, only 5 miles from Athol Lake, would show a quite different activity of water.

The case of CO_2 can be studied in the same way. At a fixed CO_2 activity, temperature, and pressure, coexisting ferroaugite, hypersthene, and calcite should have the same composition in accordance with Fig. 8. Hypersthenes higher in iron should coexist only with calcite, and those lower in iron should coexist only with ferroaugite. The clustering of hypersthenes with 36 per cent FeO coexisting with ferroaugite and calcite in the Blough Lake area, and hypersthenes with 40 per cent FeO in the Hobdad Lake area, at first hand could be taken as evidence for a system open to CO_2. In order to test this idea, hypersthenes from a number of rocks free of ferroaugite were analysed, and they all show a higher iron content. However, no specimens have been found which are free of calcite. The hypersthene in B1-3 containing only 31 per cent FeO, coexists with calcite as well as with ferroaugite. The large difference in composition between such mineral assemblages as B1-3 and B1-6 shows that significant CO_2 activity gradients can exist within such a short distance as 200 ft, the distance between the points from which these specimens were taken, assuming again that the temperature and pressure did not differ significantly between the two points. The complete absence of calcite-free assemblages, and the great variation in the composition of hypersthenes in equilibrium with ferroaugite and calcite in the Blough Lake area, again seems to show that the mineral composition mainly depends on the bulk composition. However, again, it cannot be proved that the system was completely tight.

In conclusion, it appears that the rock in most places has been closed either to CO_2 or H_2O, as shown by the low variance of the assemblage ferrohypersthene–ferroaugite–cummingtonite–calcite–quartz. If the system was open to one component, material did not diffuse over long distances, as shown by the presence of

appreciable local activity gradients for both of the volatile components. Possibly the system was open to H_2O in some places, to CO_2 in some places, to both in some places, and maybe to other components as well in some places, depending on whether the local activity gradients happened to be steep enough to drive the diffusion. Such rocks represent reaction zones between beds of strongly contrasting mineralogical compositions.

The inefficiency of long-distance diffusion raises the problem of the fate of the volatiles released in the course of the reactions taking place during progressive metamorphism.

12. THE METHOD OF ESCAPE OF VOLATILES DURING METAMORPHIC REACTIONS

One of the most powerful arguments that has been put forward in support of open systems is that water and carbon dioxide apparently have been able to escape during the reactions accompanying progressive metamorphism. Yoder (1955) discusses the problem and mentions the alternatives that water may stay on in the rock or diffuse away. The second alternative is not valid for closed systems. If diffusion is fast enough to remove water or carbon dioxide as it is liberated, there is no reason why the diffusion could not start already at a lower temperature since the necessary activity gradients are just as real below the reaction temperatures as above it. This is, of course, the same as an open system.

If the speed of diffusion is too slow to remove the liberated gas phase from the system, it will start accumulating as a new phase or expanding any volatile phase already present. If the reaction continues, the pressure is built up and the reaction must stop. The only way for the reaction to continue is to increase the volume of the rock or to increase the temperature so that the reaction will continue at the new pressure. However, since temperature and pressure are externally controlled, it is unlikely that the increase in pressure and temperature will follow the univariant reaction curve. The only alternative seems to be that the water finds open pores into which to flow. If the recrystallization is accompanied by tectonic deformation, the regional stress might give energy for such an expansion of the rock. It is questionable whether the fact that we do not find evidence for expansion in metamorphic rocks is a valid observation. On the contrary, the complicated structures found in high-grade metamorphic rocks might be a result of increased plasticity due to the presence of water in the rock. Any textural evidence would tend to be obliterated in the course of retrograde metamorphism.

During the deformation, the water vapour and carbon dioxide gas could be squeezed around in the rock and migrate upward towards areas of lower pressure, propelled by mechanical pressure gradients in the same way as a wet sponge is squeezed dry. As the gas phase moved through the rock, it would have reacted with the wall rock in places where the wall rock was not in equilibrium with such a fluid phase.

Moving gases and solutions, like diffusion, would tend to even out activity

gradients by reaction with rocks with which they are not in equilibrium. It is likely, however, that such reactions would be sporadic and incomplete, and leave rocks essentially closed in places where solutions and gases did not penetrate.

13. ORIGIN OF THE IRON FORMATION

The geochemistry of sedimentary iron formations has been discussed by Huber & Garrels (1953), by James (1954), and others, and will not be presented in detail in this paper. James differentiates between four main facies of iron formation, namely, oxide iron formation, carbonate iron formation, silicate iron formation, and sulphide iron formation. Each type is regarded as a primary chemical precipitate. The old view held by van Hise, Leith (1911), and others, that siderite is the only primary iron mineral, is now only of historical interest. Huber & Garrels have shown that each type of iron formation is precipitated within a certain range of oxidation potential and acidity of water. In sea-water the acidity is relatively constant, so that it is mainly the oxidation potential that has controlled the type of sediments precipitated at a given place at a given time. Oxide iron formations presumably are precipitated under shallow water conditions where excess oxygen is present, carbonate iron formations in deeper waters, and sulphide iron formation, mainly in the presence of organic matter in stagnant basins where the water circulation is slow. The silicate iron formations presumably form in about the same environment as the carbonate iron formation where the carbon dioxide content is too low for siderite to precipitate. Fayalite and greenalite are probably the only primary iron silicates, since they are the only ones that are stable in the presence of water (Yoder, 1957).

The iron oxides were regarded earlier as replacement products of siderite. The primary nature of ferric oxide is now generally accepted. The role of magnetite is not as clear. Haematite is known to occur interbedded with siderite (Gruner, 1946), so it appears as if it would not be stable at high CO_2 pressures under surface conditions. James suggests that its apparent occurrence as a primary mineral may be interpreted to indicate both low O_2 and low CO_2 atmospheric pressures at the time of its deposition (James, 1954).

Haematite is a major constituent in jaspilite, a common rock type both in the Lake Superior district and in Labrador. The rock consists of interlayered chert and finely crystalline haematite. Magnetite-banded facies are also common. In the Labrador trough the magnetite-bearing facies has been called cherty metallic iron formation (Perrault, 1955). It consists of fine metallic oxides, chiefly magnetite, disseminated in a cherty groundmass and also segregated into metallic bands. Minnesotaite, stilpnomelane, and siderite commonly are mixed in with the chert and magnetite.

There is hardly any reason to doubt that the specularite iron formation and the magnetite iron formation of the Mount Reed area are direct metamorphic equivalents of the jaspilite and the cherty metallic iron formation respectively of the Knob Lake area.

The origin of the silicate iron formation is a more difficult problem. Cummingtonite and hypersthene could form both by metamorphism of primary iron silicates and by reaction between quartz and siderite. Both siderite and the silicates greenalite and minnesotaite are common in the Knob Lake area.

Minnesotaite is the main constituent of the so-called minnesotaite iron formation. This rock consists of bands of minnesotaite in the form of radiating aggregates of needles and felted masses interlayered with chert. Greenalite is found as granules within the minnesotaite iron formation and also in the metallic iron formations. It commonly is intermixed with minnesotaite, greenalite being concentrated in certain layers and minnesotaite in others. From field evidence, Perrault concludes that some of the minnesotaite is definitely an alteration product of greenalite but that some may be primary. In some places minnesotaite replaces siderite, indicating that siderite starts breaking down in the presence of water already at this stage of the metamorphism.

Siderite is the main constituent in cherty carbonate iron formation in the Knob Lake area. In this rock type it is mixed in all proportions with chert. It is also found as granules and nodules in the cherty metallic iron formation and in the minnesotaite iron formation.

Ferrodolomite is present in places within the cherty carbonate, apparently secondary after siderite. It has also been found as fine laminae within cherty metallic iron formation. Generally, ferrodolomite does not appear to be as common in the Knob Lake area as it probably was in the Mount Reed iron formation before the metamorphism.

14. THE METAMORPHIC HISTORY OF THE IRON FORMATION

Unfortunately the information needed to reconstruct the metamorphic history of the iron formations in its entirety is not available. However, from information obtained in the Mount Reed area and from information available in the literature, we can at least suggest a possible model of the phase-equilibrium changes in the course of the metamorphism. The sequence of events leading up to the present state of the iron formation can best be represented by a series of phase diagrams. This has been done in Fig. 10. Most minerals in the silicate iron formation are phases in the system CaO–FmO–SiO_2–CO_2–H_2O. By assuming an excess of quartz in all assemblages, SiO_2 can be ignored in the graphical representation. The component FmO can be defined as FeO+MgO in the ratio they most commonly occur in the Mount Reed area, say 3 to 1. For other FeO/MgO ratios the reactions take place at different temperatures, usually the higher the FeO/MgO ratio the lower the temperature of the reaction. Also in magnesium-rich rocks the sequence of events will probably be different, as was demonstrated in section 8. In extremely iron-rich magnesium-poor rocks the sequence of events may also be somewhat different because of the possibilities of fayalite+quartz being stable (section 6), and high iron augite unstable (section 7).

The solubility relationships between CO_2 and H_2O are not very well known

(Ellis, 1959) and have not been shown on the diagrams. Above the critical point of water these components presumably are completely miscible.

The mineral assemblages in equilibrium with volatile phases at each stage represented in Fig. 10, and the chemical reactions assumed to produce the changes in the phase equilibria, are listed below:

(*a*) siderite–ferrodolomite–greenalite
calcite–ferrodolomite–greenalite

(1) siderite + quartz + water → greenalite + CO_2 gas

(*b*) siderite–ferrodolomite–greenalite
calcite–ferrodolomite–greenalite

(2) greenalite + siderite + quartz → minnesotaite + water − CO_2 gas

(*c*) calcite–ferrodolomite–greenalite
ferrodolomite–greenalite–minnesotaite
ferrodolomite–minnesotaite–siderite

(3) greenalite + quartz → minnesotaite + water

(*d*) calcite–ferrodolomite–minnesotaite
siderite–ferrodolomite–minnesotaite

(4) minnesotaite + siderite + quartz → cummingtonite + water − Co_2 gas

(5) minnesotaite → cummingtonite + quartz + water

(*e*) calcite–ferrodolomite–cummingtonite
siderite–ferrodolomite–cummingtonite

(6) siderite + quartz → ferrohypersthene + CO_2 gas

(*f*) calcite–ferrodolomite–cummingtonite
ferrodolomite–cummingtonite–ferrohypersthene

(7) ferroactinolite → ferroaugite + cummingtonite + quartz + water

(*g*) calcite–ferrodolomite–cummingtonite
ferrodolomite–cummingtonite–ferrohypersthene

(8) ferrodolomite + quartz → ferroaugite + CO_2 gas

(*h*) calcite–ferroaugite–cummingtonite
ferroaugite–cummingtonite–ferrohypersthene

(9) ferroaugite + CO_2 gas → calcite + ferrohypersthene + quartz

(*i*) calcite–ferroaugite–ferrohypersthene–cummingtonite

(10) calcite + quartz → wollastonite + CO_2 gas

(11) cummingtonite → ferrohypersthene + quartz + water

(*j*) wollastonite–ferroaugite
ferroaugite–ferrohypersthene

Fig. 10*a* represents the assumed stability relationships at surface temperatures and pressures.

The primary minerals are assumed to be greenalite, calcite, ferrodolomite, and siderite. It is also assumed that greenalite is able to form as a reaction product of siderite and quartz in the presence of water. Ferroactinolite could only form

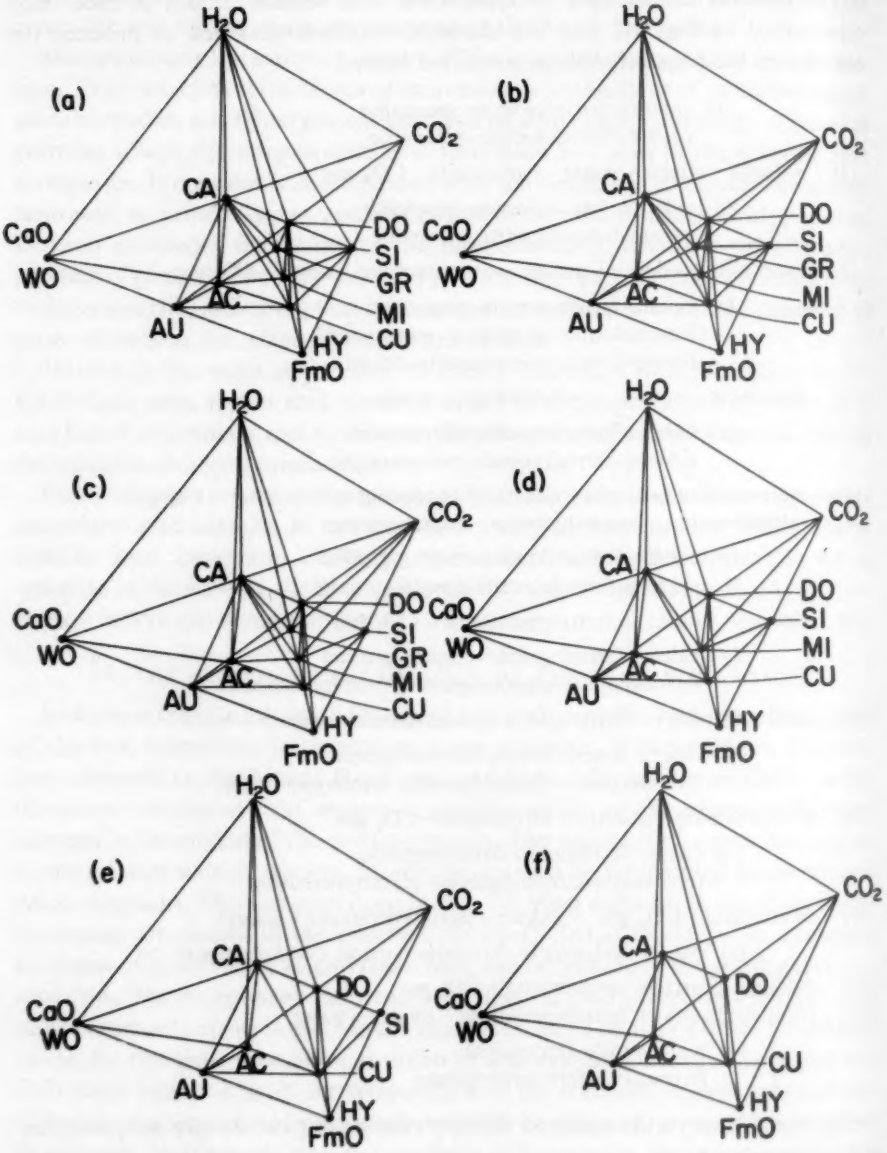
(a)
H2O
CO2
CA
CaO
WO
DO
SI
GR
AC
MI
AU
CU
HY
FmO
(b)
H2O
CO2
CA
CaO
WO
DO
SI
GR
AC
MI
AU
CU
HY
FmO
(c)
H2O
CO2
CA
CaO
WO
DO
SI
GR
AC
MI
AU
CU
HY
FmO
(d)
H2O
CO2
CA
CaO
WO
DO
SI
MI
AC
CU
AU
HY
FmO
(e)
H2O
CO2
CA
CaO
WO
DO
SI
AC
CU
AU
HY
FmO
(f)
H2O
CO2
CA
CaO
WO
DO
AC
CU
AU
HY
FmO

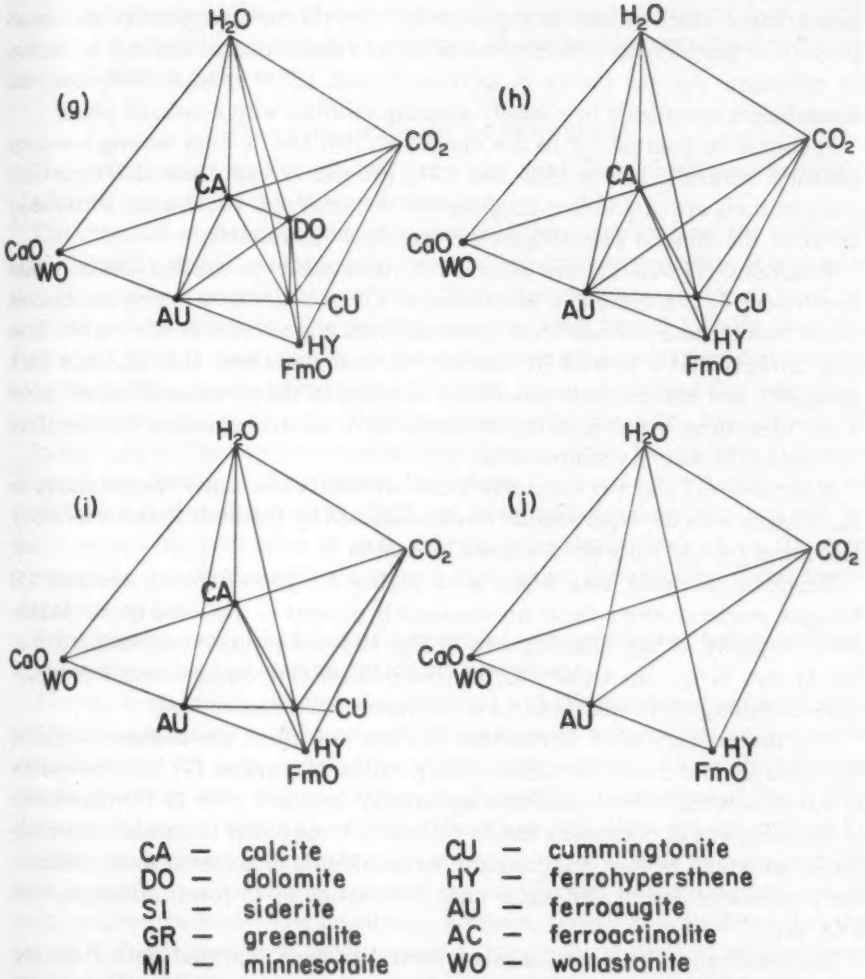

CA	—	calcite	CU	—	cummingtonite
DO	—	dolomite	HY	—	ferrohypersthene
SI	—	siderite	AU	—	ferroaugite
GR	—	greenalite	AC	—	ferroactinolite
MI	—	minnesotaite	WO	—	wollastonite

FIG. 10. Hypothetical phase diagrams showing possible changes in the mineral stability relationships with increasing metamorphism in the system FeO–MgO–CaO–SiO_2–CO_2–H_2O.

from waters with a very low CO_2 pressure and a high CaO content, probably non-existent in nature. Ferrodolomite may not actually form as a primary mineral but only by ordering or reaction of a mixture of calcite and siderite in the zone of diagenesis analogous with dolomite. Beside each diagram are listed the mineral assemblages which would be expected to form through progressive metamorphism and partial or complete removal of the volatile phases through squeezing or diffusion. As was shown in sections 11 and 12, it appears likely that the assemblages are mostly in a steady state equilibrium with a volatile phase.

It should be pointed out in this connexion that the tie lines among low-temperature minerals, low in H_2O and CO_2, are purely hypothetical. These bulk compositions are rare in low-temperature metamorphic rocks and, where they do exist, the mineral assemblages are very likely metastable.

Reactions (1) and (2) are assumed to take place to explain the common coexistence of greenalite and minnesotaite. The minnesotaite in this association could hardly have formed from greenalite since greenalite is still stable. It is also unlikely that it formed by reaction between water and siderite, since both greenalite and minnesotaite should not be stable in the presence of excess water at the same time, unless possibly the higher ferric content common in greenalites influences the stability relationships.

Reactions (3) and (4) may take place at nearly the same temperatures in accordance with the experimental results obtained by Flaschen & Osborn (1957). Reactions (4) and (5) were discussed in section 5.

Reaction (6) must take place at a higher temperature than reaction (5) because grunerite and siderite are commonly present in the same rocks (James, 1956; Murphy, 1959). The diagrams of Fig. 10 *f* and *g* may be representative of the Mount Wright area where Gross (1955) found ferrohypersthene–ferrodolomite–cummingtonite–quartz to be a common mineral assemblage.

The decomposition of ferroactinolite does not affect the common mineral assemblages in the iron formation. The position of reaction (7) in the sequence is purely arbitrary. Ferrodolomite apparently does not alter to ferroactinolite in the same way as dolomite alters to tremolite. It may alter to calcite–cummingtonite, although in this interpretation ferrodolomite is assumed to be stable in the presence of quartz and water until it decomposes to form ferroaugite and CO_2 gas.

The association grunerite–calcite–quartz has been reported both from the Lake Superior area (Richarz, 1927) and from Labrador (Mueller, 1958).

Reactions (8) and (9) have been discussed in section 7, and reactions (10) and (11) can be assumed to take place under high temperatures and pressures characteristic for the granulite facies.

It should be emphasized again that the above sequence of reactions is highly hypothetical. No doubt other phase diagrams could be drawn which would fit available evidence just as well. At the present time it is very frustrating to try to deduce stability relationships from the literature because of the habit of geolo-

gists to report the minerals occurring in a rock sequence without specifying the exact mineral assemblages in individual specimens. In the above summary the writer has tried to illustrate how useful it would be to know more about the stable mineral assemblages in studying the metamorphic grade of rocks. It is hoped that the discussion will encourage other geologists to present data which will make it possible to construct a sequence of similar diagrams based more on facts and less on guess-work.

15. SUMMARY AND CONCLUSIONS

The present study has contributed some new data about the phase chemistry of silicates and carbonates in iron formations.

The chemical analyses of coexisting minerals have shown how the different major elements distribute themselves between the different minerals. It is shown that the mineral assemblages of the silicate iron formations are at least in approximate equilibrium. The general rule has been found to hold that the FeO/MgO ratio is always lower in the calcium-bearing pyroxenes and amphiboles than in the pure ferromagnesian minerals. It was also found that cummingtonite generally has a lower FeO/MgO ratio than the coexisting hypersthene.

In the light of the new petrological and chemical data, the stability relationships of amphiboles and pyroxenes have been discussed. It is hoped that, as more facts are compiled from the field and from the laboratory, the data will be useful in helping geologists to gain a better quantitative idea about the way temperature, pressure, and bulk composition affect the stability of the ferromagnesian minerals.

Some general conclusions have been arrived at regarding the factors influencing the mineralogy of metamorphic iron formations.

The study does not support the idea that volatile components can diffuse freely through the rocks. The partial pressures of all components appear to be determined by the bulk composition of the rocks rather than by the physical conditions of the environment. The most important consequence of this is that the temperatures at which the different reactions take place are determined by equilibria in a closed system where the pressure of the volatile phase equals the rock pressure. It is, of course, too early to say whether this is a general rule in metamorphic reactions. The possibility, however, should be considered that the reason H_2O can commonly be disregarded in a graphical study of metamorphic grades is the old classical idea that volatiles are ever present in the rocks rather than the more recently advanced idea that the rocks are open to volatile components. If the volatile component is nearly pure water, it would be difficult to determine from a study of the mineral assemblages which of the two concepts are valid, as the type of mineral assemblages in either case would be the same. The iron formations are more favourable for a study of this kind, because the presence of two volatile components in the solid phases makes it possible to demonstrate the non-variance of the partial pressures of the volatile components

at constant temperatures and pressures. In the case of the Mount Reed iron formations the volatile phase is believed to have been removed by reaction of ferroaugite with CO_2 gas to form hypersthene and calcite. The mineral assemblages therefore reflect an environment deficient in a volatile phase. Therefore the tightness of the rock to one volatile component can be demonstrated with the help of the phase rule and the tightness of the rock to both H_2O and CO_2 strongly indicated by demonstrating the presence of appreciable local activity gradients for both these components. It is also suggested that chemical reactions involving volatile components are strongly influenced by tectonic processes.

The second general conclusion which can be drawn is that FeO–SiO_2 systems often behave very differently from their MgO–SiO_2 analogues. This was shown in the discussion on the stability of actinolite (Fig. 6). It was also shown that hedenbergite may not be stable at high CO_2 pressures, but is replaced by the association ferrohypersthene–calcite. The opinion has been prevalent that hypersthene and calcite are not compatible (Ramberg, 1952*b*). This does not hold for ferrohypersthene.

To summarize, the study has, at least in the mind of the writer, pointed out how badly in need theoretical geologists are of more chemical data of minerals from the field. In order that laboratory studies of the stability of minerals can help the field geologist, he must be able to point out what chemical equilibria it would be most significant to study. For this purpose more data are needed on the mineral assemblages occurring in the field as well as a better knowledge of the chemistry of coexisting minerals.

16. ACKNOWLEDGEMENTS

The writer wants to express his great appreciation to Mr. L. J. Severson, president of the Quebec Cartier Mining Company, and to Dr. R. W. Marsden, manager of explorations of the Oliver Iron Mining Company, for permission to publish information obtained in the Mount Reed area. The company generously furnished time and transportation for the collection of the rock specimens. The help and advice of Dr. R. W. Marsden, Dr. D. F. Bradley, Mr. E. C. Ferreira, and Dr. T. H. Moore in the course of the field work is greatly appreciated.

At Massachusetts Institute of Technology the encouragement and advice given by Prof. H. W. Fairbairn was very valuable. The help of Prof. W. H. Pinson, Mr. A. Brownlow, and Mr. W. Phinney is also appreciated. The theoretical approach used in this study is a direct application of methods developed by Prof. J. B. Thompson in lectures at Harvard University. The writer wishes to thank Prof. Thompson for discussions about the problems dealt with in the paper and for pointing out a few weaknesses in the original presentation, the most serious of which have been corrected.

APPENDIX A

Chemical Analysis of Minerals in Mafic Rocks

A-12. Garnet–hornblende–pyroxenite. A dark green, massive, medium-grained xenoblastic rock-type outcropping in a horizon immediately above iron formation northwest of Athol Lake. The mineral composition is given below:

Slightly pleochroic hypersthene ($2V$ 80°)	20 per cent
Green hornblende ($Z \wedge c$ 18°, $2V$ 90°)	40 per cent
Diopside ($2V$ 54°, $Z \wedge c$ 36°)	30 per cent
Garnet	10 per cent

Hypersthene

	Wt. %	*Mol. props.*	*Metal atoms per 6 oxygens*	
SiO_2	52·6	874	1·887	2·000
Al_2O_3	4·0	39	0·168 (0·113 + 0·055)	
Fe_2O_3	1·4	9	0·037	2·009
FeO	13·7	191	0·412	
MnO	0·23	3	0·006	
MgO	26·9	669	1·444	
CaO	1·2	21	0·045	
Na_2O	0·09	2	0·009	
K_2O	0·02	—	0·001	
	100·1			

Diopside

	Wt. %			*Metal atoms per 6 oxygens*	
	Individual analyses	*Average*	*Mol. props.*		
SiO_2	—	53·5	889	1·961	2·000
Al_2O_3	—	1·1	11	0·048 (0·039 + 0·009)	
Fe_2O_3	—	1·4	9	0·040	2·000
FeO	3·67 3·85	3·8	53	0·117	
MnO	0·11 0·12	0·11	2	0·004	
MgO	16·58 16·98	16·8	418	0·922	
CaO	22·97 22·66	22·8	407	0·898	
Na_2O	0·08 0·11	0·10	2	0·009	
K_2O	0·03 0·03	0·03	—	0·001	
		98·2			

Hornblende

	Wt. %			
	Individual analyses	*Average*	*Mol. props.*	*Metal atoms per 23 oxygens*
SiO_2	—	48·8	813	6·93
Al_2O_3	—	9·5	93	1·58 (1·07 + 0·51)
Fe_2O_3	—	1·9	12	0·20
FeO	5·44 5·43	5·4	76	0·69
MnO	0·12 0·11	0·11	2	0·02
MgO	18·41 18·72	18·6	463	3·94
CaO	11·33 11·64	11·4	203	1·73
Na_2O	0·80 0·82	0·81	13	0·22
K_2O	0·13 0·16	0·14	2	0·04
		96·6		

8·00 | 5·32 | 1·99

Garnet

	Wt. %	*Mol. props.*	*Metal atoms per 12 oxygens*
SiO_2	40·7	677	3·013
Al_2O_3	21·8	214	1·905
Fe_2O_3	4·8	30	0·134
FeO	15·0	209	0·930
MnO	0·89	13	0·058
MgO	10·9	271	1·206
CaO	6·9	116	0·516
Na_2O	0·05	1	0·001
K_2O	0·03	—	—
	100·6		

2·039 | 2·710

H-1. Hobdadite. This rock type has been termed hobdadite after Hobdad Lake, the location where it is found. Its mineralogical composition is so unique that a special name is warranted for the rock type. Hobdadite is a massive, dark grey, rusty weathering, very tough rock which outcrops on the top of Hobdad Mountain just west of Hobdad Lake. The rock is xenoblastic, coarse-to-medium grained. A thin section studied is composed of the following minerals:

Light-coloured hypersthene 30 per cent: light green amphibole is intermixed with the hypersthene in small amounts in myrmekite-like intergrowths.

Colourless chlorite 35 per cent: occurring partly as flaky masses filling up areas between hypersthene granules, partly as euhedral grains sometimes growing parallel with the cleavage of the hypersthene, in other places cutting across hypersthene and olivine grains. It appears, at least partly, to be in textural equilibrium with the other ferromagnesian minerals. Under polarized light it has a very fine striated appearance, the birefringence and relief are low. In thin sections the mineral is colourless;

in thicker masses it is light green. The chemical composition given below and the X-ray pattern show that the mineral is a chlorite.

Olivine-like mineral 10 per cent: this is a reddish-orange mineral with high relief. It is strongly pleochroic in yellow, orange, and red. $2V = 69°+$. The chemical composition is shown below and indicates that the mineral is related to olivine or humite.

The thin section also shows small amounts of spinel, magnetite, carbonate, and cordierite.

Hypersthene

	Wt. %	*Mol. props.*	*Metal atoms per 6 oxygens*	
SiO_2 . . .	54·2	901	1·888	2·000
Al_2O_3 . . .	5·8	57	0·239 (0·112 + 0·127)	
Fe_2O_3 . . .	1·7	11	0·046	1·973
FeO . . .	9·1	127	0·266	
MnO . . .	0·2	3	0·006	
MgO . . .	29·1	723	1·520	
CaO . . .	0·1	2	0·004	
Na_2O . . .	0·02	1	0·004	
K_2O . . .	0·05	—	—	
	100·3			

Olivine

	Wt. %	*Mol. props.*	*Metal atoms per 4 oxygens*	
SiO_2 . . .	35·9	598	0·905	1·000
Al_2O_3 . . .	3·4	39	0·106 (0·095 + 0·011)	
Fe_2O_3 . . .	2·4	15	0·045	2·023
FeO . . .	11·4	159	0·241	
MnO . . .	0·06	1	0·002	
MgO . . .	45·4	113	1·710	
CaO . . .	0·3	6	0·009	
Na_2O . . .	0·05	1	0·004	
K_2O . . .	0·01	—	0·000	
	99·0			

Chlorite

	Wt. %	*Mol. props.*	*Metal atoms per 10 oxygens*
SiO_2	29·7	494	2·84 → 3·00
Al_2O_3	20·5	201	2·42 → (0·16 → 3·00; 2·26 → 2·33 → 2·00; 0·33)
Fe_2O_3	1·0	6	0·07 → 2·33
FeO	3·8	53	0·31 → 4·77
MnO	0·01	—	— → 4·77
MgO	30·8	766	4·41 → 4·77
CaO	0·2	4	0·03 → 4·77
Na_2O	0·09	2	0·02 → 4·77
K_2O	0·02	—	— → 4·77
	86·1		0·33 + 4·77 → 5·10

APPENDIX B

Silicate Iron Formation from the Southern Area

B1-1. A heavy, light-bluish-grey homogeneous rock composed of 85 per cent ferrohypersthene, 10 per cent quartz, and 5 per cent calcite. A partial analysis of the hypersthene showed it to contain 44·8 per cent FeO.

B1-2. A grey, indistinctly banded rock composed of 30 per cent quartz, 30 per cent ferrohypersthene, 20 per cent ferroaugite, and 20 per cent calcite. The ferrohypersthene contains 36·0 per cent FeO.

B1-3. A well-bedded rock consisting of alternating rusty-weathering layers rich in calcite and more resistant layers rich in quartz and silicates. The mineral composition of a thin section is 15 per cent quartz, 25 per cent calcite, 30 per cent hypersthene, and 30 per cent ferroaugite. The chemical compositions of the pyroxenes are given below:

Hypersthene

	Wt. %	*Mol. props.*	*Metal atoms per 6 oxygens*
SiO_2	50·1	833	2·075
Al_2O_3	0·2	2	0·009
Fe_2O_3	2·4	15	0·075
FeO	31·8	443	1·103
MnO	0·37	5	0·810
MgO	13·1	325	0·012 → 2·112
CaO	2·2	39	0·097
Na_2O	0·08	1	0·005
K_2O	0·03	—	0·001
	100·3		

Ferroaugite

	Wt. %			
	Individual analyses	*Average*	*Mol. props.*	*Metal atoms per 6 oxygens*
SiO_2	—	51·7	859	1·987 } 2·001
Al_2O_3	—	0·3	3	0·014 }
Fe_2O_3	—	2·0	12	0·056
FeO	15·15	15·2	212	0·491
	15·30			
MnO	0·18	0·18	3	0·006
	0·19			
MgO	9·75	9·6	239	0·553 } 1·981
	9·55			
CaO	21·09	21·0	374	0·865
	20·97			
Na_2O	0·12	0·12	2	0·009
	0·13			
K_2O	0·02	0·03	—	0·001
	0·06			
		100·1		

Bl-6. A thin-bedded phase of the silicate iron formation, composed of 35 per cent quartz, 30 per cent ferrohypersthene, 25 per cent ferroaugite, 10 per cent calcite, and small amounts of graphite. Some layers consist of only one mineral, others are composed of the different minerals in varying proportions. The chemical compositions of the pyroxenes are given below:

Ferrohypersthene

	Wt. %			
	Individual analyses	*Average*	*Mol. props.*	*Metal atoms per 6 oxygens*
SiO_2	—	48·8	813	1·980 } 1·990
Al_2O_3	—	0·2	2	0·010 }
Fe_2O_3	—	2·3	14	0·068
FeO	36·36	36·6	509	1·240
	36·62			
MnO	—	1·14	16	0·039
MgO	8·94	9·0	224	0·546
	9·03			
CaO	1·68	1·7	30	0·073 } 2·016
	1·81			
Na_2O	0·59	0·61	10	0·049
	0·62			
K_2O	0·03	0·02	—	0·001
	0·02			
		100·3		

Ferroaugite

	Wt. %			
	Individual analyses	*Average*	*Mol. props.*	*Metal atoms per 6 oxygens*
SiO_2	—	50·5	839	1·970 } 1·979
Al_2O_3	—	0·2	2	0·009 }
Fe_2O_3	—	1·9	12	0·056
FeO	16·90 17·18	17·1	238	0·559
MnO	0·56 0·67	0·57	8	0·019
MgO	7·61 7·90	7·7	191	0·448 } 2·016
CaO	21·04 21·30	21·2	378	0·887
Na_2O	0·61 0·68	0·64	10	0·046
K_2O	0·02 0·05	0·03	—	0·001
		99·8		

B1-21. A medium-grained granoblastic rock with indistinct banding composed of about 35 per cent ferrohypersthene, 25 per cent ferroaugite, 30 per cent quartz, and 10 per cent calcite. The compositions of the pyroxenes are given below:

Ferrohypersthene

	Wt. %			
	Individual analyses	*Average*	*Mol. props.*	*Metal atoms per 6 oxygens*
SiO_2	—	49·2	818	1·977 } 1·991
Al_2O_3	—	0·3	3	0·014 }
Fe_2O_3	—	3·1	19	0·092
FeO	36·27 35·72	35·9	500	1·211
MnO	0·14 0·15	0·14	2	0·588
MgO	9·90 9·78	9·8	243	0·005 } 1·97
CaO	1·85 1·63	1·7	30	0·073
Na_2O	0·06 0·08	0·07	1	0·005
K_2O	0·02 0·02	0·02	—	—
		100·2		

Ferroaugite

	Wt. %		Mol. props.	Metal atoms per 6 oxygens	
	Individual analyses	Average			
SiO_2	—	50·8	845	1·993	2·000
Al_2O_3	—	0·3	3	0·014 (0·007 / 0·007)	
Fe_2O_3	—	1·9	12	0·056	1·973
FeO	17·41, 17·48	17·4	242	0·570	
MnO	—	0·06	1	0·002	
MgO	—	7·7	191	0·450	
CaO	—	21·0	374	0·882	
Na_2O	—	0·61	1	0·005	
K_2O	—	0·05	125	0·001	
		99·9			

A-50. Magnetite–silicate iron formation. A heavy, dark-coloured homogeneous rock composed of 50 per cent quartz, 25 per cent magnetite, 20 per cent aegirine–hedenbergite, and 15 per cent ferrohypersthene. Calcite is not present. Cummingtonite is present in small amounts in another similar thin section studied. The rock is quite coarse grained and is easily crushed up.

Ferrohypersthene

	Wt. %		Mol. props.	Metal atoms per 6 oxygens	
	Individual analyses	Average			
SiO_2	—	47·1	784	1·987	1·988
Al_2O_3	—	0·2	2	0·001	
Fe_2O_3	—	4·1	26	0·131	1·953
FeO	40·21, 40·15	40·1	558	1·292	
MnO	3·08, 3·12	3·1	94	0·238	
MgO	3·58, 3·30	3·4	84	0·213	
CaO	1·62, 1·65	1·6	29	0·073	
Na_2O	0·11, 0·10	0·10	1	0·005	
K_2O	0·03, 0·03	0·03	—	0·001	
		99·7			

Aegirine–hedenbergite

	Wt. %			
	Individual analyses	*Average*	*Mol. props.*	*Metal atoms per 6 oxygens*
SiO_2	—	49·7	827	2·001
Al_2O_3	—	0·1	1	0·005
Fe_2O_3	—	9·6	60	0·290
FeO	17·80 18·06	17·9	249	0·603
MnO	—	2·03	28	0·068
MgO	1·75 1·90	1·8	45	0·109
CaO	15·25 15·46	15·3	273	0·661
Na_2O	2·95 3·05	3·0	47	0·227
K_2O	—	0·03	—	0·001
		100·4		

1·963

Si-4. A medium-grained massive rock similar to B1-1, composed of 85 per cent hypersthene, 15 per cent calcite, and 10 per cent quartz. The hypersthene contains 40·4 per cent FeO by weight.

A-8. A medium-grained homogeneous granoblastic rock composed of 55 per cent quartz, 25 per cent ferrohypersthene, 10 per cent ferroaugite, 5 per cent cummingtonite, 5 per cent calcite, and small amounts of magnetite. All the minerals are scattered fairly evenly in the rock. Calcite and cummingtonite generally are separated from each other by hypersthene. The hypersthene contains 39·1 per cent FeO.

A-30. A coarse-grained rock which in hand specimens appears to consist only of large crystals of hypersthene. A thin section shows that ferrohypersthene is intermixed with 10 per cent cummingtonite, 5 per cent calcite, and 5 per cent quartz. The ferrohypersthene contains 40·5 per cent FeO.

A-31. Magnetite–arfvedsonite iron formation. The rock is composed of bands of coarse crystals of bluish amphibole in a fine-grained mixture of quartz and magnetite. The amphibole is an arfvedsonite with the following pleochroic formula: X = yellow, Y = green, Z = blue; $2V$ is 40° and negative. The chemical compositions are given below:

Arfvedsonite

	Wt. %	*Mol. props.*	*Metal atoms per 6 oxygens*
SiO_2	54·8	910	8·00
Al_2O_3	3·7	37	0·47
Fe_2O_3	10·4	65	1·14
FeO	8·6	120	1·05
MnO	9·2	30	0·26
MgO	1·9	228	2·00
CaO	2·1	34	0·30
Na_2O	4·7	76	1·34
K_2O	1·7	18	0·32
	97·1		

4·92

1·96

B-9. A light green, homogeneous silicate rock composed of granular quartz and ferroaugite mixed with needles of cummingtonite. The mineral composition consists of 35 per cent ferroaugite, 55 per cent quartz, and 10 per cent cummingtonite. An analysis of the ferroaugite and a partial analysis of the cummingtonite is given below.

Cummingtonite

	Wt. %	*Mol. props.*	*Metal atoms per 7 oxygens (16 oxygens are assumed to be taken up in SiO_2 and Al_2O_3)*	
SiO_2	n.d.	—	—	
Al_2O_3	n.d.	—	—	
Fe_2O_3	2·5	16	0·30	6·95
FeO	28·6	398	3·69	
MnO	0·23	3	0·03	
MgO	9·9	246	2·28	
CaO	3·8	68	0·63	
Na_2O	0·10	2	0·02	
K_2O	0·03	—	—	
	97·9			

Ferroaugite

	Wt. %			*Metal atoms per 6 oxygens*	
	Individual analyses	*Average*	*Mol. props.*		
SiO_2	—	50·1	835	1·976	1·990
Al_2O_3	—	0·3	3	0·014	
Fe_2O_3	—	2·3	14	0·006	2·099
FeO	16·69 16·95	16·8	233	0·552	
MnO	0·34 0·37	0·35	1	0·002	
MgO	8·35 8·17	8·2	204	0·483	
CaO	20·61 20·98	20·8	372	0·881	
Na_2O	0·15	0·17	3	0·114	
K_2O	0·03 0·03	0·03	—	0·001	
		99·0			

B-18. A rock similar to B-9 and from the same locality. The cummingtonite content is higher (about 30 per cent).

Ferroaugite

	Wt. %			
	Individual analyses	*Average*	*Mol. props.*	*Metal atoms per 6 oxygens*
SiO_2	—	50·7	844	1·980 } 1·996
Al_2O_3	—	0·3	3	0·014 }
Fe_2O_3	—	2·8	18	0·084
FeO	17·06 17·17	17·1	238	0·558
MnO	0·15 0·16	0·15	2	0·005
MgO	8·02 8·21	8·1	201	0·472 } 1·983
CaO	20·30 20·54	20·4	364	0·854
Na_2O	0·15 0·14	0·15	2	0·009
K_2O	0·03 0·02	0·03	—	0·001
		99·7		

Cummingtonite

	Wt. %	*Mol. props.*	*Metal atoms per 23 oxygens*
SiO_2	51·5	857	7·92 } 7·98
Al_2O_3	0·3	3	0·06 }
Fe_2O_3	3·5	22	0·41
FeO	31·2	434	4·01
MnO	0·23	3	0·03
MgO	9·1	226	2·09 } 6·90
CaO	1·9	34	0·31
Na_2O	0·16	2	0·04
K_2O	0·03	—	0·01
	97·9		

R-7. A green massive medium-grained granoblastic rock composed of 45 per cent diopside, 15 per cent dark green amphibole, and 35 per cent quartz.

Diopside

	Wt. %	*Mol. props.*	*Metal atoms per 6 oxygens*
SiO_2	54·6	908	1·991 } 2·000
Al_2O_3	0·7	7	0·031 { 0·009 } 0·022
Fe_2O_3	2·7	17	0·075
FeO	5·7	79	0·173
MnO	0·03	—	0·001
MgO	14·8	368	0·808 } 1·958
CaO	22·1	394	0·865
Na_2O	0·17	3	0·013
K_2O	0·03	—	0·001
	100·8		

Hornblende

	Wt. %	*Mol. props.*	*Metal atoms per 23 oxygens*	
SiO_2	54·2	900	7·77	
Al_2O_3	5·0	49	0·85 (0·23 + 0·62)	8·00
Fe_2O_3	0·3	2	0·03	
FeO	7·7	107	0·92	4·76
MnO	0·03	—	0·01	
MgO	14·8	368	3·18	
CaO	13·0	232	2·00	
Na_2O	0·14	2	0·03	2·06
K_2O	0·18	2	0·03	
	96·3			

APPENDIX C

Specimens of Silicate Iron Formations of the Northern Area

H-3. Magnetite–silicate iron formation. A medium-grained banded rock consisting of 55 per cent quartz, 15 per cent magnetite, 15 per cent ferroaugite, and 10 per cent cummingtonite.

Cummingtonite

	Wt. %	*Mol. props.*	*Metal atoms per 6 oxygens*	
SiO_2	53·3	887	7·95	7·99
Al_2O_3	0·2	2	0·04	
Fe_2O_3	2·5	16	0·29	
FeO	26·3	365	3·27	
MnO	4·5	64	0·57	
MgO	11·2	279	2·50	6·90
CaO	1·6	29	0·26	
Na_2O	0·09	1	0·01	
K_2O	0·02	—	—	
	99·7			

Ferroaugite

	Wt. %	*Mol. props.*	*Metal atoms per 6 oxygens*	
SiO_2	51·1	850	1·984	1·993
Al_2O_3	0·2	2	0·009	
Fe_2O_3	3·7	23	0·107	
FeO	13·5	188	0·439	
MnO	2·54	36	0·084	1·992
MgO	8·9	221	0·516	
CaO	18·9	338	0·789	
Na_2O	0·71	12	0·056	
K_2O	0·03	—	0·001	
	99·5			

H-4. A coarse-grained, dark green, massive rock consisting of 50 per cent ferrohypersthene, 30 per cent ferroaugite, 10 per cent calcite, and 10 per cent quartz.

Ferrohypersthene

	Wt. %				
	Individual analyses	*Average*	*Mol. props.*	*Metal atoms per 6 oxygens*	
SiO_2 . .	—	47·8	795	1·978	1·988
Al_2O_3 . .	—	0·2	2	0·010	
Fe_2O_3 . .	—	2·3	14	0·070	
FeO . .	40·67	40·4	562	1·398	
	40·30				
MnO . .	0·50	0·52	7	0·017	
	0·55				
MgO . .	6·68	6·67	166	0·413	1·981
	6·66				
CaO . .	1·75	1·74	31	0·077	
	1·73				
Na_2O . .	—	0·09	1	0·005	
K_2O . .	—	0·02	—	0·001	
	99·7				

Ferroaugite

	Wt. %				
	Individual analyses	*Average*	*Mol. props.*	*Metal atoms per 6 oxygens*	
SiO_2 . .	—	51·0	849	2·009	
Al_2O_3 . .	—	0·2	2	0·008	
Fe_2O_3 . .	—	2·7	17	0·080	
FeO . .	20·33	19·9	277	0·657	
	19·73				
MnO . .	0·26	0·26	4	0·009	
	0·26				
MgO . .	5·96	6·0	148	0·350	1·943
	6·00				
CaO . .	19·21	19·3	344	0·814	
	19·44				
Na_2O . .	—	0·28	5	0·024	
K_2O . .	—	0·03	—	0·001	
		99·7			

H-7. The rock consists of large rosettes of cummingtonite needles mixed with coarse-grained ferroaugite and ferrohypersthene and small amounts of magnetite, calcite, and quartz. Magnetite grains sometimes are concentrated in the centres of cummingtonite rosettes. The hand specimen represents a silicate-rich layer in banded silicate iron formation.

Ferroaugite

	Wt. %				
	Individual analyses	*Average*	*Mol. props.*	*Metal atoms per 6 oxygens*	
SiO_2	50·9	50·9	847	2·009	
Al_2O_3	—	0·4	4	0·019	
Fe_2O_3	—	2·8	18	0·085	
FeO	19·85	19·6	273	0·643	
	19·43				
MnO	0·73	0·74	10	0·024	
	0·74				
MgO	5·75	5·8	144	0·340	1·954
	5·91				
CaO	19·46	19·5	348	0·823	
	19·51				
Na_2O	0·25	0·27	4	0·019	
	0·29				
K_2O	0·03	0·03	—	0·001	
	0·03				
		100·0			

Cummingtonite

	Wt. %				
	Individual analyses	*Average*	*Mol. props.*	*Metal atoms per 23 oxygens*	
SiO_2	—	50·9	847	7·93	
Al_2O_3	—	0·4	4	0·06	
Fe_2O_3	—	1·3	8	0·15	
FeO	35·51	35·4	494	4·62	
	35·23				
MnO	1·25	1·25	18	0·17	
	1·25				7·02
MgO	7·61	7·7	191	1·79	
	7·80				
CaO	1·27	1·3	23	0·22	
	1·36				
Na_2O	0·10	0·11	1	0·01	
	0·12				
K_2O	0·03	0·03	—	—	
	0·03				
		98·4			

Ferrohypersthene

	Wt. %			
	Individual analyses	*Average*	*Mol. props.*	*Metal atoms per 6 oxygens*
SiO_2	—	47·8	795	1·987 } 1·997
Al_2O_3	—	0·2	2	0·010 }
Fe_2O_3	—	1·9	12	0·060
FeO	39·43 39·71	39·5	549	1·372
MnO	1·53 1·50	1·51	21	0·052
MgO	7·15 7·07	7·1	176	0·440 } 1·983
CaO	1·21 1·26	1·2	22	0·055
Na_2O	0·09 0·10	0·09	1	0·003
K_2O	0·03 0·03	0·03	—	0·001
		99·3		

H-9. A medium-grained, dark greyish-green rock. In thin sections the rock exhibits a distinct micro-banding. In places the bands are monomineralic layers consisting of calcite, hypersthene, quartz, or cummingtonite. In places the different mineral constituents are mixed in varying proportions. Cummingtonite and calcite layers are generally separated from each other by hypersthene. The mineral composition of one thin section consists of 10 per cent ferroaugite, 10 per cent quartz, 20 per cent cummingtonite, 45 per cent ferrohypersthene, and 15 per cent calcite.

Ferrohypersthene

	Wt. %	*Mol. props.*	*Metal atoms per 6 oxygens*
SiO_2	48·4	807	1·994
Al_2O_3	0·2	2	0·010
Fe_2O_3	1·7	11	0·133
FeO	38·8	539	1·332
MnO	1·61	23	0·056 } 1·981
MgO	7·6	189	0·467
CaO	1·3	23	0·057
Na_2O	0·07	1	0·005
K_2O	0·02	—	—
	99·7		

Ferroaugite

	Wt.%	*Mol. props.*	*Metal atoms per 6 oxygens*	
SiO_2	50·4	838	1·996	
Al_2O_3	0·2	2	0·010	
Fe_2O_3	2·1	13	0·062	
FeO	19·4	270	0·643	
MnO	0·75	11	0·026	1·978
MgO	6·6	164	0·391	
CaO	19·6	349	0·831	
Na_2O	0·20	3	0·014	
K_2O	0·03	—	0·001	
	99·3			

Cummingtonite

	Wt.%	*Mol. props.*	*Metal atoms per 23 oxygens*	
SiO_2	51·7	859	7·98	8·00
Al_2O_3	0·1	1	0·02	
Fe_2O_3	1·2	8	0·15	
FeO	35·2	490	4·56	
MnO	1·25	18	0·17	6·93
MgO	8·0	199	1·85	
CaO	1·1	20	0·19	
Na_2O	0·03	—	—	
	98·7			

F-73. Mineral specimens are taken from reaction zone between quartz–magnetite iron formation and dolomite. The reaction zone consists of 6 in. of pure magnetite, 7–9 in. of hornblende, and 5 in. of diopside. In a narrow zone hornblende and diopside are intermixed, hornblende occurring as unreplaced remnants in a diopside matrix.

Hornblende

	Wt.%		*Mol. props.*	*Metal atoms per 23 oxygens*		
	Individual analyses	*Average*				
SiO_2	—	47·2	784	6·83		8·00
Al_2O_3	—	8·9	87	1·52	1·17 / 0·35	
Fe_2O_3	—	6·0	38	0·66		
FeO	9·31 9·28	9·3	129	1·12		5·03
MnO	0·16 0·15	0·15	2	0·02		
MgO	13·31 13·31	13·3	330	2·88		
CaO	11·83 11·33	11·6	208	1·81		2·26
Na_2O	—	1·0	16	0·28		
K_2O	—	0·90	10	0·17		
		98·1				

Diopside

	Wt. %		Mol. props.	Metal atoms per 6 oxygens	
	Individual analyses	Average			
SiO_2	—	53·2	884	1·973	2·000
Al_2O_3	—	0·8	8	0·035 (0·027 + 0·008)	
Fe_2O_3	—	2·5	16	0·071	1·991
FeO	4·57 4·60	4·6	64	0·143	
MnO	0·14 0·14	0·14	2	0·005	
MgO	14·88 15·01	14·9	369	0·824	
CaO	22·47 22·80	22·6	403	0·899	
Na_2O	0·58 0·55	0·57	9	0·040	
K_2O	0·04 0·03	0·04	—	0·001	
		99·3			

F-1. Anthophyllite–hornblende rock probably representing an altered ultramafic intrusive. The rock consists mainly of a mass of subhedral prismatic grains of anthophyllite without any discernible preferred orientation. Clusters of hornblende are present in parts of the hand specimen. The two amphiboles are sometimes intergrown in one grain. Biotite and minor garnet also are present in the hand specimen.

Anthophyllite

	Wt. %	Mol. props.	Metal atoms per 23 oxygens	
SiO_2	52·0	866	7·33	8·00
Al_2O_3	7·1	70	1·19 (0·67 + 0·52)	
Fe_2O_3	3·0	15	0·25	6·95
FeO	15·5	216	1·83	
MnO	0·16	2	0·02	
MgO	19·7	489	4·14	
CaO	1·0	18	0·15	
Na_2O	0·06	1	0·02	
K_2O	0·12	1	0·02	
	98·7			

Hornblende

	Wt. %	*Mol. props.*	*Metal atoms per 23 oxygens*
SiO_2 . . .	48·3	804	6·72 } 8·00 (1·28 + 1·01)
Al_2O_3 . . .	14·0	137	2·29
Fe_2O_3 . . .	3·9	24	0·39 } 5·61
FeO . . .	8·8	123	1·03
MnO . . .	0·14	2	0·02
MgO . . .	15·2	378	3·16 } 6·99
CaO . . .	8·4	150	1·25 } 1·38
Na_2O . . .	0·30	5	0·08
K_2O . . .	0·30	3	0·05
	99·3		

REFERENCES

BOWEN, N. L., & TUTTLE, O. F., 1949. The system MgO–SiO_2–H_2O. *Bull. geol. Soc. Amer.* **60**, 439–60.

BOYD, F. R., 1959. Hydrothermal investigations of amphiboles. In *Researches in geochemistry*, Abelson ed. New York: Wiley & Co., 377–96.

CARSTENS, C. W., 1924. Zur Frage der Genesis der Eulysitgesteine. *Geol. Fören. Stockh. Förh.* **46**, 248–52.

DUFFELL, S., & ROACH, R. A., 1959. Mount Wright, Quebec–Newfoundland. *Geol. Survey Can. Map*, **6-1959**.

ECKERMANN, H. VON. The rocks and contact minerals of the Mansjo Mountain. *Geol. Fören. Stockh. Förh.* **44**, 203–410.

ELLIS, A. J., 1959. The solubility of carbon dioxide in water at high temperatures. *Amer. J. Sci.* **257**, 217–34.

ESKOLA, P., 1950. Paragenesis of cummingtonite and hornblende from Muuruvesi, Finland. *Amer. Min.* **35**, 728–34.

FLASCHEN, S. S., & OSBORN, E. F., 1957. Studies of the system iron oxide–silica–water at low oxygen partial pressures. *Econ. Geol.* **52**, 923–43.

FYFE, W. S., TURNER, F. J., & VERHOOGEN, J., 1958. Metamorphic reactions and metamorphic facies. *Mem. geol. Soc. Amer.* **73**.

GEIJER, P., 1925. Eulysitic iron ores in northern Sweden. *Sverig. Geol. Unders. Afh.* ser. C., No. **324**.

GOLDSMITH, J. R., 1959. Some aspects of the geochemistry of carbonates. In *Researches in geochemistry*, Abelson ed. New York: Wiley & Co., 336–58.

GROSS, G. A., 1955. *The metamorphic rocks of the Mount Wright and Matonipi Lake areas of Quebec.* Ph.D. thesis, Univ. of Wisconsin.

GROUT, F. F., 1919. The nature and origin of the Biwabik iron-bearing formation of the Mdsabi Range, Minnesota. *Econ. Geol.* **14**, 452–64.

—— & BRODERICK, T. M., 1919. The magnetite deposits of the eastern Mesabi Range, Minnesota. *Bull. Minn. geol. Surv.* **17**.

GRUNER, J. W., 1946. The mineralogy and geology of the taconites and iron ores of the Mesabi Range, Minnesota. *Iron Range Resources and Rehabilitation*, St. Paul, Minn.

HARRY, W. T., 1950. Aluminium replacing silicon in some silicate lattices. *Miner. Mag.* **29**, 142–9.

HISE, C. R. VAN, & LEITH, C. K., 1911. The geology of the Lake Superior region. *Mon. U.S. geol. Surv.* **52**.

HUBER, N. K., & GARRELS, R. M., 1953. Relation of pH and oxidation potential to sedimentary iron mineral formation. *Econ. Geol.* **48**, 337–57.

JAMES, H. L., 1954. Sedimentary facies of iron formation. *Econ. Geol.* **49**, 235–85.

—— 1956. Zones of regional metamorphism in the Precambrian of northern Michigan. *Bull. geol. Soc. Amer.* **66**, 1455–88.

KRANCK, S. H., 1959. *Chemical petrology of metamorphic iron formations and associated rocks in the Mount Reed area, in northern Quebec.* Ph.D. thesis, Massachusetts Institute of Technology.

KUNITZ, W., 1930. Die Isomorphieverhältnisse in der Hornblende Gruppe. *N. Jb. Min. Geol. Paläont.* **60**, Abt. A, 171–250.

LINDROTH, G. T., 1926. Bidrag till fragan om kalk-skarnjarn-malmernas genesis. *Geol. Fören. Stockh. Förh.* **48**, 357–410.

MILES, K. R., 1943. Grunerite in western Australia. *Amer. Min.* **28**, 25–38.

MILTON, C., & EUGSTER, H. P., 1959. Mineral assemblages of the Green River Formation. In *Researches in geochemistry*, Abelson ed. New York: Wiley & Co., 118–50.

MUELLER, R. F., 1958. Chemical petrology of a metamorphosed iron formation (abstract). *Bull. geol. Soc. Amer.* **69**.

MUIR, I. D., & TILLEY, C. E., 1958. The compositions of coexisting pyroxenes in metamorphic assemblages. *Geol. Mag. Lond.* **95**, 336–58.

MURPHY, D. L., 1959. Preliminary report on Mount Wright area. *Dept. Min. Quebec.*

PALMGREN, J., 1916. Die Eulysite von Sodermanland. *Bull. geol. Inst. Univ. Upsala*, **14**, 108–225.

PERRAULT, G., 1955. *Geology of the western margin of the Labrador trough.* Ph.D. thesis, Univ. of Toronto.

RABBITT, J. C., 1948. A new study of the anthophyllite series. *Amer. Min.* **33**, 263–323.

RAMBERG, H., 1952*a*. Chemical bonds and the distribution of cations in silicates. *J. Geol.* **60**, 331–56.

—— 1952*b*. *The origin of metamorphic and metasomatic rocks.* Univ. of Chicago Press.

RICHARZ, S., 1927. Grunerite rocks of the Lake Superior region and their origin. *J. Geol.* **35**, 690–708.

—— 1930. A peculiar blue-green amphibole from the metamorphosed iron formation of the eastern Mesabi Range, Minnesota. *Amer. Min.* **15**, 65–69.

SHAPIRO, L., & BRANNOCK, W. W., 1956. Rapid analysis of silicate rocks. *Bull. U.S. geol. Surv.* **1036C**.

SMITH, J. R., 1957. Reconnaissance in the system FeO–Fe_2O_3–SiO_2–H_2O. In Annual report of the Director, Geophysical Laboratory, for 1956–7, *Yearb. Carneg. Instn.* **56**, 230–1.

SUNDIUS, N., 1933. Über die Mischungslücken zwischen Anthophyllite–Gedrit, Cummingtonit-Grunerit, und Tremolit Actinolith. *Tscherm. Mitt.* **43**, 422–40.

—— 1946. The classification of the hornblendes and the solid solution relations in the amphibole group. *Sverig Geol. Unders. Afh.* **40**, No. 4, 1–36.

THOMPSON, J. B., 1959. Local equilibrium in metasomatic processes. In *Researches in geochemistry*, Abelson ed. New York: Wiley & Co., 427–57.

TILLEY, C. E., 1936. Eulysites from Ross-shire. *Miner. Mag.* **24**, 331–42.

TURNER, F. J., & VERHOOGEN, J., 1951. *Igneous and metamorphic petrology.* New York: McGraw-Hill.

WEEKS, W. F., 1956. A thermochemical study of equilibrium relations during metamorphism of siliceous carbonate rocks. *J. Geol.* **64**, 245–70.

WULFING, E. A., 1891. *Beiträge zur Kenntnis der Pyroxenefamilie in der chemischer und optischer Beziehung.* Heidelberg.

YODER, H. S., 1952. The MgO–Al_2O_3–SiO_2–H_2O system and the related metamorphic facies. *Amer. J. Sci.*, Bowen Volume, 569–627.

—— 1955. The role of water in metamorphism. In *Crust of the Earth, Geol. Soc. Amer. Spec. Pap.* **62**, 505–24.

—— 1957. Isograd problems in metamorphosed iron-rich sediments. In Annual report of the Director, Geophysical Laboratory, for 1956–7, *Yearb. Carneg. Instn.* **56**, 232–7.

Basic and Ultrabasic Xenoliths from Volcanic Rocks of New South Wales

By H. G. WILSHIRE *and* R. A. BINNS

Department of Geology and Geophysics, University of Sydney,[1] *and Department of Mineralogy and Petrology, Cambridge*

ABSTRACT

Basic and ultrabasic xenoliths found in Tertiary basaltic and lamprophyric volcanic rocks from New South Wales are predominantly peridotites, but mineralogical gradations between these and associated pyroxenites and gabbros also occur. The xenoliths are unstable in their host rocks and show marked marginal reactions. Evidence of xenocrystal material derived from such xenoliths has been observed in 40 per cent of other basaltic rocks in the New South Wales Tertiary volcanic province. A review of evidence from New South Wales and that available in the literature favours the hypothesis that such xenoliths represent portions of the earth's mantle incorporated in magmas originating from within that zone. Analyses of xenoliths and host rocks, and seven new analyses of clinopyroxenes from xenoliths are presented.

INTRODUCTION

PLATEAU basalts and minor intrusions belonging to the Tertiary alkali olivine basalt province of New South Wales commonly contain basic and ultrabasic xenoliths. These are of a wide range of rock types including various types of peridotite, pyroxenites, hornblende–biotite pyroxenite, glimmerite, hornblendite, norite, and gabbro. In most cases peridotite is the dominant rock type. A number of occurrences described here have been dealt with in previous publications, but are apparently unknown outside of Australia. This, as well as the unusually well-preserved reactions between host rocks and xenoliths, stimulated this study. The present study has not involved a systematic field search for xenoliths and as such is by no means an exhaustive study of New South Wales occurrences.

PREVIOUS WORK

Although there are many brief references to the occurrence of basic xenoliths in New South Wales volcanic rocks, only a few detailed descriptions are available. Benson (1910) and Osborne (1920) have given detailed descriptions of basic and ultrabasic xenoliths in massive basalts which are associated with some diatremes near Sydney. Süssmilch (1905) gave brief descriptions of peridotite xenoliths from a dyke near Kiama, and Jensen (1907) noted a remarkable xenolithic sill in the Nandewar Mountains. Brown (1929) recorded gabbro and other xenoliths from a dyke near Moruya, and Harvey & Joplin (1940) described biotite and pyroxene xenocrysts and peridotite xenoliths from a leucite lamprophyre neck near Murrumburrah.

[1] *Present address*: Dept. of Geophysics, The Australian National University, Canberra, A.C.T.

[Journal of Petrology, Vol. 2, Part 2, pp. 185–208, 1961]

0233.2

OCCURRENCES OF XENOLITHS

Peridotite

The following occurrences of peridotite xenoliths in basalt and lamprophyre dykes, and in basalt flows have been studied in detail.

1. *Dyke No. 13* (Jaquet *et al.*, 1905); No. 46 (Harper, 1915), 2 miles south of Kiama. The dyke is a monchiquite 3 to 5 ft wide intruded into the Permian Westley Park tuffs and overlying Bombo latite flow. It has well-developed joints parallel to the dyke walls filled with fibrous green clay and carbonates. Well-rounded to sub-rounded peridotite xenoliths up to 4 in. in diameter and xenocrysts derived from these are abundant in all exposures of the dyke, while angular fragments of the Westley Park tuffs are locally abundant. The larger xenoliths tend to be concentrated in the centre of the dyke.

2. *The MacAlister Trigonometrical Survey Station*, 4 miles east of Taralga, is situated on a basalt flow which is at least 50 ft thick. About the lower half of the exposure contains abundant ovoid olivine xenoliths from ¼ to 2 in. in maximum dimension. These are absent from the upper half, and while it is possible that the outcrops represent two flows, it is more likely that only one flow is present and the xenoliths settled to the bottom following extrusion (see Lausen, 1927). Xenoliths of the underlying sandstone also occur and have reacted strongly with the magma.

3. *Nandewar Mountains.* Lamprophyre sill 2 to 3 ft thick intruded into Permo-Carboniferous sandstones (Jensen, 1907). Rounded peridotite xenoliths and xenocrysts up to 2 in. long derived from the xenoliths make up about 60 per cent of the sill, which is one of many feeders to the alkaline lavas and plugs comprising the Nandewar Mountains. Rounded books of biotite (polymorph 2 M) up to 2 in. long are fairly common, but nothing of comparable size was found in xenoliths. The occurrence is noteworthy for the considerable diversity in grain size and modes exhibited by the xenoliths.

4. *Armidale.* Basalt flow ¼ mile north of the New England University. A small quarry in this flow, which is one of many flows carrying peridotite xenoliths in the area (B. Chappell, personal communication), has revealed an abundance of angular to rounded peridotite xenoliths up to 9 in. long which show striking marginal reactions to be described below.

5. *The Drogheda Trigonometrical Survey Station*, about 15 miles south-east of Oberon, is situated on a thin basalt flow which is crowded with peridotite xenoliths. The xenoliths range up to 6 in. in diameter and are ovoid, tabular with rounded edges, or sharply angular. No banding is apparent in the xenoliths, but there is a large range in grain size and occasionally a xenolith shows some fissility. Another flow near Ginkin, 4 miles to the north-east, contains peridotite xenoliths which exhibit a more pronounced fissility.

In several localities peridotite xenoliths are closely associated with pyroxenite and gabbro xenoliths. Two such occurrences are the Dundas (Benson, 1910) and Norton's Basin (Osborne, 1920) breccia pipes. These are similar to many

diatremes of the Western Coalfield (Carne, 1908), and probably more of these than are listed in Table 1 are xenolithic but they have not been studied in detail. The best-preserved xenoliths occur in massive basalts associated with the breccia, but identical ones are also found in the breccia. With the exception of well-bedded fragments such as shales, many of the large fragments of the breccia, including sandstone, basalt, granite, and others, are well-rounded. The rounding is probably due largely to attrition (see Powers, 1915), which likewise appears to be the cause of rounding of ultrabasic xenoliths though this is often attributed to magmatic corrosion.

Other types of xenoliths

One occurrence (*dyke No. 36*, Jaquet *et al.*, 1905; No. 59, Harper, 1915) was studied in which hornblende–biotite pyroxenite, hornblendite, and glimmerite are the dominant xenoliths. The dyke is one of five monchiquite dykes exposed in Bombo Quarry, 1 mile north of Kiama. The dyke ranges from a few inches to 2 ft in width and varies considerably in fabric from point to point. Long stretches are free of xenoliths and here the dyke rock may be either aphanitic or markedly porphyritic. Vesicle trains parallel to the dyke walls are often present where xenoliths are absent. Locally the xenoliths make up 60 per cent or more of the volume of the dyke and may be scattered from margin to margin or be concentrated in the centre. The xenoliths, excepting schistose ones, are generally well-rounded and are up to 1 ft in diameter. Although few of the xenoliths approximate peridotite in composition, the xenoliths described by Süssmilch (1905) from the Bombo Quarry are mainly peridotites identical with those of other occurrences. Unfortunately, Süssmilch's specimens were not found in place, and considerable deepening of the quarries has exposed five monchiquite dykes, any of which might conceivably have been the source. Only the dyke described here and one immediately south of it contain xenoliths in the present exposures, and none of these are peridotites similar to those described by Süssmilch. The other three dykes are free from macroscopically visible xenoliths, but exposures are no larger than barren areas of the xenolithic dykes. If the dyke here described was the source of peridotite xenoliths, it is significant that so small a change in elevation has produced so drastic a change in type of xenoliths. It is further noteworthy that peridotite, hornblende pyroxenite, and biotite peridotite xenoliths occur side by side in a number of other occurrences, and that peridotite xenocrystal debris is present in the dyke here described.

Miscellaneous occurrences from which specimens were obtained but which were not studied in the field, include a monchiquite dyke in Bulli Colliery (Harper, 1915) which contains tabular peridotite xenoliths up to 1½ in. long, large oxyhornblende xenocrysts, and small hornblende pyroxenite and green spinel-bearing gabbro xenoliths; a basalt dyke at Sherbrook containing xenoliths nearly identical with those from Bulli; and the leucite lamprophyre of Murrumburrah (Harvey & Joplin, 1940), which contains peridotite xenoliths,

TABLE 1

Tabulated occurrences of basic and ultrabasic xenoliths and derived xenocrysts

Location (listed alphabetically by county (Co.) and parish (Ph.))	*Host rock*	*Xenoliths*			*Xenocrysts*						
		1	2	3	4	5	6	7	8	9	10
		Peridotite	*Pyroxenite*	*Gabbro*	*Deformed olivine*	*Clino-pyroxene*	*Ortho-pyroxene or granular ol.*	*Spinel*	*Plagioclase*	*Hornblende*	*Biotite*
Co. Buller											
Ph. Coutts, Portion 24	Olivine basalt				×						
Co. Camden											
Ph. Bargo, Myrtle Crk., Bargo Rd.	Lamprophyre				×	×	×	×			
Ph. Broughton, 1 m. S. Gerringong on coast	Monchiquite dyke	×			×	×	×	×			
Ph. Couridjah, Thirlmere	Olivine basalt				×	×	×	×			
Ph. Weromba, The Oaks	Olivine basalt dyke				×	×	×				
Ph. Wonona, Rixons Pass, sill No. 1 (Harper, 1915)	Olivine basalt sill				×		×	×			
Co. Cook											
Ph. Barton, Green Hill*	Olivine basalt neck			×							
Ph. Barton, Murrays Mt.*	Olivine basalt neck				×	×	×	×	×	(and apatite)	
Co. Cowper											
Capitan, Byrock	Leucite basalt neck			×							
Co. Cumberland											
Ph. Appin, 2 m. W. Appin	Olivine basalt dyke				×	?					
Ph. Minto, ½ m. from Minto	Olivine basalt	×			×	×	×	×			
Ph. Southend, 5½ m. from Bulli on Appin Rd.	Olivine basalt dyke	×		×	?	×			×	×	
Ph. Southend, Dyke 70, Cataract R.	Olivine basalt	×			×	×	×	×			
Ph. Southend, Dyke 53, Crk. near Bulli no. 4 Colliery	Olivine basalt	×			×	×	×	×			
Ph. Southend, Stanwell Park	Dolerite sill	×	×		×	×	×				
Co. Dampier											
Ph. Noorooma, between Tilba and Dynums Crk.	Olivine basalt				×	×					×
Co. Durham											
Ph. Balmoral, Portion 110, Muswellbrook	Monchiquite plug				×	?	×				
Ph. Rowan, Portion 12, Muswellbrook	Monchiquite plug				×	?	×				
Co. Gloucester											
Ph. Knowla, Rawdon	Olivine basalt	×			×	×	×	×			
Co. Hawes											
Ph. Barry, headwaters of Barnard R. Not in place	Olivine basalt	×		×	×	×	×	×			
Co. Hunter											
Ph. Bulga, Green Hill*	Olivine basalt neck				×	×	×	?			
Ph. Bulga, Stony Crk.*	Olivine basalt				×		×	?			
Ph. Coorongooba, Grassy Pt.	Olivine basalt				×	×					
Ph. Coorongooba, Grassy Ridge Waterholes	Olivine basalt				×		?	?			
Ph. Coorongooba, Mt. Coorongooba*	Olivine basalt neck	×									
Ph. Glen Alice, The Nile, Glen Alice, Capertee	Olivine basalt neck				×	×	×				
Ph. Gullongulong, Marsdens Arm*	Olivine basalt neck				×						
Ph. Innes, Uraterer	Olivine basalt				?	×	×				
Ph. Kindarum, Green Hill*	Olivine basalt neck	×									
Ph. Myrtle, Mt. Kindarum*	Olivine basalt neck				×	×	×	×			
Ph. Nullo, Pinnacles near Kerry Mt.	Olivine basalt neck				×		×				
Ph. Nullo, Mt. Nullo*	Nepheline basalt	×									
Ph. Poppong, Mt. Poppong*	Olivine basalt neck	×			×		×	×			
Ph. Putty, Snake's Valley neck*	Olivine basalt neck	×									
Ph. Tollagong, Box Bump*	Olivine basalt neck				×	×	×	×			
Ph. Tupa, Gospers Hill*	Olivine basalt	×			×	×	×	×			
Ph. Wareng, Boorowal Swamp*	Olivine basalt neck	×			×	×	×	×			
Wollamoi, Putty	Olivine basalt				×	×			×		
Co. Phillip											
Ph. Burrumbelong, W. side Burrumbelong Crk.	Olivine basalt				×	×	×	×	×		
Ph. Dabee, Mt. Brace*	Olivine basalt	×			×		×				
Ph. Dabee, E. Cox's Crk. Bridge	Monchiquite sill				×	×	×	×			
Ph. Growee, Mt. Graham	Olivine basalt neck				×	×	×				
Ph. Browee, Gulph neck*	Olivine basalt dyke				×	×		?			

* Brief descriptions given by Carne (1908).

TABLE 1 (*contd.*)

Location (listed alphabetically by county (Co.) and parish (Ph.))	*Host Rock*	*Xenoliths*			*Xenocrysts*						
		1	2	3	4	5	6	7	8	9	10
		Peridotite	*Pyroxenite*	*Gabbro*	*Deformed olivine*	*Clino-pyroxene*	*Ortho-pyroxene or granular ol.*	*Spinel*	*Plagioclase*	*Hornblende*	*Biotite*
Ph. Kelgoola, Bin Ben Mt.	Monchiquite				×	×	×	×			
Ph. Kelgoola, Mt. Darcy*	Olivine basalt				×	×	×				
Ph. Kelgoola, Mt. Kelgoola*	Olivine basalt neck	×									
Ph. Kelgoola, Native Dog Mt.*	Olivine basalt				×	×	×	×			
Ph. Kelgoola, White Gum Forest	Olivine basalt				×						
Ph. Never Never, Mt. Touwouwan*	Olivine basalt				×	×	×	×			
Ph. Pomany, Mt. Davis*	Monchiquite				×	×					
Ph. Pomany, Pinnacle*	Olivine basalt neck	×									
Ph. Widdin, Mt. Cox*	Olivine basalt	×									
Ph. Wollar, 1 m. N. Wollar	Olivine basalt	×			×						
Co. Pottinger											
Ph. Johnston, Battery Mt.	Nepheline basalt				×	×					
Ph. Wilson, 5 m. W. Tambar Springs	Nepheline basalt				×	×	×	?			
Co. Roxburgh											
Ph. Burrowang, Spring Crk.	Olivine basalt	×								×	
Ph. Ganguddy, Mt. Durambang*	Olivine basalt		×								
Ph. Ganguddy, Currant Hill*	Monchiquite neck				×	×	×	?			
Co. Sandon											
Ph. Armidale, 5 m. N. Halls Peak, Armidale	Olivine basalt					×			×		
Co. Wallace, Selwyn											
Ph. Kiandra, Phoenix Claim	Olivine basalt				×						
Kosciusko 1 m. Military sheet grid references:											
230 019 Lake Albina	Monchiquite			×	×	×					
263 984 Merritt's Crk.	Olivine basalt	×			×	×					
242 975	Monchiquite				×	×		?			
245 045	Monchiquite	×		×	×	×					
218 033	Olivine basalt				×		×	×			
Co. Wellesley											
Ph. Hayden, Mollombibby, Snodgrass	Limburgite				×	×	×	×			
Co. Wellington, Bald Hill, Hill End	Olivine basalt				×	×	×	×			
Co. Westmoreland											
Ph. Bulgarres, Ginkin Crk.	Olivine basalt	×									
Ph. Oberon, ½ m. W. Oberon	Olivine basalt	×			×	×	×	×			

* Brief descriptions given by Carne (1908).

rounded books of biotite, and large clinopyroxene xenocrysts identical with those from the Nandewar Mountains sill.

In addition to these occurrences it was found from examination of 260 thin sections of New South Wales basaltic rocks that 40 per cent show unequivocal evidence of the presence of peridotite and gabbro xenocrystal debris even where xenoliths as such are absent. Occurrences which show a high degree of contamination and the type of foreign material are tabulated in Table 1.

PETROLOGY

Peridotite xenoliths

Although peridotite xenoliths exhibit a wide range of modal composition (Table 2, Nos. 1–13), the essential constituents are always olivine, ortho- and clinopyroxene, and brown spinel. Moreover, the compositions of these minerals are remarkably uniform in all studied occurrences which are up to 400 miles apart (Fig. 1). The fabric of all xenoliths is allotriomorphic granular, but minor

TABLE 2

Modal compositions of xenoliths

Mineral	*Peridotite*												
	1	2	3	4	5	6	7	8	9	10	11	12	13
Olivine	58·3	85·4	55·3	52·0	65·2	67·0	45·4	70·0	66·6	72·5	56·2	75·2	67·3
Clinopyroxene	41·0	14·6	24·8	14·5	8·6	13·2	34·4	18·8	8·4	11·5	8·2	2·1	10·8
Orthopyroxene	—	—	17·2	32·7	24·9	19·0	19·7	9·0	21·8	13·9	32·7	21·1	21·0
Spinel	—	—	2·7	0·8	1·3	0·8	0·5	2·2	3·2	2·1	2·9	1·6	0·9
Mica	0·5	—	tr.	—	—	—	—	—	—	—	tr.	tr.	—
Magnetite	0·2	—	—	—	—	—	—	—	—	—	—	—	—
Amphibole	—	—	tr.	—	—	—	—	—	—	—	—	—	—

	Gabbro					*Hornblende–biotite pyroxenite*		
	14	15	16	17	18	19	20	21
Olivine	—	—	3·3	—	—	—	—	—
Clay &c. = olivine and/or orthopyroxene	12·1	7·5	—	22·0	12·7	21·8	8·0	6·2
Clinopyroxene	2·2	20·4	49·1	12·0	28·7	59·0	46·5	52·2
Orthopyroxene	—	tr.	17·0	—	1·0	—	—	—
Magnetite	tr.	2·4	tr.	6·8	4·4	tr.	0·4	18·2*
Spinel	—	—	6·6	—	—	—	—	—
Mica	—	—	—	—	—	12·1	6·7	0·2
Plagioclase	85·7	69·7	24·0	47·5	53·2	—	—	—
Amphibole	—	—	—	11·7	tr.	6·8	38·3	16·5
Apatite	—	—	—	tr.	—	0·3	0·1	6·7

* Includes some pyrite. 1–2, Nandewar Mts. sill. 3, Dundas. 4–6, dike, 2 m. S. Kiama. 7, MacAlister Trig. flow. 8–10, Drogheda Trig. flow. 11–13, Armidale flow. 14–16, Dundas. 17, Dyke, 2 m. S. Kiama. 18–21, Bombo Quarry dyke.

TABLE 3

Chemical analyses of peridotite xenoliths and host basalts

	Peridotite xenoliths			*Host basalts*	
	1	2	3	4	5
SiO_2	43·25	44·20	43·43	44·48	44·29
TiO_2	0·28	0·12	0·12	2·42	2·49
Al_2O_3	2·55	2·95	2·74	13·47	13·98
Fe_2O_3	2·09	1·16	1·01	3·50	2·94
FeO	7·33	7·70	7·21	9·09	9·19
MnO	0·12	0·14	0·12	0·24	0·24
MgO	37·77	40·01	40·98	9·43	10·18
CaO	2·07	2·65	2·12	8·12	9·09
Na_2O	0·20	0·16	0·19	4·08	3·55
K_2O	0·006	0·07	0·006	2·23	1·15
H_2O^+	2·58	0·17	0·74	1·29	1·73
H_2O^-	0·07	0·29	0·68	0·38	0·28
CO_2	nil	0·06	nil	nil	nil
P_2O_5	0·01	nil	nil	0·97	0·71
Cr_2O_3	0·35	0·31	0·25	0·09	0·11
NiO	0·24	0·27	0·23	0·04	0·03
TOTAL	99·916	100·26	99·826	99·83	99·96
S.G.	3·27	3·33	3·29	2·96	2·94

1, dyke, 2 m. S. Kiama. 2, Armidale flow. 3, Drogheda Trig. flow. 4, Armidale flow. 5, Drogheda Trig. flow. Nos. 1, 3–5 analysed by W. H. Herdsman, Glasgow, Scotland. No. 2 analysed by J. Pyle, Dept. of Mines, Sydney.

structures such as narrow fracture bands, fissility, grain-size banding, and, rarely, mineralogical banding occur.

Olivine is invariably very magnesian (Fo 88–89) and usually exhibits either undulose extinction in wide-spaced bands sub-parallel to (100) or translation lamellae parallel to (100) (Turner, 1942). Orthopyroxene is similarly magnesian

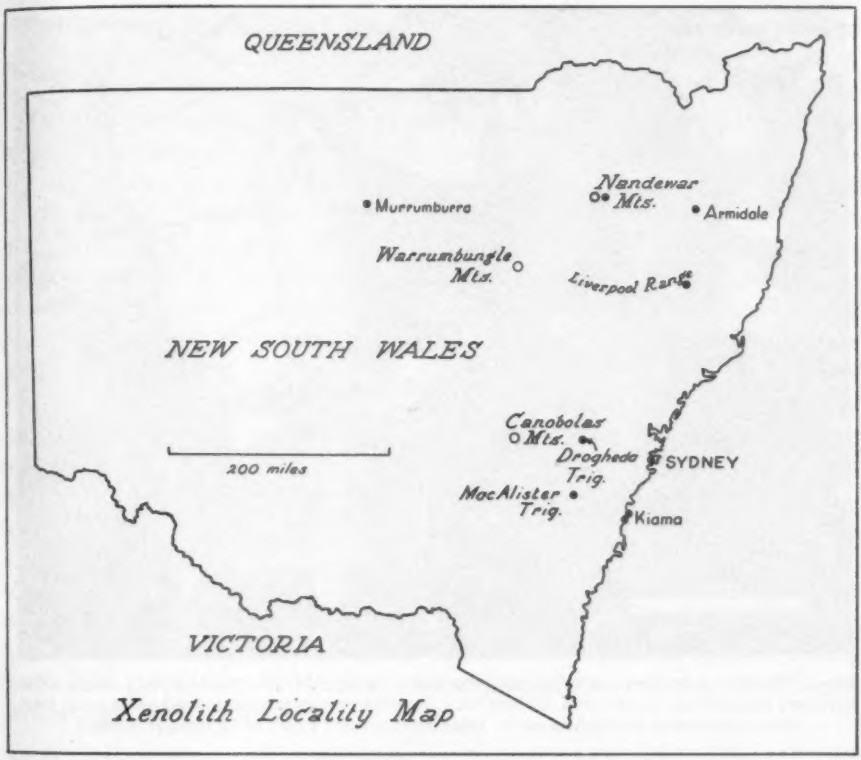

FIG. 1.

(En 87–89) and frequently contains exsolution lamellae of clinopyroxene. Clinopyroxene is slightly more variable in composition (see Tables 4, 5), and often contains exsolution lamellae of orthopyroxene. Both pyroxenes occasionally exhibit patchy undulose extinction or translation lamellae. Brown spinel grains (probably Cr-rich; see Ross *et al.*, 1954) are a common accessory. Three analyses of peridotite, each representing several xenoliths, are given in Table 3.

Marginal reactions between peridotite xenoliths and host rock

The constituents of most peridotite xenoliths show marked reaction rims where they are exposed at xenolith margins. Olivine generally shows the least reaction effects which consist only of an occasional normal zoning. Clino-

pyroxene has a spongy intermediate zone, which extinguishes in the same position as unaltered parts of the grain, followed towards the host rock by a newly precipitated, euhedral rim of salite. The spongy zones appear to be riddled with opaque inclusions in plane-polarized light, but with the condenser these are seen to be cavities which are frequently filled with carbonate and clay. These probably

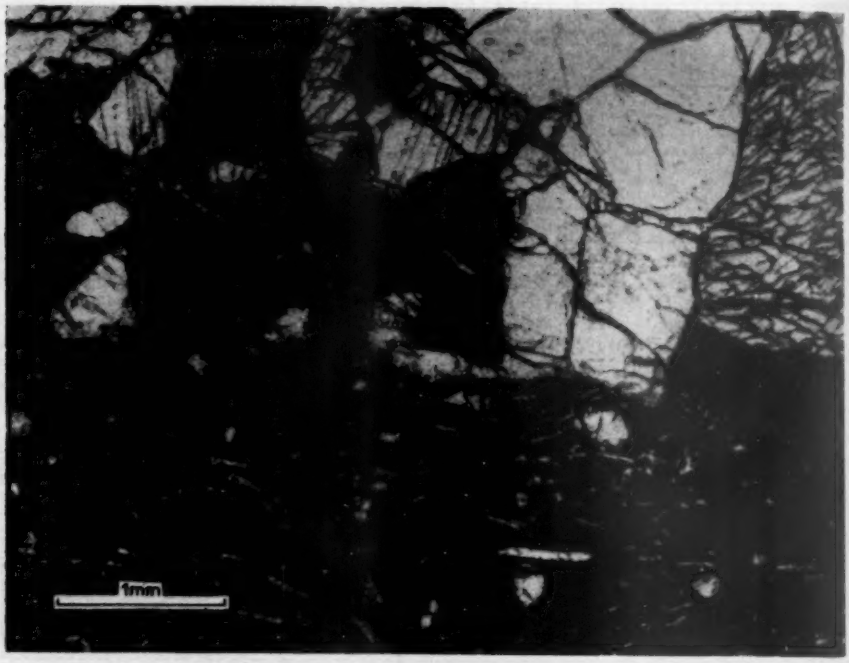

FIG. 2. Margin of peridotite xenolith showing slight embayments and reaction rims where orthopyroxene grains are in contact with the host rock. Reaction has proceeded inward along grain boundaries converting orthopyroxene to turbid material and spinel to an opaque mineral.

represent devitrified glass (Walker & Ross, 1954). Orthopyroxene generally has a rim of turbid, finely divided material with high birefringence followed towards the host rock by a corona of granular olivine with or without magnetite. The turbid zone is probably finely divided olivine which directly replaces orthopyroxene. The position of orthopyroxene grains is generally marked by embayments in xenolith margins (Fig. 2) indicating preferential resorption, and the corona is sometimes surrounded by a thin zone of salite. Spinel grains exposed at margins are always converted to an opaque mineral.

These reaction relationships are similar to those described by Ernst (1936) as occurring between peridotite xenoliths and melilite basalts from Westberges, Germany. Ernst, however, observed that the reaction product of orthopyroxene was a granular mixture of olivine and glass ($n = 1{\cdot}49$–$1{\cdot}51$). The reaction thus appears to be one of incongruent melting of orthopyroxene. In New South

Wales occurrences no glass was observed in the outer rim of granular olivine, but is conceivably present in the inner turbid zone. Ernst also concluded that the spongy zones ('exhaustion zone') of clinopyroxenes are due to small enclosures of glass.

Pyroxenite xenoliths

Pyroxenite xenoliths (Table 2, Nos. 19–21) were found in three occurrences and grade, on the one hand, into hornblendites or glimmerites, and, on the other, into gabbros. Occurrence of these with hornblende– and biotite–peridotite suggests mineralogical gradation between these and pyroxenites also. These xenoliths are generally coarse-grained hypidiomorphic granular and only infrequently show signs of solid state deformation. The clinopyroxenes vary from colourless through pale green or pink to fairly strongly pleochroic ones (X = grey-brown, Y = yellow, Z = grey-green). A complex schiller structure is frequently encountered. Hornblende occurs both as large plates poikilitically enclosing pyroxene and as small, optically continuous grains enclosed by pyroxene. Biotite (polymorph 2 M) may occur as large plates interstitial to pyroxene, as small flakes enclosed in hornblende, or what appear to be coronas around olivine and/or orthopyroxene, now completely altered to carbonate, clay, and quartz. These pseudomorphs are often subhedral and such grains isolated by disintegration of xenoliths cannot be distinguished from altered olivine phenocrysts of the host rock. Magnetite and coarse, stumpy apatite prisms are frequently abundant and some pyrite occurs. In one specimen pyroxenite grades into a rock made up almost entirely of apatite prisms in a matrix of magnetite. Although alteration is severe, some xenoliths appear to consist largely of olivine and/or orthopyroxene with biotite.

These xenoliths and their constituent minerals are similar to those described by Frechen (1948) from Eifel and the Siebengebirge, Germany, and by Holmes & Harwood (1937) from Africa.

Marginal reactions between pyroxenite xenoliths and host rock

The margins of these xenoliths show marked disintegration, not only disaggregation of constituent minerals but also splitting of individual crystals. The most pronounced marginal reactions are shown by hornblende, which is converted to salite and opaque material with or without plagioclase and apatite. Biotite often has a narrower reaction rim than hornblende, but the same reaction products have formed. Clinopyroxene generally has a spongy intermediate zone followed outward by a newly precipitated salite rim.

Gabbro xenoliths

Gabbro xenoliths are widespread in occurrence, but only rarely, as at Dundas, are they abundant. Their fabric is generally hypidiomorphic granular, and occasionally signs of solid-state deformation are evident. The gabbros consist, in

widely varying proportions (Table 2, Nos. 14–18), of plagioclase (An 52–68), clinopyroxene ($2V$ 54°–57°), magnetite, orthopyroxene (En about 80) and/or olivine. Olivine and orthopyroxene are frequently completely altered. Amphibole and biotite are common accessories and green spinel is sometimes present, as in the remarkable graphic intergrowths with ortho- and clinopyroxene described by Benson (1910).

Reactions between host and mafic constituents of the xenoliths are the same as those described above. Although Benson (1910) stated that embayments in gabbro xenoliths where plagioclase is exposed at the margin indicates solution of the feldspar, little supporting evidence was found in the present study. Mechanical disintegration is, however, common, and angular chips of all constituent minerals are found in the host rocks.

Host rocks

The host rocks include alkali basalts (Table 3, Nos. 4, 5) and a variety of lamprophyres. Basalts consist of olivine phenocrysts (Fo 77–86) set in a groundmass of salite, plagioclase, opaque ores, and olivine. It was not possible to select rocks for analysis which were free of peridotite xenocrystal debris, and a higher proportion of this material is reflected in the Drogheda basalt analysis as compared with that of the Armidale basalt. Olivine compositions approaching Fo 85 probably represent xenocrysts. The lamprophyres, generally monchiquite, are often badly altered and only occasionally are groundmass constituents other than salite and opaque ores distinguishable. An ocellar structure, consisting of salite or amphibole needles and alkali feldspar, is common. Olivine and salite are present in all of the host rocks both as groundmass constituents and as large crystals.

In most of these rocks there is unmistakable evidence of a high degree of contamination by peridotite, pyroxenite, and gabbro xenocrystal debris. The criteria used to identify foreign material are the structural characteristics of the constituents of xenoliths and their marginal reactions with the host rock. Although reaction with the host magma has proceeded so far in some cases that phenocrysts may be confused with modified xenocrysts, every stage may be traced from incipient reactions at xenolith margins to complete replacement of xenocrysts by new minerals or lower temperature members of solid-solution series.

Olivine rarely shows any pronounced reaction (normal zoning where reaction occurs) so that structures such as translation lamellae and banded undulose extinction which characterize olivines of the inclusions (Turner, 1942) are useful guides to xenocrystal origin (Hamilton, 1957). Not uncommonly the bulk of coarse olivine in the host rock is xenocrystal (Fig. 5), and where the olivine of xenoliths is badly sheared or shattered, much of the groundmass olivine is also foreign.

Much of the coarse clinopyroxene of host rocks is also xenocrystal. The typical green or colourless clinopyroxenes of xenoliths contrast sharply with the purple

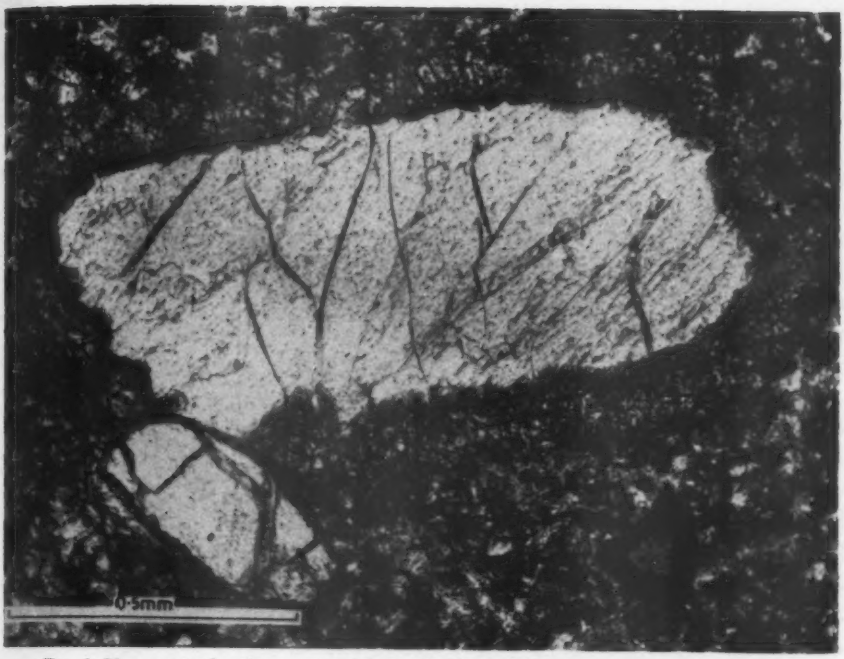

FIG. 3. Xenocryst of orthopyroxene surrounded by turbid and granular olivine corona.

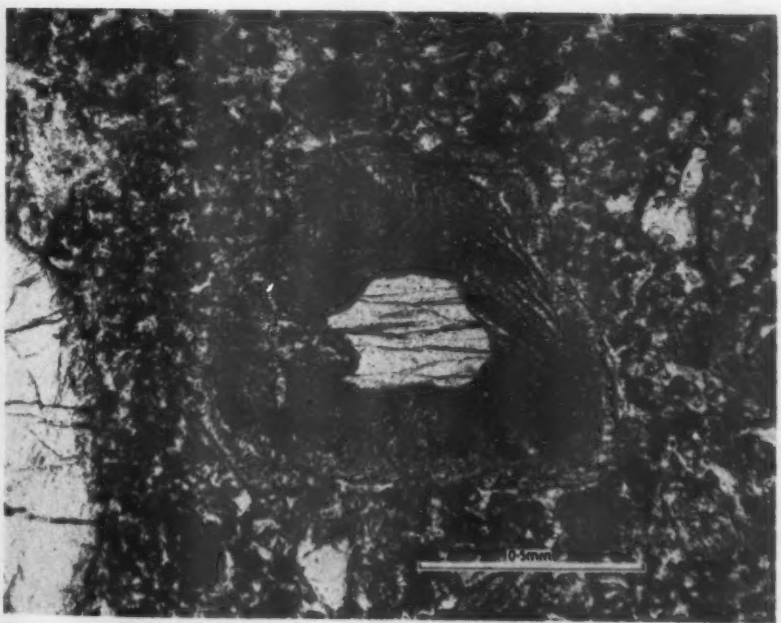

FIG. 4. Corroded colourless clinopyroxene xenocryst surrounded by spongy zone and outer rim of titansalite.

salites of the host, and ragged cores of the former are frequently found encased in subhedral to euhedral salite rims (Fig. 4). In advanced stages of reaction only spongy cores attest to the former presence of a xenocryst.

Complete replacement of amphiboles and micas sometimes gives rise to aggregates which are difficult to distinguish from ocelli, but more frequently a fine intergrowth of opaque ores, salite, and feldspar is ultimately encased in one or several large salite crystals. The large variation in proportions of reaction products suggests that simple dehydration at low pressure is not the only factor involved in the breakdown of amphiboles and micas; furthermore, crystallization of amphiboles in ocelli has commonly followed the breakdown of xenocrystal hornblende.

Orthopyroxene xenocrysts usually exhibit the same reaction rims as those found at margins of orthopyroxene-bearing xenoliths. These consist of a turbid zone followed outward by a granular olivine corona (Fig. 3). Products of complete replacement or sections randomly cut through the corona without exposing the orthopyroxene core are unmistakable in fine-grained host rocks, but are difficult to distinguish from glomeroporphyritic olivine aggregates in coarse hosts. In a few cases the turbid zone is followed outward by a salite rim, and rarely granular olivine pseudomorphs after orthopyroxene are encased in euhedral salite crystals (Fig. 6). Where small aggregates of orthopyroxene and clinopyroxene occur, overgrowths of salite on the clinopyroxene nucleus may enclose the olivine reaction products of orthopyroxene.

Translucent brown, green, and blue spinels are always converted to opaque minerals in contact with the host. Frequently only the larger xenocrysts retain spinel cores, and completely replaced grains may be indistinguishable from opaque microphenocrysts.

It is evident from the foregoing descriptions that some problems may arise because of the presence of xenocrysts. Thus, the distinction between pyroxene, olivine, and opaque phenocrysts and xenocrysts may become obscured as reaction between xenocrysts and host magmas nears completion. The same applies to some groundmass constituents, especially olivine. Anhedral groundmass olivine may as well represent fragments of shattered xenoliths, or relicts of olivine in the process of fusion as products of surface crystallization.

Where strongly reactive minerals such as hornblende, biotite, orthopyroxene, and spinels are common, reaction undoubtedly leads to modifications of liquid compositions. In addition, many of the rocks listed in Table 1 contain so much peridotite xenocrystal debris that these constituents must contribute significantly to the undersaturation shown by bulk compositions. It is evident, however, that the liquid phase is generally undersaturated (see, for example, Fenner, 1938; Drever & Johnston, 1958), for the products of differentiation beyond the basaltic stage are those of undersaturated parent basalts. One of the main interpretative problems which arises from the presence of unmelted peridotite debris is that separation and accumulation of this material will not affect liquid

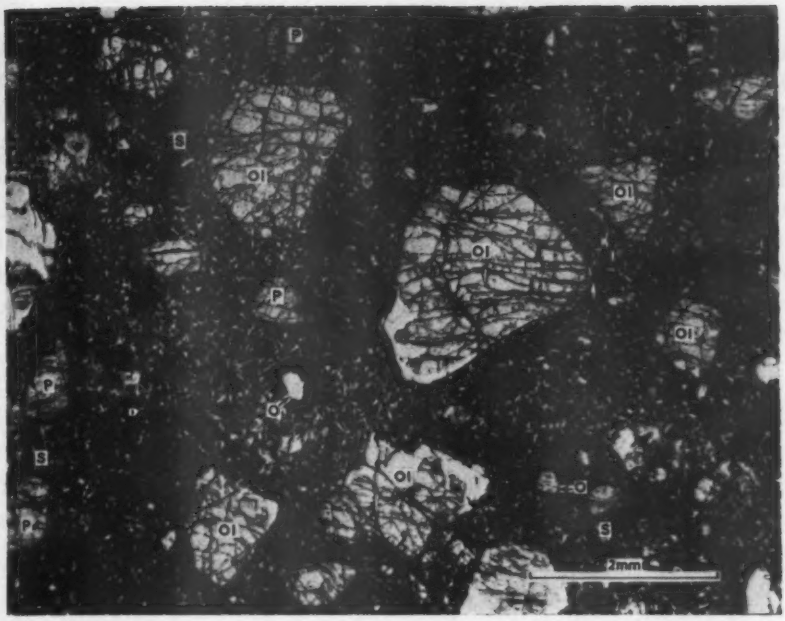

FIG. 5. Xenocrysts of anhedral olivine (*Ol*), orthopyroxene (*O*) with turbid and granular olivine coronas, clinopyroxene (*P*), and spinel (*S*) with opaque reaction rims.

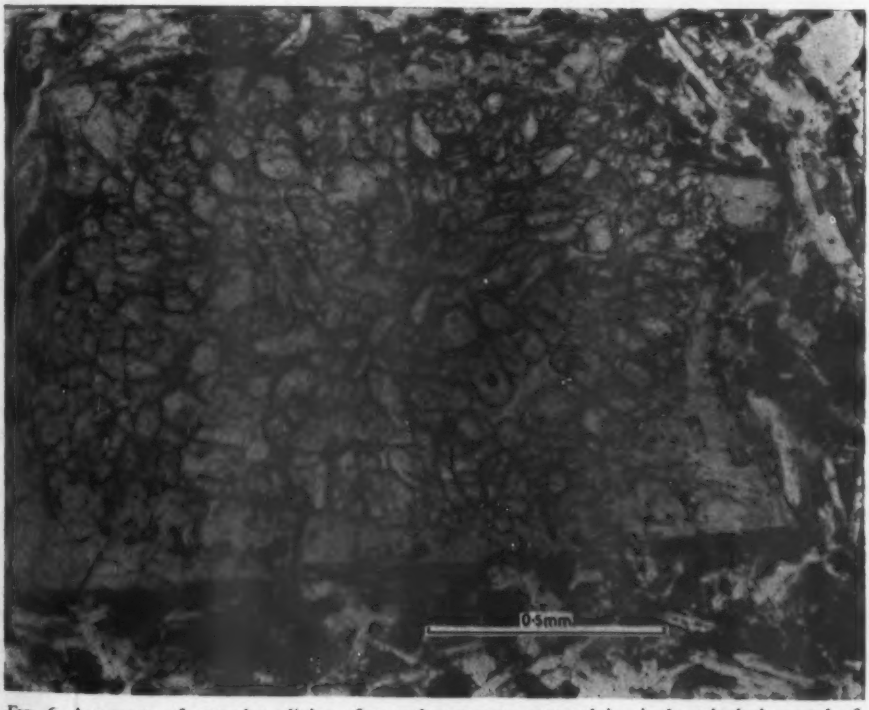

FIG. 6. Aggregate of granular olivine after orthopyroxene encased in single euhedral crystal of titansalite.

compositions, and accumulative rocks so formed cannot be considered as complements of acid differentiates.

A different type of problem may arise if it is assumed that peridotite xenoliths or xenocrysts of peridotite origin are early precipitates from the host magma. Fenner (1938) attempted to prove that compositional trends shown by pyroxene 'phenocrysts' and groundmass pyroxenes were inconsistent with experimental results which have been used to support the theory of fractional crystallization. From Fenner's descriptions it seems probable that the 'phenocrysts' are constituents of peridotite xenoliths, and no such correspondence with experimental results need be expected.

CHEMISTRY OF THE MAFIC MINERALS OF XENOLITHS

Seven analyses (Table 4*a*) of clinopyroxenes from peridotite, pyroxenite, and gabbro xenoliths and one clinopyroxene from the pyroxenite phase of the Mount Dromedary laccolith (Brown, 1930) were prepared by Mr. Pyle of the Department of Mines, Sydney. The analyses and purity of samples were tested

TABLE 4*a*

Chemical analyses of clinopyroxenes

	1	2	3	4	5	6	7	8
SiO_2	50·94	51·91	47·91	46·80	48·64	46·41	46·70	49·68
TiO_2	0·46	0·26	1·39	1·75	2·13	2·11	0·60	2·01
Al_2O_3	5·78	4·77	5·45	5·72	5·24	7·80	6·74	3·40
Fe_2O_3	1·39	0·92	3·91	7·87	4·00	5·60	8·94	4·41
FeO	2·77	2·39	6·64	5·06	5·20	4·70	4·67	3·36
MnO	0·10	0·07	0·21	0·35	0·25	0·31	0·32	0·25
MgO	17·47	16·02	11·23	10·29	12·26	11·51	11·71	15·46
CaO	19·43	21·75	19·95	20·49	21·01	20·05	19·14	20·55
Na_2O	0·72	0·74	1·70	1·57	1·21	1·22	1·16	0·71
K_2O	0·03	0·04	0·04	0·14	0·14	0·14	0·15	0·16
H_2O^+	0·02	0·09	0·45	0·02	0·04	0·09	0·03	0·05
H_2O^-	0·07	0·11	0·20	0·06	0·06	0·06	0·02	0·04
CO_2	0·40	0·12	0·97	nil	nil	nil	nil	nil
P_2O_5	—	—	—	nil	nil	nil	nil	nil
Cr_2O_3	0·59	0·80	tr.	tr.	0·05	0·02	tr.	tr.
NiO	0·03	0·04	tr.	tr.	0·06	0·03	0·02	0·03
TOTAL	100·20	100·03	100·05	100·12	100·29	100·05	100·20	100·11
S.G.	3·278	3·314	3·377	3·373	3·280	3·342	3·218	3·276
	22·7° C	22·4°	22·8°	—	23·0°	23·0°	23·4°	23·4°

Analyst: J. Pyle, Dept. of Mines, Sydney. 1, from peridotite, 2 m. S. Kiama. 2, from peridotite, Drogheda Trig. 3, xenocryst, Nandewar Mts. 4–5, from pyroxenites, Bombo Quarry. 6, from gabbro, Bombo Quarry. 7, from gabbro, Dundas. 8, from pyroxenite, Mt. Dromedary (Brown, 1930).

by Hess's method (1949), and, with the exception of No. 3, were found to be well within the permissible limits of error quoted by Hess. Calculations of cations per 6 oxygens are given in Table 4*b*. Where the CO_2 content was significant, analyses were recalculated to 100 per cent excluding CO_2 as $CaCO_3$ before these computations were made. Although the results compare well with requirements of the pyroxene formula, compensating errors in the $X+Y$ value may result

from the assumption that CO_2 is present entirely in $CaCO_3$. Compositions determined from physical properties (Table 5) were made, using data in Tröger (1952) and Hess (1949). An effort was made to use Zwaan's (1954) data for composition determination from X-ray powder photographs, but the equipment available did not permit sufficiently accurate measurement of reflections.

Pyroxene xenocrysts from the Nandewar Mountains sill (Table 4*a*, No. 3) are associated with peridotite xenoliths, but it is noteworthy that total Fe,

TABLE 4*b*

Pyroxene compositions in cations per 6 oxygens ($Z = 2$)*

	1	2	3	4	5	6	7	8
Si	1·858	1·894	1·841	1·770	1·813	1·738	1·755	1·837
Al_z	0·142	0·106	0·159	0·230	0·187	0·262	0·245	0·148†
Al_y	0·107	0·099	0·088	0·025	0·043	0·082	0·053	—
Ti	0·013	0·007	0·040	0·050	0·060	0·059	0·017	0·056
Fe^{3+}	0·038	0·025	0·113	0·224	0·112	0·158	0·253	0·123
Fe^{2+}	0·084	0·073	0·213	0·160	0·162	0·147	0·147	0·104
Cr	0·017	0·023	—	—	0·001	—	—	—
Mg	0·949	0·871	0·643	0·580	0·681	0·642	0·656	0·852
Mn	0·003	0·002	0·007	0·011	0·008	0·010	0·010	0·008
Ni	0·001	0·001	—	—	0·002	0·001	0·001	0·001
Na	0·051	0·052	0·127	0·115	0·087	0·089	0·084	0·051
K	0·001	0·002	0·002	0·007	0·007	0·007	0·007	0·008
Ca	0·739	0·844	0·770	0·830	0·839	0·804	0·770	0·814
W	0·791	0·898	0·899	0·952	0·933	0·900	0·861	0·873
X+*Y*	1·212	1·101	1·104	1·050	1·069	1·099	1·137	1·144
W+*X*+*Y*	2·003	1·999	2·003	2·002	2·002	1·999	1·998	2·017
Ca	40·7	46·5	45·5	46·0	46·6	45·7	41·9	42·8
Mg	52·3	48·0	36·8	32·1	37·8	36·5	35·7	44·8
Fe	7·0	5·5	17·7	21·9	15·6	17·8	22·4	12·4

* Analyses 1–3 recalculated free of CO_2 as $CaCO_3$ before computation.

† Because Al is insufficient to make $Z = 2$, there is presumably Ti for Si substitution.

alkalis, TiO_2, and Cr_2O_3 are different from those of clinopyroxenes from peridotite xenoliths (Nos. 1, 2). This is presumably due to magmatic reaction, but the resemblance to pyroxenes from gabbro and pyroxenite xenoliths of other occurrences is conspicuous.

The analysis of pyroxene from the Mount Dromedary pyroxenite (No. 8) was prepared for comparison with those of the Bombo pyroxenites (Nos. 4, 5) (see p. 202) because Brown (1929) suggested the possibility of accidental incorporation of accumulates similar to those present in the Dromedary complex as an explanation of the origin of pyroxenite xenoliths.

The compositions of olivine, ortho- and clinopyroxene of peridotite xenoliths as determined from optical properties are given in Table 5 as well as comparisons of compositions as determined both by analysis and optical properties of the clinopyroxenes in Table 4*a*. Minor elements in olivine and orthopyroxene are probably the same as those reported by Ross *et al.* (1954).

As might be expected, the clinopyroxenes from gabbro and hornblende-biotite pyroxenites are richer in Fe than those of peridotite. The additional charge of Fe^{3+} is balanced by Al in the Z group, and to a lesser extent by Na in the W group. The relatively high alumina and alkali contents of the pyroxenes provide potential sources of these materials in the magma source area. These

TABLE 5

Optical properties and compositions of mafic minerals from xenoliths

Locality, host rock and anal. no. (Table 4a)	*Xenolith*	*Mineral*	n_x	n_y	n_z	*2V*	*Composition*
1. Kiama	Peridotite	Olivine	1·656	1·674	1·692		Fo 89 Fa 11
Monchiquite		Orthopyroxene	1·669	1·675	1·680		En 88 Fs 12
		Clinopyroxene	1·678	1·684	1·707	55	Ca 44 Mg 48 Fe 8*
							Ca 40·7 Mg 52·3 Fe 7·0
MacAlister Trig.	Peridotite	Olivine	1·656	1·674	1·692		Fo 89 Fa 11
Olivine basalt		Orthopyroxene	1·668	1·674	1·678		En 89 Fs 11
		Clinopyroxene	1·679	1·686	1·708	52–55	Ca 44 Mg 46 Fe 10*
2. Drogheda	Peridotite	Olivine	1·657	1·674	1·692		Fo 89 Fa 11
Trig.		Orthopyroxene	1·669	1·674	1·678		En 89 Fs 11
Olivine basalt		Clinopyroxene	1·675	1·683	1·703	51	Ca 41 Mg 52 Fe 7*
							Ca 46·5 Mg 48·0 Fe 5·5
3. Nandewar Mts.	Peridotite	Olivine	1·656	1·674	1·691		Fo 89 Fa 11
Lamprophyre		Clinopyroxene	1·682	1·688	1·711	52–55	Ca 44 Mg 45 Fe 12*
	Xenocryst	Clinopyroxene	1·706	1·712	1·733		Ca 45·5 Mg 36·8 Fe 17·7
4–6. Bombo	Pyroxenite	Clinopyroxene	1·702	1·708	1·730	59	Ca 50 Mg 23 Fe 27*
Quarry							Ca 46·0 Mg 32·1 Fe 21·9
Monchiquite	Pyroxenite	Clinopyroxene	1·693	1·701	1·723	55	Ca 45 Mg 32 Fe 23*
							Ca 46·6 Mg 37·8 Fe 15·6
		Hornblende	1·675	1·693	1·700		
	Gabbro	Clinopyroxene	1·697	1·703	1·726	54–57	Ca 44 Mg 30 Fe 26*
							Ca 45·7 Mg 36·5 Fe 17·8
7. Dundas	Peridotite	Olivine		1·674			Fo 89 Fa 11
Olivine basalt		Orthopyroxene	1·669	1·674	1·679		En 89 Fs 11
		Clinopyroxene		1·686		55–56	Ca 46 Mg 44 Fe 10*
	Gabbro	Clinopyroxene				57	Ca 41·9 Mg 35·7 Fe 22·4
Bulli Colliery	Xenocryst	Hornblende	1·672	1·682	1·698		
Monchiquite			1·678	1·690	1·706		

* Composition determined from $2V$ and n .

values are not as high as those experimentally achieved with eclogites (Yoder & Tilley, 1959), but where gabbro is a potential source rock the alumina and alkali content of pyroxene is of little consequence.

DEUTERIC ALTERATION OF XENOLITHS AND HOST ROCKS

A common feature of both xenoliths and host rocks is extensive deuteric alteration which has resulted in the formation of abundant clays, carbonate, and quartz. It is evident from the literature that altered rocks have frequently been analysed (generally expressed in high CO_2 and H_2O values). That bulk compositions of such rocks may be far removed from original compositions is amply illustrated in Table 6, and consequently the value of such analyses is strictly limited. The altered rock in Table 6 was originally described by David *et al.* (1893) as a 'chromite-anorthite' rock, but Benson (1910) showed that this is actually a peridotite in which all constituents except the spinel have been replaced by quartz, carbonate, and clay. Perfect preservation of the original fabric permits calculation of absolute changes in composition without volume change,

these figures appearing in Table 6, col. *A*. Both altered and unaltered xenoliths are probably large enough (8 in.) to have avoided marked modal differences which characterize smaller ones, but there can be no certainty of this. Compositional changes are so drastic, however, that pronounced effects due to alteration are obvious. In this particular case the compositional changes accompanying alteration have produced a more acid rock than the original; that opposite changes may also take place is evident from the data presented by Wilshire (1959).

TABLE 6

Compositional changes accompanying equal volume alteration of a peridotite xenolith

	1	2	*A*
SiO_2	39·13	46·29	+ 98
Al_2O_3	3·48	4·66	+ 25
Fe_2O_3	1·83	1·93	− 2
FeO	7·58	10·10	+ 53
MgO	42·15	7·13	−1,152
CaO	0·07	9·36	+ 273
H_2O^-	2·80	—	—
		0·11	
H_2O^+	0·80	—	− 23
CO_2	3·05	19·34	+ 470
TiO_2	0·16	0·12	− 1
Cr_2O_3	0·20	0·24	+ 1
MnO	0·21	0·19	− 1
(Ni, Co)O	0·04	0·05	0
TOTAL	101·50	99·52	
S.G.	3·19	2·93	

1, slightly altered peridotite xenolith (Benson, 1910, p. 532).
2, badly altered peridotite xenolith (Benson, 1910, p. 535).
A, compositional differences (mg/c.c.) between 1 and 2. Analyses recalculated to 100 per cent excluding H_2O_- before computation of figures in column *A*.

ORIGIN OF XENOLITHS AND HOST MAGMAS

Although the xenoliths described here include a wide range of rock types, they share many features, and mineralogical gradations among rock types are common. The occurrence together of peridotite, hornblende–biotite peridotite, pyroxenites, and gabbros suggests a common origin. Many of the variants, including small monomineralic specimens, are doubtless due to disintegration of inhomogeneous rocks (Holmes & Harwood, 1937), and among the peridotites, the occasional mineral banding, diverse modes, and grain-size variation suggest that the source rock is banded. In addition to these features, many of the rocks show evidence of solid-state deformation and most have orthopyroxene as a constituent.

Hypotheses which have been advanced to explain the origin of peridotite xenoliths include: accidental incorporation of fragments of peridotite intrusions, or of ultrabasic portions of differentiated intrusions; accumulation, by gravity

settling or other mechanisms, of crystals precipitated from the host magma; subvolcanic crystallization of the host magma in conduits with fragments subsequently ripped off by movement of the host magma; and unmelted parts of a peridotite layer from which the host magma is thought to originate by partial fusion.

Gabbro, pyroxenite, and related xenoliths are far more frequently attributed to subvolcanic intrusions representing shallow level differentiates of the lavas (Washington, 1927; Lacroix, 1893, 1912; Edwards, 1938), but are occasionally thought to be accidental (Brown, 1929). Lacroix (1912) suggested that all the rock types under consideration are derivatives of subvolcanic intrusions. This hypothesis was supported by Turner & Verhoogen (1951), but these authors subsequently (1960, p. 202) concluded that peridotite xenoliths are derived from the mantle.

Accidental origin

As shown by Ross *et al.* (1954), the world-wide occurrence and similarity of peridotite xenoliths is strongly opposed to an accidental origin. That the same thing is true of hornblende–biotite pyroxenite and related xenoliths is clear from the many occurrences cited by Holmes & Harwood (1937) as well as those reported here, by Edwards (1938), and by Frechen (1948). This relationship is further enhanced by mineralogical gradations among all these rock types (Holmes & Harwood, 1937; Edwards, 1938; Benson, 1910; Macdonald, 1949; Harumoto, 1952; Frechen, 1948). Although the similarity of pyroxenes (Table 4*a*, No. 8) from such pyroxenite-bearing intrusions as Mount Dromedary (Brown, 1930) to those of pyroxenite xenoliths (Table 4*a*, Nos. 4, 5) may support an accidental origin, Dromedary is, as is true of some of the intrusions cited by Holmes & Harwood (1937), largely composed of feldspathic rocks with only subordinate amounts of ultrabasic rocks. Xenoliths of similar acid rocks are absent from the New South Wales occurrences. Finally, Kuno's observation (1959*a*) that these xenoliths are absent from tholeiitic basalts compels rejection of an accidental origin.

Cognate origin

The hypothesis of origin by accumulation of crystals precipitated from the host magma or from products of subvolcanic crystallization has wide support (Lacroix, 1893, 1912, 1932; Arnold-Bemrose, 1910; Benson, 1910; Thompson, 1916; Lausen, 1927; Andreatta, 1938; Edwards, 1938; Chudoba & Frechen, 1941; Frechen, 1948; Macdonald, 1949; and more recently from Turner & Verhoogen (1951), Brown (1955), and Searle (1960)). These authors have generally based their conclusions on the contention that mineralogical features of peridotite xenoliths are those expected of early precipitates of the host magma. Chudoba & Frechen have shown that olivine compositions in xenoliths are more magnesian where olivine is present in greatest quantity. It is argued that increase

in Fa content (from Fa 8 to Fa 16) with increase in pyroxene content is expected of fractional crystallization and continues th ugh the stage of intratelluric and surface crystallization of olivine in the host magmas. Andreatta arrived at similar conclusions using normative compositions plotted on variation diagrams. These conclusions have no support from chemical data presented by Ross *et al.* (1954), by Deriu (1959), and in the present study.

Most of the writers favouring a cognate origin are agreed that the xenoliths have not formed in place, but rather represent segregations formed at depth (i.e. subvolcanic differentiates). This conclusion is based on the shape of xenoliths, sharp contacts with the host, absence of macroscopic ultrabasic segregations in lavas, flow structures related to xenolith boundaries, and frequent occurrence in diatremes. For example, Thompson (1916) stated, 'The fact that the inclusions themselves form a differentiation series comparable with that which would have been expected had the various basic volcanic rocks enclosing them consolidated under plutonic conditions suggests that they are actually fragments from such a series which has arisen from the differentiation in depth of a portion of the primary basic magma.' Formation at depth is generally required by recent authors who are aware of the difficulties in reconciling xenolith mineralogy with modern information on pyroxene crystallization in basaltic magmas. Thus, Turner & Verhoogen (1951) concluded that, 'The olivine and associated minerals of the xenoliths crystallized or accumulated at depths sufficiently great to allow continuous crystalline masses with the mineralogical composition and fabric of peridotites to be built up.'

Chudoba & Frechen (1941) concluded that the fabric of xenoliths results from deposition of euhedral crystals with long dimensions oriented by flow. Phillips (1938) also compared the fabric of inclusions with that of accumulative ultrabasic rocks, and stated, 'the resemblance of the rocks from Rhum and Skye to the nodules of basalts in texture, grain size, oriented fabric, and prominent development of translation lamellae is so close that these criteria at least suggest no need to look further afield for the source of such nodules than to an earlier phase of the same period of activity'.

Searle (1960) noted the occurrence of peridotite xenoliths in tuffs from Auckland, New Zealand, and considered the relation to explosive vulcanism as evidence for derivation of the xenoliths from upper parts of a parent magma body where early magmatic fractions separated along the margins. On a world-wide scale a relation with explosive vulcanism has little support. This suggestion is likewise inconsistent with Searle's conclusion that pegmatoid segregations (generally thought to form in place, Walker, 1953) are complements of the peridotite. Localized distribution of xenoliths, cited as evidence for spasmodic disruption of accumulates (Searle, 1960; Turner & Verhoogen, 1951) and consequently as evidence for this origin, is in the writers' opinion due to mechanical sorting during movement through channels of variable width and attitude (see description of dyke in Bombo Quarry, p. 187).

The chief difficulties with this hypothesis lie in the typical fabric of peridotite xenoliths, the presence of orthopyroxene, and rarity of these xenoliths in tholeiitic basalts. Contrary to the claims of Phillips (1938), there is little resemblance between fabrics of ultrabasic accumulates of intrusions and those of xenoliths (see Hess, 1955, p. 394). The allotriomorphic granular fabric of xenoliths contrasts with that of accumulates which exhibit subhedral, tabular olivine crystals, and pyroxene, where present, as intercumulate rather than as discrete gains. Intercumulate plagioclase is common in differentiated intrusions (Wager *et al.*, 1960), but plagioclase is a rare mineral in peridotite xenoliths, and rarer still in intergranular arrangement. Moreover, the chromian diopsides of inclusions contrast with the augites of accumulate rocks belonging to smaller basic intrusions. Additional problems in fabric interpretation arise from this hypothesis, for accumulation of crystals precipitated freely from the magma does not explain the allotriomorphic granular fabric of xenoliths and provides no explanation for severe solid-state deformation and the presence of exsolution lamellae in both orthopyroxene and clinopyroxene. Orthopyroxene lamellae in clinopyroxene react with the host magma to produce olivine in the same way as individual enstatite grains which emphasizes the very complex physico-chemical history inherent in this hypothesis.

Kuno (1959*a*) has also pointed out that the presence of orthopyroxene in xenoliths is not consistent with the crystallization history of host alkali basalts, for neither orthopyroxene nor pigeonite is a product of intratelluric or surface crystallization of understaturated basalts (Wilkinson, 1956). Because orthopyroxene melts incongruently to olivine, the early crystallization of orthopyroxene followed by crystallization of olivine without orthopyroxene or pigeonite requires drastic changes in physical or chemical conditions (Kuno *et al.*, 1957), which is not compatible with the close relation implied by subvolcanic differentiation.

Finally, Kuno (1959*a*) has pointed out the difficulty of reconciling this hypothesis with the general absence of peridotite xenoliths in tholeiites. There is little reason to believe that alkali basalts are more prone to subvolcanic differentiation than are tholeiites.

None of the above objections, however, rule out the fact that intrusions of appropriate mineralogy have been found in the cores of some volcanoes (Lacroix, 1912, 1932). Whether these represent differentiates of the lavas is an altogether different question, for it is noteworthy that such intrusions have been reported only from oceanic volcanoes. There is no dearth of deeply eroded continental volcanoes, yet peridotite intrusions, if they occur, cannot be common. In New South Wales the three central volcanic eruptions comprising the Canobolas, Warrumbungle, and Nandewar Mountains are all deeply dissected, but no intrusions resembling peridotite have been reported. Coarse dolerite intrusions have a gabbroic fabric, but the mineralogy is that of alkali basalt. In volcanic terrains such as Hawaii, where both tholeiitic and alkali basalt occur together,

it may be possible to find orthopyroxene-bearing gabbro xenoliths in alkali basalts, but Kuno (personal communication) regards such xenoliths as possibly derived from the layer just above the *M* discontinuity. It is perhaps more plausible to consider the peridotite intrusions of oceanic volcanoes, where the crust overlying the peridotite mantle is thin, as direct derivatives from the mantle which need not represent advanced stages of liquefaction.

Derivation from the mantle

Ross *et al.* (1954) have made a valuable chemical study of peridotite xenoliths, which, with the support of further data in Deriu (1959) and the present work, has stressed the remarkable uniformity in mineralogy and composition of minerals from peridotite xenoliths all over the world, and from a variety of host rocks. The independence of mineral composition of host rocks is in itself difficult to reconcile with accumulation-differentiation hypotheses. It suggests rather that there is a world-wide source of ultrabasic material, varying little in composition of minerals though variable in proportions of minerals. Because this material must be abundantly present beneath both continental and oceanic regions, the upper mantle appears to be the most likely source of both peridotite xenoliths and of the host magmas. Turner & Verhoogen (1960) suggested that primary basalt magmas are derived from the mantle by partial fusion, and this hypothesis is supported by modern seismic studies of active volcanic regions (see Kuno, 1959*b*; Powers, 1955). Seismic properties of the mantle are consistent with the physical characteristics of both peridotite and eclogite (Lovering, 1958, 1959), but petrological evidence clearly points to the predominance of peridotite. Objections to a mantle origin of peridotite xenoliths raised by Tilton *et al.* (1956) and by Lovering (1959) were based on data subsequently found to be in error, and there is as yet insufficient reliable data on U/Pb ratios to support any conclusions (Tilton, personal communication).

Although the xenoliths are most easily accounted for as unmelted relicts from the magma source area, some problems arise with this hypothesis. Kuno (1959*a*, *b*) and Turner & Verhoogen (1960, p. 443) suggest that both tholeiite and alkali basalt are derived by partial fusion of peridotite, alkali basalt being derived from lower levels than tholeiite. It is the writers' opinion that the presence of xenoliths is due largely to accidental structural conditions which permit spalling and incorporation of unmelted fragments of the source rock. If such is the case it is hardly to be supposed that the requisite structural conditions consistently occur where alkali basalt is generated but not where tholeiite is generated from the same source rock. Kuno's suggestion (1957) that tholeiites have a shorter distance to travel through peridotite and consequently contain fewer xenoliths does not seem adequate, and in itself provides no explanation for differences in composition of liquid phases between alkali basalts and tholeiites. Melting of olivine before orthopyroxene (Kuno *et al.*, 1957) in deep levels of the mantle from which alkali basalt is supposedly derived is not consistent with the

xenocrystal mineralogy of some accumulative rocks in alkali basalts from Lord Howe Island and Kerguelen which will be dealt with at a later date.

A partial solution may be found in the wide variety of rock types[1] found as xenoliths, all of which may be relicts from the magma source area. It is evident from the analyses of peridotite xenoliths (Table 3, Nos. 1–3) that a very large volume of peridotite would be required to produce significant quantites of basaltic liquid by partial fusion. The quantity is correspondingly reduced if less basic rocks are present as well as peridotite. It has been demonstrated that rocks of basaltic composition may have widely different mineralogical compositions depending on *TP* conditions and presence or absence of H_2O (Yoder & Tilley, 1956, 1959). This probably accounts for some of the variants described in this paper and points to the possibility of differentiates of variable composition (but with similar physical properties) occurring in the mantle. Hornblendites, glimmerites, and hornblende–biotite pyroxenites and peridotites may occur as local differentiates within the mantle, while gabbros possibly occur in the lower crust or as quantitatively minor differentiates within the upper mantle. It has been experimentally demonstrated (Boyd & England, 1960) that large amounts (10–20 wt. %) of alumina can enter the orthopyroxene structure at very high pressures (15–20 kilobars). Thus, the graphic intergrowths of pyroxene and spinel of some gabbro xenoliths suggest a deep-seated origin followed by exsolution of Al to form spinel as xenoliths are brought to the surface (A. E. Ringwood, personal commmunication). Recent studies of alpine peridotites in the Caribbean area (MacKenzie, 1960) have revealed the presence of 'pseudo-gabbro' masses within a high-temperature peridotite intrusion. These are interpreted (MacKenzie, 1960, p. 311) as fragments of metamorphosed country rock, but, in the light of common association of contrasted differentiates, the argument raised against their origin as differentiates of the peridotite is not convincing. It is possible that differentiation within the mantle has given rise to the gabbros and other, non-peridotite rocks which appear as xenoliths. Heterogeneity (involving rocks with different physical properties) in the upper mantle is not inconsistent with recorded variations in wave velocities (Hill, 1957; Gutenberg, 1955), but these measurements are affected by many other factors (Gutenberg, 1955), and Hess (1960) attributes some variations to different degrees of serpentinization of peridotite. In the writers' opinion the direct evidence must be accounted for and it is therefore proposed that the alkali basalt and lamprophyre host rocks in New South Wales originated by partial (and locally complete) fusion of a composite source rock in which peridotite is dominant, and that xenoliths of all types represent unmelted fragments of this source rock, which is probably located at the top of the mantle.

[1] In the absence of a distinguishing terminology, the xenolith lithologies have been named as though they were igneous rocks. The authors consider it likely that they were formed by transformation in the solid state, for xenolith fabrics are frequently more akin to those of metamorphic than to igneous rocks.

ACKNOWLEDGEMENTS

New xenolith localities were brought to the authors' attention by several people. In particular Dr. C. V. G. Phipps, Mr. B. Chappell, and Mr. O. Shiels are thanked for their assistance in collecting specimens, and Mr. D. Pinkston of the Department of Mines, Sydney, for his help in making available specimens held by the Mining Museum. Dr. F. Booker and Mr. St. J. Mulholland are again thanked for their kind permission that chemical analyses be carried out by Mr. J. Pyle. The high quality of Mr. Pyle's work has made the mineral analyses a valuable addition to the study. Dr. H. Kuno is thanked for having commented on the manuscript. The cost of some of the rock analyses was defrayed by the Sydney University Research Grants Committee, 125 thin sections were prepared by Mr. E. J. Armstrong, and the photography was done by the Medical Illustrations Department, Sydney University, for which the writers are grateful.

REFERENCES

ANDREATTA, C., 1938. Basalti della valle dell'Alpone e loro inclusi peridotitici. *Bol. Soc. geol. ital.* **57**, 239–64.

ARNOLD-BEMROSE, H. H., 1910. On olivine nodules in the basalt of Calton Hill, Derbyshire. *Geol. Mag. Lond.* **7**, 1–4.

BENSON, W. N., 1910. The volcanic necks of Hornsby and Dundas near Sydney. *J. roy. Soc. N.S.W.* **44**, 529–55.

BOYD, F. R. & ENGLAND, J. L., 1960. Minerals of the mantle. *Yearb. Carneg. Instn.*, No. **59**, 47–52.

BROWN, D. A., 1955. The geology of Siberia Hill and Mt. Dasher, North Otago. *Trans. roy. Soc. N.Z.* **83**, 347–72.

BROWN, I. A., 1929. A garnet-bearing dyke near Moruya, New South Wales. *Proc. Linn. Soc. N.S.W.* **39**, 447–53.

—— 1930. The geology of the South Coast of New South Wales. Pt. 3: The monzonitic complex of the Mount Dromedary District. *Proc. Linn. Soc. N.S.W.* **55**, 637–98.

CARNE, J. E., 1908. Geology and mineral resources of the Western Coalfield. *Mem. geol. Surv. N.S.W.* **6**.

CHUDOBA, K. F., & FRECHEN, J., 1941. Die frühmagmatische Bildung der Olivinausscheidungen vom Finkenberg (Siebengebirge) und Dreiser Weiher (Eifel). *Geol. Rdsch.* **32**, 257–78.

DAVID, T. W. E., SMEETH, W. F., & WATT, J. A., 1893. Preliminary note on the occurrence of a chromite-bearing rock in the basalt at the Pennant Hills quarry near Parramatta. *J. roy. Soc. N.S.W.* **27**, 401–6.

DERIU, M., 1959. Olivini e pirosseni di noduli inclusi in basalti della Sardegna centro-occidentale. *Period. Miner.* **28**, 259–83.

DREVER, H. I., & JOHNSTON, R., 1958. The petrology of picritic rocks in minor intrusions—a Hebridean group. *Trans. roy. Soc. Edinb.* **63**, 459–98.

EDWARDS, A. B., 1938. Tertiary lavas from the Kerguelen Archipelago. *B.A.N.Z. Antarctic Expedit. 1929–1931 Rept.*, ser. A, Pt. **5**, 72–100.

ERNST, T., 1936. Der Melilith-Basalt des Westberges bei Hofgeismar, nördlich von Kassel, ein Assimilationsprodukt ultrabasischer Gesteine. *Chem. d. Erde*, **10**, 631–66.

FENNER, C. N., 1938. Olivine fourchites from Raymond Fosdick Mountains, Antarctica. *Bull. geol. Soc. Amer.* **49**, 367–400.

FRECHEN, J., 1948. Die Genese der Olivinausscheidungen von Dreiser Weiher (Eifel) und Finkenberg (Siebengebirge). *N. Jb. Min. Geol. Paläont.* **79**, 317–406.

GUTENBERG, B., 1955. Wave velocities in the earth's crust. *Geol. Soc. Amer.*, Spec. Pap., **62**, 19–34.

HAMILTON, J., 1957. Banded olivines in some Scottish basalts. *Geol. Mag. Lond.* **97**, 135–9.

HARPER, L. F., 1915. Geology and mineral resources of the Southern Coalfield. *Mem. geol. Surv. N.S.W.* **7**, 276–405.

HARUMOTO, A., 1952. Melilite–nepheline–basalt, its olivine nodules, and other inclusions from Nagahama, Japan. *Mem. Coll. Sci. Kyoto*, ser. B, **20**, 69–88, 311–22.

HARVEY, M. H., & JOPLIN, G. A., 1940. A note on some leucite-bearing rocks from N.S.W., with special reference to an ultrabasic occurrence at Murrumburrah. *J. roy. Soc. N.S.W.* **74**, 419–42.

HESS, H. H., 1949. Chemical composition and optical properties of common clinopyroxenes. Pt. 1. *Amer. Min.* **34**, 621–66.

—— 1955. Serpentines, orogeny, and epiorogeny. *Geol. Soc. Amer.* Spec. Pap., **62**, 391–408.

—— 1960. Caribbean research project: Progress report. *Bull. geol. Soc. Amer.* **71**, 235–40.

HILL, M. N., 1957. Recent geophysical exploration of the ocean floor, in *Physics and chemistry of the earth*, vol. **2**, Pergamon Press: New York.

HOLMES, A., & HARWOOD, H. F., 1937. The petrology of the volcanic area of Bufumbira. *Mem. geol. Surv. Uganda*. **3**, Pt. 2.

JAQUET, J. B., CARD, G. W., & HARPER, L. F., 1905. The geology of the Kiama–Jamberoo district. *Rec. geol. Surv. N.S.W.* **8**, Pt. 1, 1–66.

JENSEN, H. I., 1907. The geology of the Nandewar Mountains. *Proc. Linn. Soc. N.S.W.* **32**, 842–914.

KUNO, H., 1959*a*. Discussion of paper by J. F. Lovering, The nature of the Mohorovicic discontinuity. *J. geophys. Res.* **64**, 1071–2.

—— 1959*b*. Origin of Cenozoic petrographic provinces of Japan and surrounding areas. *Bull. volcan.* **20**, 37–76.

—— YAMASAKI, K., IIDA, C., & NAGASHIMA, K., 1957. Differentiation of Hawaiian magmas. *Jap. J. Geol Geogr.* **28**, 179–218.

LACROIX, A., 1893. *Les Enclaves des roches volcaniques*. Protat Frères: Macon.

—— 1912. Les Roches grenues, intrusives dans les brèches basaltiques de la Reunion; leur importance pour l'interpretation de l'origine des enclaves homœogènes des roches volcaniques. *C.R. Acad. Sci. Paris*, **154**, 1–6.

—— 1932. La Constitution lithologique des iles volcaniques de la Polynesie Australe. *Mém. Acad. Sci. Paris*, **58**.

LAUSEN, C., 1927. The occurrence of olivine bombs near Globe, Arizona. *Amer. J. Sci.* **14**, 293–306.

LOVERING, J. F., 1958. The nature of the Mohorovicic discontinuity. *Trans. Amer. geophys. Un.* **39**, 947–55.

—— 1959. Reply to discussion by H. Kuno. *J. geophys. Res.* **64**, 1073.

MACDONALD, G. A., 1949. Petrography of the Island of Hawaii. *Prof. Pap. U.S. geol. Surv.* **214**-D.

MACKENZIE, D. B., 1960. High-temperature alpine-type peridotite from Venezuela. *Bull. geol. Soc. Amer.* **71**, 303–18.

OSBORNE, G. D., 1920. The volcanic neck at The Basin, Nepean River. *J. roy. Soc. N.S.W.* **54**, 113–45.

PHILLIPS, F. C., 1938. Mineral orientation in some olivine rich rocks from Rhum and Skye. *Geol. Mag. Lond.* **75**, 130–5.

POWERS, H. A., 1955. Composition and origin of basaltic magma of the Hawaiian Islands, *Geochim. et Cosmochim. Acta*, **7**, 77–107.

POWERS, S., 1915. Origin of dyke inclusions. *J. Geol.* **23**, 166–82.

ROSS, C. S., FOSTER, M. D., & MYERS, A. T., 1954. Origin of dunites and of olivine-rich inclusions in basaltic rocks. *Amer. Min.* **39**, 693–737.

SEARLE, E. J., 1960. Petrochemistry of the Auckland basalts. *N.Z. J. Geol. Geophys.* **3**, 23–40.

SÜSSMILCH, C. A., 1905. On the occurrence of inclusions of basic plutonic rocks in a dyke near Kiama. *J. roy. Soc. N.S.W.* **39**, 65–70.

THOMPSON, J. A., 1916. Report on the inclusions of the volcanic rocks of the Ross Archipelago. *Brit. Antarctic Expedit., 1907–1909, Rept., Geol.* **2**, 129–48.

TILTON, G. R., WETHERILL, G. W., ALDRICH, L. T., DAVIS, G. L., & JEFFERY, P. M., 1956. Ages of ancient minerals. *Yearb. Carneg. Instn.*, No. **55**, 87–100.

TRÖGER, W. E., 1952. *Tabellen zur optischen Bestimmung der gesteinsbildenden Minerale*. E. Schweizerbartsche Verlag: Stuttgart.

TURNER, F. J., 1942. Preferred orientation of olivine crystals in peridotites, with special reference to New Zealand examples. *Trans. roy. Soc. N.Z.* **72**, 280–300.

—— & VERHOOGEN, J., 1951. *Igneous and metamorphic petrology*. McGraw-Hill Inc.: New York.

—— —— 1960. *Igneous and metamorphic petrology*, 2nd ed., McGraw-Hill Inc.: New York.

WAGER, L. R., BROWN, G. M., & WADSWORTH, W. J., 1960. Types of igneous cumulates. *J. Petrol.* **1**, 73–85.

WALKER, F., 1953. The pegmatitic differentiates of basic sheets. *Amer. J. Sci.* **251**, 41–60.

WALKER, G. P. L., & ROSS, J. V., 1954. A xenolithic monchiquite dyke. *Geol. Mag. Lond.* **91**, 463–72.

WASHINGTON, H. S., 1927. The italite locality of Villa Senni. *Amer. J. Sci.* **14**, 173–98.

WILKINSON, J. F. G., 1956. Clinopyroxenes of alkali olivine-basalt magma. *Amer. Min.* **41**, 724–3.

WILSHIRE, H. G., 1959. Deuteric alteration of volcanic rocks. *J. roy. Soc. N.S.W.* **93**, 105–20.

YODER, H. S., & TILLEY, C. E., 1956. Natural tholeiite basalt-water system. *Yearb. Carneg. Instn.*, No. **55**, 169–71.

—— —— 1959. Eclogites. *Yearb. Carneg. Instn.*, No. **58**, 89–94.

ZWAAN, P. C., 1954. On the determination of pyroxenes by X-ray powder diagrams. *Leid. geol. Meded.* **19**, 167–276.

Jadeite Deposits of the Clear Creek Area, New Idria District, San Benito County, California[1]

U.S. Geological Survey, Menlo Park, California, U.S.A.

by R. G. COLEMAN

WITH ONE PLATE

ABSTRACT

Tectonic inclusions within the New Idria serpentine body contain jadeite in two distinct assemblages: (1) Lenslike inclusions containing a monomineralic green jadeite core surrounded by a calc-silicate rim. (2) Jadeite veins cross-cutting albite–crossite schist inclusions. In these veins jadeite coexists with low albite; green jadeite (Jd 75 Ac+Di+He 25) coexists with low albite within the host schist.

Albite schists are related to the pre-metamorphic keratophyres and it can be shown that desilication of such rocks produces a bulk composition similar to that of jadeite. Metamorphism of keratophyric tectonic inclusions within serpentine produced jadeite–albite schists along margins of the inclusions. Jadeite–albite veins formed from mobilized liquids rich in the jadeite molecule and deficient in water. Geological evidence such as would indicate extreme pressures or temperatures during jadeite formation is lacking; rather, a low silica and dry system allowed its formation at reduced temperatures and pressures.

INTRODUCTION

EXPERIMENTAL studies and reports on new occurrences of jadeite within the past ten years have brought this mineral from comparative obscurity to a place of importance in metamorphic petrology. It is the purpose of this paper to describe, in detail, the jadeite occurrence within the New Idria serpentine mass and, in the light of recent experimental evidence, to suggest a genesis.

Jadeite was first recorded in this area by Mielenz (1939) as small grains within quartz–albite–jadeite schist from localized metamorphic zones of the Franciscan formation of Jurassic and Cretaceous age which flanks the New Idria serpentine mass to the west. Within the serpentine mass, jadeite was originally identified by Dr. George Switzer, U.S. National Museum, in stream boulders collected by Bolander (1950) along Clear Creek. This discovery aroused considerable interest, as it was the first recorded occurrence of massive jadeite on the North American continent. Previously, the only known deposits of massive jadeite were those in Tawmaw, Upper Burma; Kotaki District, Niigata Prefecture, Japan; and Motagua Valley of Guatemala. Careful field-work by Yoder & Chesterman (1951) disclosed that the boulders found by Bolander were derived from outcrops along the slopes of Clear Creek. A preliminary mineralogical description was given by Coleman (1954, 1956) as part of a more comprehensive study of the New Idria serpentine mass (Coleman, 1957).

The massive jadeite from this locality forms in rocks distinct from the jadeitic

[1] Publication authorized by the Director, U.S. Geological Survey.

[Journal of Petrology, Vol. 2, Part 2, pp. 209–47, 1961]

metagraywackes described in recent papers by Bloxam (1956, 1959), De Roever (1955), McKee (1958), Seki & Shido (1959), and Shido & Seki (1959). These authors describe jadeitic pyroxene as an essential mineral in metagraywackes composed essentially of quartz–lawsonite–jadeitic pyroxene–glaucophane. Jadeite from Clear Creek occurs with a different mineral assemblage and is of different composition.

GENERAL GEOLOGY

The Clear Creek jadeite deposits are contained within an elongate serpentine dome about 12 miles long and 4 miles wide, situated within the New Idria District, California (Fig. 1). This District is located in the southern extension of the Diablo Range of the California Coast Ranges. The regional geology has been described by Eckel & Myers (1946), Anderson & Pack (1915), Mielenz (1939), Phillips (1939), and Jennings & Strand (1958). Their maps and discussions have been consulted, and in part incorporated into this description. A detailed map has been made of the serpentine mass (Coleman, 1957) and from this map the salient features related to this problem are taken and given in Fig. 2.

Structure. The serpentine mass lies between the San Andreas fault on the west and the Great Valley of California on the east. The sedimentary rocks in this area are folded into a series of anticlines and synclines trending N. 70° W., which is oblique to the N. 40° W. structural trend of the San Andreas fault (Jennings & Strand, 1958). The elongate oval body of serpentine is flanked by the Franciscan formation of Jurassic and Cretaceous age and the Panoche formation of Late Cretaceous age. These flanking sediments and the serpentine mass together comprise an asymmetric anticlinal dome that is the northern extension of the Coalinga anticline. Eckel & Myers (1946) have shown that the north-east flank of the dome is marked by overturned sediments that have assumed this attitude as a result of the irregular New Idria thrust fault which marks part of the serpentine-sediment contact. The remainder of the contact around the serpentine dome is marked by high-angle fault and shear zones. These structural relations suggest that the fault-bounded serpentine mass has moved upward through the Mesozoic sediments.

Serpentine body. The New Idria serpentine mass, as well as other serpentine bodies in the Franciscan formation of the California Coast Ranges, has been considered 'intrusive' into the Jurassic and Cretaceous sediments. Evidence to support intrusive emplacement is lacking. Faulted contacts and the non-existence of contact metamorphism imply that emplacement was effected by tectonic movement rather than by magmatic intrusion; therefore the age of the primary ultrabasic rock cannot be determined by the presently exposed contact relations. The original movement of the ultrabasic 'magma' into the earth's crust may well have been during the period of maximum down-warping of the Franciscan geosyncline. Tectonic movements following the original emplacement

FIG. 1. Index map showing location of the New Idria District, California. After Eckel & Myers (1946).

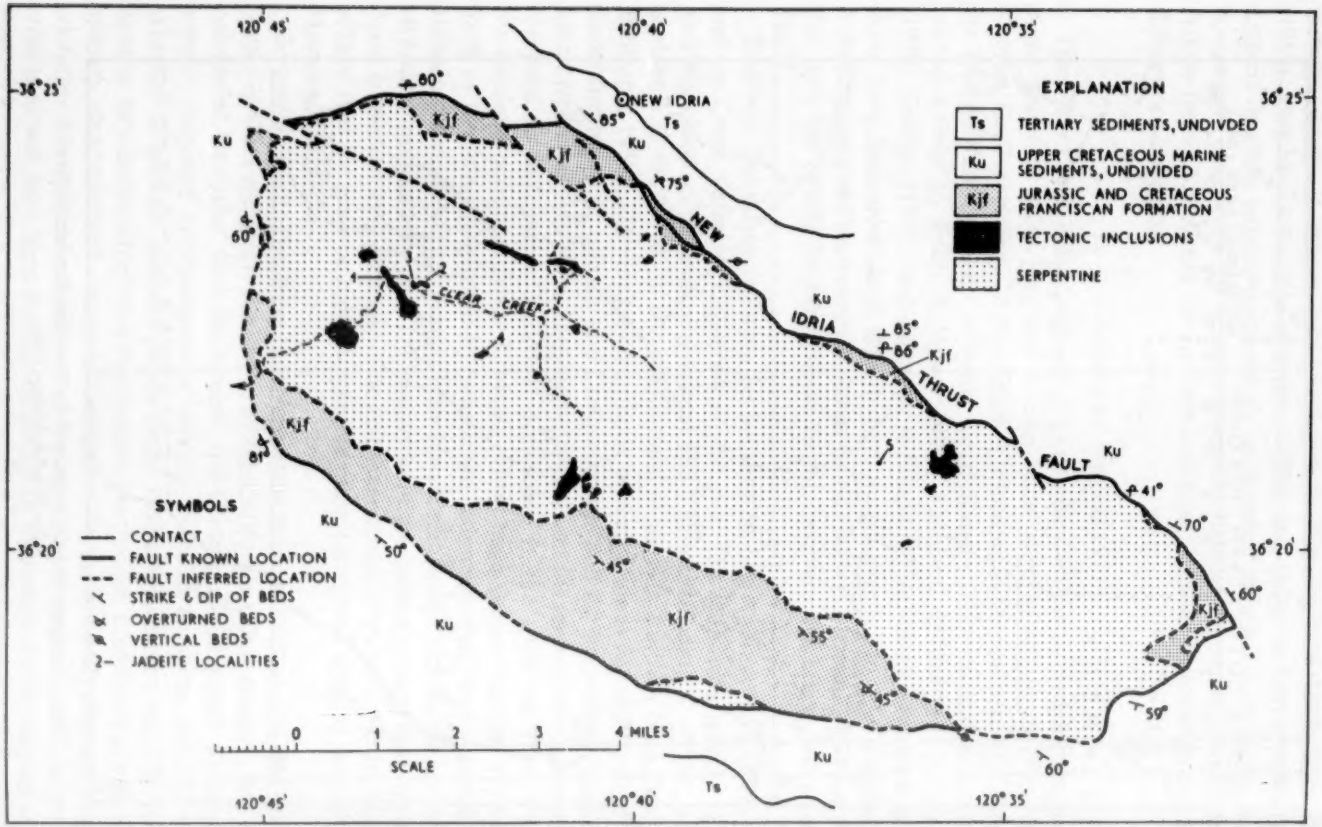

FIG. 2. Simplified geological map of the New Idria serpentine mass showing tectonic inclusions and jadeite localities. Modified from Eckel & Myers (1946).

of the ultrabasic rocks were probably instrumental in starting serpentinization and the squeezing of the mass into its present position. That emplacement of the serpentine was accomplished, undoubtedly, in several distinct stages is demonstrated by the presence of abundant serpentine debris in near-by sediments of three different ages (Eckel & Myers, 1946); Upper Cretaceous (Panoche formation), Upper Middle Miocene (Big Blue serpentinous member of the Temblor formation), and Pliocene (Tulare formation).

Tectonic inclusions. Jadeite-bearing rocks within the serpentine are found in tectonic inclusions. The distribution, size, and shape of the larger bodies are shown in Fig. 2. Smaller bodies associated with the larger masses, not shown on the map, may be less than 10 square feet in areal extent. Some of the larger bodies roughly parallel the regional NW.–SE. structural trend, but the smaller bodies are randomly orientated. Within each separate body the schistosity and planar structures are consistent; however, there is no correlation of these structures between each separate body. The inclusions were derived mainly from graywackes, tuffs, greenstones, spilites, keratophyres, and cherts characteristic of the Franciscan eugeosynclinal suite. In most cases, bedding and igneous textures have not been completely obscured by the attendant metamorphism of these inclusions.

Brothers (1954, p. 616) has described similar rock bodies within serpentines of the Berkeley Hills, California, and has referred to them as tectonic inclusions. Many other serpentine bodies within the California Coast Ranges contain foreign inclusions showing sheared contacts and random orientation. It is recommended that the term 'tectonic inclusions' be used to describe those inclusions, found within serpentines, which show random orientation and structural evidence of having been emplaced within the serpentine by tectonic movements—as originally set forth by Brothers.

The contacts between the serpentine and the inclusions are sheared and faulted; however, in some instances where macro-shearing or faulting are not apparent, microscopic examination reveals shearing and alteration of serpentine to chlorite and andradite. Careful examination of the contacts revealed no evidence of metamorphism, within the tectonic inclusions, that might have resulted from contact with an ultrabasic magma. There is some evidence of metasomatic interchange between the serpentine and inclusions. Sodium-rich pyroxenes are found to invade and replace the serpentine near the contacts and along the borders of smaller pod-like bodies, and introduction of calcium is demonstrated by the development of calc–silicate within the inclusions.

The movement of the tectonic inclusions within the New Idria serpentine mass is extremely difficult to interpret. The tabular and elongate shape of the inclusions, combined with the vertical dip of the bedding or schistosity, indicate vertical movement within the serpentine. Semi-parallel orientation of these inclusions with the bounding faults demonstrates that such an alignment may have developed during the upward squeezing of the semiplastic serpentine.

FIG. 2. Simplified geological map of the New Idria serpentine mass showing tectonic inclusions and jadeite localities. Modified from Eckel & Myers (1946).

These relations suggest that the inclusions were incorporated into the ultrabasic rock during serpentinization, or after serpentinization as part of an intense tectonic movement within the Diablo Range.

Similarity of mineralogy and bulk composition of the tectonic inclusions to the Franciscan formation suggest that the inclusions are blocks of Franciscan emplaced within the serpentine. In no instance were tectonic inclusions found that could be definitely related to rocks younger than Franciscan, nor were there rocks present that could be classed as older basement rocks.

Low-grade metamorphism is characteristic of the tectonic inclusions and is similar to that of the glaucophane schists found within the Franciscan formation. However, the inclusions do not show complete recrystallization and they are uniformly finer grained than typical California glaucophane schist facies rocks. Evidence for retrogressive metamorphism, often described in the glaucophane schists of California, was not found in these inclusions.

Diverse rock types are represented within the inclusions but, as shown by Coleman (1957), their metamorphic grade is that of the glaucophane schist facies as defined by Fyfe, Turner, & Verhoogen (1958). Albite–crossite schists similar to those found within the inclusions are not widely developed within the glaucophane schists of the Franciscan formation; however, their presence has been established by Palache (1894), and Fyfe, Turner, & Verhoogen (1958). Edgar Bailey & Julius Schlocker, U.S. Geological Survey (oral communication, 1960), have also observed albite-blue amphibole schists within metamorphic terrains of the Franciscan formation in central and northern California. A small area of albite–glaucophane–chlorite schist outcrops within the Franciscan formation flanking the north-eastern part of the New Idria serpentine mass. Even though the albite-blue amphibole schists are not well known within the schist terrains of the Franciscan, and chemical analyses are not available to allow a precise comparison, it is evident that the albite–crossite schist tectonic inclusions are similar and can be correlated with albite-blue amphibole schists of similar bulk composition within the Franciscan formation. Jadeite is restricted to these quartz-free albite–crossite schist inclusions within the serpentine mass.

The relations between the albite–blueamphibole schists and the spilite–keratophyre lavas of the Franciscan will be treated in the section on petrology.

MINERALOGY

The mineralogy of the jadeite and the associated minerals is given in detail to characterize the deposits. For this purpose, representative rock types containing jadeite and associated minerals were carefully studied, rather than using the best development of a particular mineral. Mineral separations were made and each mineral identified by optical and X-ray techniques. Paragenetic relations were established from thin sections.

Jadeite. Jadeite from this area assumes varied habits and exhibits a rather wide range in composition. Nearly pure jadeite is found within veins cross-cutting

albite–crossite–acmite schists. Within these veins, jadeite is white with only a faint green tint developing along the vein contact. Earlier generations of green fibrous jadeite associated with albite are developed within the schists containing veins of white jadeite. Green jadeite also forms in pod-like bodies where it commonly exhibits cataclastic deformation and is healed by intersecting veins of white jadeite.

TABLE 1

Chemical analyses and optical properties of the Clear Creek Jd-rich pyroxenes, with atomic ratios

	1	2	3	*Metal atoms to 6 (O)*								
					1			2			3		
SiO_2	59·38	59·06	56·54	Si	1·999	1·999 Z		1·997	1·997 Z		1·981	2·000 Z	
Al_2O_3	25·82	24·62	18·38	Al	—			—			0·019		
TiO_2	0·04	0·08	0·44	Al	1·024			0·980			0·740		
Fe_2O_3	0·45	0·41	5·67	Ti	0·011			0·002			0·011		
FeO	trace	0·18	1·05	Fe^{3+}	0·011	1·042	X	0·010	1·006	X	0·146	1·004	X
MnO	nil	0·03	0·10	Fe^{2+}	—			0·005			0·030		
MgO	0·12	0·17	1·44	Mn	—		1·921	0·001		1·996	0·003		1·988
CaO	0·13	0·35	2·69	Mg	0·006			0·008			0·074		
Na_2O	13·40	14·95	13·00	Ca	0·005			0·012			0·101		
K_2O	0·02	0·01	0·03	Na	0·873	0·879	Y	0·978	0·990	Y	0·882	0·984	Y
H_2O^+	0·22	0·07	0·20	K	0·001			—			0·001		
H_2O^-	0·16	0·03	0·05										
Li_2O	—	nil	0·01										
Cr_2O_3	0·01	—	—										
TOTAL	99·75	99·96	99·60										
S.G.	3·34±0·006	—	—										
α	1·654	1·654	1·679										
β	1·657	1·656	1·681										
γ	1·666	1·666	1·685										
Biref.	0·012	0·012	0·006										
$2V_\gamma$ (+)	70°±2°	70°±2°	64°±2°										
$Z \wedge c$	34°±1°	35°±1°	38°±1°										
Disp.	none	none	$r > v$ strong										
Jd	96·5	97·6	74·3										
Ac	2·4	1·0	15·1										
Di	1·1	0·9	7·5										
He	—	0·5	3·2										

1. White jadeite from veins (54-RGC-58) in albite-green jadeite schist from tectonic inclusions (see Fig. 5), Clear Creek, New Idria District, California (Locality No. 2, Fig. 2). Analyst: W. H. Herdsman, Glasgow, Scotland. Na_2O value is apparently in error as calculation of the formula to 6 (O) reveals a large discrepancy between Z group and the Σ (XY) groups.
2. White jadeite (J31–14) Clear Creek, New Idria District, California (Locality No. 1, Fig. 2). Collected by H. S. Yoder jr. Analysed sample loaned to the author by G. S. Switzer, U.S. National Museum. Analyst: Eileen H. Oslund, Univ. of Minnesota.
3. Green jadeite (J28–7) Clear Creek, New Idria District, California (Locality No. 1, Fig. 2). Collected by H. S. Yoder jr. Analysed sample loaned to the author by G. S. Switzer, U.S. National Museum. Analyst: Eileen H. Oslund, Univ. of Minnesota.

X-ray and optical determinations were made on splits of the analysed samples.

Two analyses of the white-vein jadeite and one of the green jadeite are given in Table 1. White-vein jadeite is very nearly pure Jd ($NaAlSi_2O_6$) whereas the green jadeite contains some Ac ($NaFe^{3+}Si_2O_6$), Di ($CaMgSi_2O_6$), and He ($CaFe^{2+}Si_2O_6$). Calculations of these analyses to the components Jd, Ac, Di, and He were made following the system used by Hess (1949). A chemical comparison of the Clear Creek jadeite with other jadeites and related jadeitic pyroxenes is shown in Fig. 3. From this comparison it can be seen that many of the pyroxenes referred to as jadeite may contain considerable amounts of the

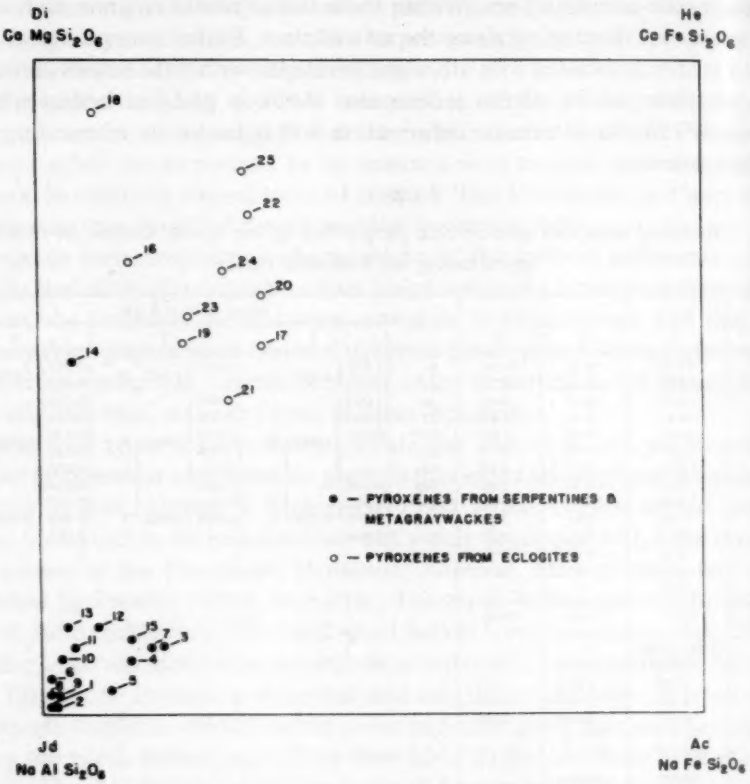

FIG. 3. Chemical variation of jadeitic pyroxenes represented by four components; Jd, Ac, Di, and He.

1, 2, 3. Clear Creek jadeites, see Table 1.

4. Jadeite from quartz–jadeite–lawsonite–glaucophane metagraywacke, 2½ miles N. 17° E. of Valley Ford, Sonoma County, California. Analysed material is impure; 12·55 per cent SiO_2 (quartz) was subtracted from the analysis before calculations were made. Analyst: Eileen H. Oslund, Univ. of Minnesota (Bloxam, 1956). (Jd 80·0, Ac 11·2, Di 6·5, He 2·3.)

5. Jadeite from quartz–jadeite–lawsonite–muscovite metagraywacke (blasto-psammitic quartzite) from Roesek River, between Korontowoe and Pompangeo Mountains 1° 48′ S., 120° 59′ W., Eastern Central Celebes. Analysed material impure; 5 per cent quartz, 0·44 per cent TiO_2 as rutile, and 0·15 per cent H_2O, subtracted by De Roever from analysis. Analyst: J. H. Scoon, Cambridge University (De Roever, 1955). (Jd 87·0, Ac 8·9, Di 2·7, He 1·5.)

6. Jadeite associated with quartz in veins cutting glaucophane schist. Boulders collected 2½ miles north of the Sonoma County–Mendocino County line in the bed of the Russian River, Cloverdale, California. Analysed material impure; 6 per cent quartz subtracted by Wolfe from analysis. Analyst: Eileen H. Oslund, Univ. of Minnesota (Wolfe, 1955). (Jd 93·1, Ac 0·9, Di 5·5, He 0·5.)

7. Jadeite from glaucophane schist, Valley Ford, Sonoma County, California. Supplied by Dr. George Switzer, U.S. National Museum. Analyst: Eileen H. Oslund, Univ. of Minnesota. (Jd 93·1, Ac 0·9, Di 5·5, He 0·5.)

8. Jadeite from Burma (U.S. N.M. No. 94829). It is assumed that this material came from the Tawmaw deposits within the serpentine mass. Analyst: E. G. Zies (Yoder, 1950a). (Jd 97·2, Ac 0·9, Di 1·9, He 0·0.)

9. White jadeite associated with albite in zoned pods surrounded by serpentine from Kotaki District, Niigata Prefecture, Japan. Recalculation of the analysis to fit the pyroxene formula shows the Na_2O determination is in error as in No. 1. Data taken from Yoder (1950a) as derived from Omori (1939) and Kawano (1939). (Jd 94·7, Ac 2·1, Di 3·2, He 0·0.)

10. Green jadeite associated with albite in zoned pods surrounded by serpentine from Kotaki District, Niigata Prefecture, Japan. Comments identical with those above. (Jd 89·2, Ac 2·3, Di 8·0, He 0·5.)

11–15. 'Blue Jade', Mexico. (Jd 86·4, Ac 3·2, Di 8·7, He 0·7.) 12. Jadeite from large pea-green coloured celt, Guatemala. (Jd 80·4, Ac 6·4, Di 11·7, He 1·5.) 13. Jadeite from boulder (No. 2078) tomb, Kaminaljuyu, Guatemala. (Jd 84·5, Ac 1·9, Di 11·9, He 1·7.) 14. Diopside–jadeite rough fragment, Kaminaljuyu, Guatemala. (Jd 44·6, Ac 2·4, Di 50·8, He 2·2.) 15. Chloromelanite from greyish-green celt, Guatemala. (Jd 76·0, Ac 12·2, Di 10·4, He 1·5.) These Meso-American jadeites are associated with low albite and, to a lesser extent, muscovite, sphene, actinolite, and zoisite. Although they have not been found in place, Foshag (1955) suggests that these gemstones form in and near the serpentine bodies of Guatemala. Analyst: Joseph Fahey, U.S. Geological Survey (Foshag 1955, 1957).

16–18. Omphacite in eclogite (omphacite 57 per cent, garnet 34 per cent, quartz-mica 7·9 per cent) from Silden, Nord-

other pyroxene components. For instance, green jadeite (Table 1, No. 3) from Clear Creek contains 25·9 per cent of other pyroxene components, yet it is clearly much closer to pure jadeite composition than much other 'jadeite'. Substitution of other components into pure jadeite produces an increase in the indices and extinction angle, but lowers the density, birefringence, and optic angle. It is not possible at this time, to correlate these changes in optical properties with variation of Ac, Di, and He components within jadeitic pyroxenes. A characteristic of the jadeitic pyroxenes containing between 10 and 30 per cent Di, He, and Ac, however, is worthy of special comment (see especially Nos. 3, 4, 5, and 7, Fig. 3). These pyroxenes have a very strong dispersion ($r > v$) combined with a low birefringence (0·006–0·008) in this compositional range. These properties have been previously observed by Bloxam (1956) and De Roever (1955) for jadeitic pyroxenes within metagraywackes and Shido & Seki (1959) report the same optical character for jadeitic pyroxenes in metamorphosed mafic intrusives. The strong dispersion and low birefringence in jadeitic pyroxenes of this composition may cause serious errors in identification, as clinozoisite could easily be confused with jadeite when the determination is based on a thin-section study.

In Table 2, X-ray diffraction patterns of the analysed jadeites from Clear Creek are compared with jadeitic pyroxene from metagraywacke, and the data given by Yoder (1950*a*) for an analysed Burmese jadeite. The Clear Creek white-vein jadeite closely matches the spacings given for the Burma material; however, the jadeitic pyroxenes rich in Ac, Di, and He components show noteworthy changes in the (330), (441), (310), and (311) spacings. In addition to the shift in *d*-spacings, a weak but persistent peak at 21·0 Å is characteristic for the Ac–Di–He-rich jadeites (Table 2). This peak at 21·0 Å (001?) indicates the possibility of a super cell for jadeites of this composition and having a *c*-dimension exactly four times that given for pure jadeite. These changes reflect an increase in the *a* and *b* cell dimensions as it has been shown by Yoder (1950*a*), Wolfe (1955), Schüller (1958), and Warren & Biscoe (1931), that the *c*-dimension for all pyroxenes is essentially constant. Again, it is apparent that substitution of Di,

---

fjord, Norway. Analyst: P. Eskola. (Jd 22·2, Ac 8·1, Di 64·3, He 6·5.) 17. Omphacite in Duen type eclogite (omphacite 38 per cent, garnet 55 per cent, apatite 5 per cent), Norway. Analyst: L. Thomasen. (Jd 36·4, Ac 16·8, Di 30·0, He 16·8.) 18. Omphacite in eclogite (omphacite 55 per cent, garnet 44·8 per cent) from Rodhaugen, Almklovdalen, Sondmore, Norway. Analyst: P. Eskola. (Jd 3·3, Ac 4·5, Di 88·0, He 4·2.) These are typical omphacites from eclogites (Eskola, 1921).

19. Omphacite in eclogite (omphacite 57 per cent, garnet 28 per cent, glaucophane 2 per cent, hornblende 3 per cent, chloride 4 per cent, sphene 4 per cent, and rutile 2 per cent) from Healdsburg, Sonoma County, California. Analyst: F. A. Gonyer (Switzer, 1945). (Jd 31·4, Ac 11·6, Di 46·9, He 10·1.)

20. Omphacite in eclogite (omphacite and garnet) from Ardintoul, Glenelg, Scotland. Analyst: A. R. Alderman (Alderman, 1936). (Jd 31·5, Ac 11·5, Di 46·9, He 10·1.)

21. Omphacite in eclogite (omphacite, garnet, rutile, and apatite) from Fay, France. Analyst: Raoult (Briere, 1920). (Jd 35·0, Ac 16·9, Di 36·8, He 11·3.)

22. Omphacite in a garnet–hornblende–pyroxene–scapolite gneiss from Ghana, Africa. Pyroxene from this rock is considered transitional between the amphibolite and eclogite facies. Analyst: O. von Knorring (von Knorring & Kennedy, 1958). (Jd 1·8, Ac 11·2, Di 66·0, He 21·0.)

23. Omphacite in eclogite (omphacite and garnet) from Valley Ford, Sonoma County, California. This eclogite is in close association with the jadeite-bearing metagraywackes of this area. Analyst: T. W. Bloxam (Bloxam, 1959). (Jd 32·0, Ac 6·9, Di 45·9, He 15·2.)

24. Omphacite in eclogite (omphacite and garnet), hills west of 'Postman's Path' to Ardintoul, Glenelg, Scotland. Analyst: J. H. Scoon, Cambridge University (Yoder & Tilley, 1959). (Jd 18·7, Ac 13·2, Di 53·3, He 14·8.)

25. Omphacite in eclogite (omphacite and garnet), ½ mile south-east of the Pier, Totaig, Loch Duich, Ross-shire (Yoder & Tilley, 1959). (Jd 6·1, Ac 10·7, Di 63·0, He 20·3.)

TABLE 2

*X-ray powder diffraction data on Jd-rich pyroxenes**

Space Group C_{2h}^{5} hkl	1		8		3		B-48	
	d	*I*	*d*	*I*	*d*	*I*	*d*	*I*
	(Å)		(Å)		(Å)		(Å)	
?	—	—	—	—	21·0	½	21·0	½
110	6·20	2	6·18	1	6·27	2	6·20	2
200	4·50	½	4·49	½	N.O.	—	W.B.	—
020	4·29	4	4·27	3	4·34	2	4·29	3
021	3·25	½	3·25	1	3·26	½	3·25	½
220	3·10	3	3·10	3	3·13	2	3·11	2
221	2·92	7	2·92	8	2·94	6	2·93	5
310, 311	2·83	10	2·83	10	2·85	10	2·84	10
130	N.O.	—	2·68	½	N.O.	—	N.O.	—
202, 002, 131, 112	2·49	4	2·49	2	2·50	2	2·49	2
$\bar{2}21$	2·42	5	2·42	9	2·44	2	2·42	3
$13\bar{1}$	N.O.	—	2·31	½	N.O.	—	N.O.	—
400	N.O.	—	2·24	½	N.O.	—	N.O.	—
312	2·21	1	2·20	2	2·22	1	2·21	1½
022	2·16	½	2·15	1	2·18	1	2·17	½
330	2·067	6	2·067	3	2·081	2	2·073	2
421	2·045	½	2·043	1	2·062	½	2·054	1
420	1·993	½	1·991	½	N.O.	—	1·997	½
041	1·969	4	1·966	1	1·982	½	1·973	1
241	1·888	½	1·887	1	1·914	½	1·892	½
511	1·831	½	1·835	½	N.O.	—	1·842	½
510	1·762	1	1·760	2	1·772	1	1·765	1
422	1·810	½	1·807	½	1·822	½	1·820	½
332	1·683	½	1·683	2	1·698	½	1·689	1
042	1·623	½	1·623	½	1·642	½	1·629	½
313	1·653	½	1·652	½	1·675	½	1·656	½
441	1·573	3	1·570	4	1·583	½	1·577	1
223	1·610	½	1·608	½	1·615	½	1·613	½
440	1·550	2	1·551	1	1·559	½	1·556	½
530	1·523	½	1·523	½	N.O.	—	1·528	½
600	1·499	1	1·498	1	1·502	½	1·504	½
350	1·487	1	1·488	1	W.B.	—	1·497	½

* X-ray patterns were obtained with a Norelco high-angle diffractometer using Cu K_α radiation. *d*-spacings between 3° and 62° 2θ are recorded. $I = I_{hkl}/I_{110}$; N.O. = not observed; W.B. = weak and broad peak.

1. White jadeite (54-RGC-58) from vein. Analysed, Table 1, No. 1 (Jd 96·5, Ac 2·4, Di 1·1).
8. Jadeite from Burma (U.S. N.M. No. 94829). Analysed (Jd 95·8, Ac 0·9, Di 2·9). X-ray data taken from Yoder (1950*a*).
3. Green jadeite (J28-7). Collected by H. S. Yoder jr. Analysed, Table 1, No. 3 (Jd 74·3, Ac 15·1, Di 7·6, He 3·2).
B-48. Jd-rich pyroxene from quartz–jadeite–lawsonite-sericite schist (metagraywacke), Angel Island, San Francisco Bay, California. Analysis of this jadeite pending.

Ac, and He components produce marked changes in the properties of jadeite; however, as shown earlier, it is not possible to determine the effect of each individual component.

Further observations can be made from Fig. 3 that apply directly to the Clear Creek deposits and their relations to other jadeitic pyroxenes described in the literature. From the figure, it is readily apparent that jadeites from serpentines and metagraywackes form a distinct group containing less than 30 molecular per cent of Di, He, and Ac, whereas pyroxenes from eclogites, containing as much as 64 molecular per cent Jd, have a much wider range of solid solution but do not overlap the jadeites. This difference in the two types of pyroxene was defined earlier by Yoder (1950*a*) on the basis of geological association. The present study demonstrates that the pyroxenes from the Clear Creek deposits are clearly different from the omphacites reported from eclogites.

In the discussion to follow, the use of the term '*white* jadeite' will be used to designate pyroxene with at least 95 molecular per cent Jd and '*green* jadeite' will be used to describe pyroxene containing 5–30 molecular per cent of combined Di, Ac, and He. Optical and X-ray studies of various types of green jadeite, both in the pods and in albite–jadeite schists, demonstrate that their composition is similar to the analysed green jadeite (Table 1, No. 3).

Within the albite–crossite schists, small porphyroblasts of a green pyroxene are commonly developed along iron-rich stringers of the schists. Insufficient material was available for analyses, but the determined optical properties are similar to those of acmite: $\alpha = 1{\cdot}740 \pm 0{\cdot}002$; $2V_{\gamma} = 75$–$80°$ (−), $X \wedge c = 16°$, X = light green, Y = colourless, Z = light yellow. Similar pyroxenes (Ac 48±, Jd 7±, Di 45±) are reported from albite–aegirine–augite and aegirine–augite–blue amphibole–garnet–albite–quartz schists from Sikoku, Japan (Banno, 1959).

Albite. Plagioclase is a common associate of jadeite formed within the schistose tectonic inclusions, but within the pod-like jadeite deposits albite is not present. The following discussion, therefore, will refer only to albite coexisting with jadeite in veins or as a major constituent of the schist making up the tectonic inclusions.

Coarsely crystalline, vein albite develops as radiating clusters intergrown with, or partially replacing, jadeite. Later veins of albite cut the jadeite veins and within these late veins albite is intergrown with pectolite and thomsonite. Simple albite twinning is observed in some grains, but many individuals do not exhibit twinning. Within the tectonic inclusions, albite may make up as much as 50 per cent of the schists. Here the albite is extremely fine-grained and untwinned; however, the larger porphyroblasts of albite within the groundmass are characterized by simple albite twinning.

To establish the composition of the albite it was separated from the veins and schists by carefully controlling a bromoform–acetone mixture between a density of 2·64 and 2·65, and centrifuging. This density suggested a compositional range near that of pure albite, which was confirmed by a spectrographic analysis of the

vein feldspar (0·1–0·5 per cent Ca, and less than 0·3 per cent K). The structural state was established by the X-ray diffraction technique described by J. V. Smith (1956) and J. R. Smith & Yoder (1956).

TABLE 3

Composition of the plagioclase determined by the separations ($\bar{1}32$–131), (131–$1\bar{3}1$), *and* (111–$1\bar{1}1$) *after J. V. Smith* (1956)

	$\bar{1}32$–131	% An	131–$1\bar{3}1$	% An	111–$1\bar{1}1$	% An
54-RGC-58 Albite from jadeite veins; analysed jadeite from same specimen	2·725	2·0	1·051	0·0	0·48	2·0
54-RGC-58-1 Albite from albite–crossite schist*	2·72	3·0	1·10	2·0	0·47	1·0
54-RGC-58-2 Albite from albite–crossite–stilpnomelane schist	2·725	2·0	1·053	0·0	0·48	2·0
54-RGC-58-3 Albite from albite–crossite–acmite schist	2·735	1·3	1·10	2·0	0·46	0·0
54-RGC-58-4 Albite from albite–crossite schist	2·73	2·0	1·095	2·0	0·48	2·0
54-RGC-58-5 Albite from albite–crossite–acmite schist	2·705	3·0	1·062	0·0	0·46	0·0
54-RGC-58-6 Albite from albite–crossite schist (analysed rock, see Table 8, No. 3)	2·715	3·0	1·09	1·8	0·48	2·0
54-RGC-58-7 Albite from albite–crossite schist	2·71	2·6	1·043	0·0	0·45	0·0
54-RGC-58-8 Albite from albite–crossite–acmite schist	2·72	3·0	1·07	0·4	0·47	1·0
54-RGC-58-9 Albite from albite–crossite–acmite schist	2·72	3·0	1·08	1·0	0·45	0·0

* Schist samples represent a series of samples taken across the tectonic inclusion shown in Fig. 4.

The separation 2θ ($\bar{1}32$)–2θ (131) on all samples ranged between 2·705 and 2·735 (Table 3). From fig. 4 of J. V. Smith's paper, these values all fall close to the low-temperature curve at Ab_{100} composition. Measurements of the separation 2θ (131)–2θ ($1\bar{3}1$) gave values ranging from 1·05 to 1·10, which, from fig. 3 of Smith, correspond to compositions lying between An_0 and An_2 (Table 3). Thus, as suggested by Smith, the separations 2θ ($\bar{1}32$)–2θ (131) and 2θ (111)–2θ ($1\bar{1}1$) can be used to establish the composition of low albites, as has been done in Table 3.

It has been pointed out by J. R. Smith & Yoder (1956), J. V. Smith (1956), and MacKenzie (1957) that the values so determined are only reliable within ± 2 per cent An and that curves constructed from synthetic and natural feldspars may be valid only for those plagioclases used to establish them. However, the composition and structural state of the albite associated with the jadeite is now as well known as it conveniently can be, namely, between An_0 and An_2 and of the low form.

Zeolites. The presence of zeolites was established in all the tectonic inclusions bearing jadeite; however, some zeolites were restricted in their distribution.

Identification was based on optical and X-ray powder patterns of separated fractions obtained from the various rock types.

Thomsonite is present within the jadeite vein systems of the tectonic inclusions and also within the calc–silicate zone surrounding the pod-like jadeite bodies. It occurs as equigranular aggregates rarely exhibiting euhedral forms. Natrolite and pectolite occur as inclusions or are intergrown with the thomsonite. X-ray diffraction and optical data for thomsonite from the calc–silicate zone surrounding the jadeite pods are given in Table 4. Following Hey's (1932) data for thomsonite, this material must have a composition near that of the calcium-rich types.

TABLE 4

*X-ray diffraction and optical data for thomsonite**

d (Å)	*I*	*d* (Å)	*I*	*d* (Å)	*I*	*Optics*
6·55	50	3·52	60	2·69	60	$\alpha = 1{\cdot}528 \pm 0{\cdot}002$
5·94	10	3·29	15	2·585	20	$\beta = 1{\cdot}529 \pm 0{\cdot}002$
5·40	10	3·22	15	2·437	10	$\gamma = 1{\cdot}541 \pm 0{\cdot}002$
4·65	100	3·19	15	2·259	30	$2V(+) = 50°$ *ca*
4·39	15	2·96	20	2·197	60	
4·15	50	2·93	20	2·181	60	

Cu K_α radiation; $I = I_{hkl}/I_{100}$; *d*-spacings given for first 18 lines.

* Thomsonite associated with pectolite and hydrogarnet in veins cutting calc-silicate zone, jadeite pods (105-RGC-58), shown in Fig. 6.

Natrolite tends to crystallize as equigranular masses similar to thomsonite. However, within the jadeite vein system of the tectonic inclusions, it may be seen as large radiating groups intergrown with pectolite. It is most abundant within the veins and is of only minor importance in the calc–silicate zone of the jadeite pods. The following optical constants were obtained on the natrolite from veins cutting schist: $\alpha = 1{\cdot}476 \pm 0{\cdot}002$, $\beta = 1{\cdot}478 \pm 0{\cdot}002$, $\gamma = 1{\cdot}488 \pm 0{\cdot}002$, $2V(+) = 56° \pm 2°$.

Analcime is the least abundant zeolite and is generally restricted to veins within the tectonic schist inclusions. It replaces jadeite and/or albite as irregular wormy patches. Recent work by Saha (1959) on natural and synthetic analcimes allows us to estimate its composition by use of refractive index and unit cell measurements. For the Clear Creek analcime, a unit cell of 13·74 Å and a mean index of refraction of $1{\cdot}488 \pm 0{\cdot}003$ were recorded. Using figs. 1 and 3 of Saha (op. cit., pp. 303, 304) the molecular ratio of SiO_2 was found to be 4, and from this we can say that the composition of this analcime is very near the ideal, i.e $NaAlSi_2O_6 . H_2O$.

Hydrogrossular. Within the calc–silicate zone surrounding the jadeite pods, hydrogrossular forms as irregular masses intergrown with pectolite and thomsonite. Late veins of thomsonite–pectolite invading the calc–silicate rim contain irregular blebs of hydrogrossular closely associated with pectolite. Individual grains within these veins exhibit distinct zoning manifested by differences in

refractive index; the indices increase from the core outward. Hydrogrossular was not identified in the veins cutting the tectonic inclusions.

To establish the compositional range of the hydrogrossular in the calc-silicate zone and in the later veins cutting it, −300 mesh material was centrifuged in liquids of known densities to produce a series of fractions. The resultant density fractions, although contaminated with pectolite, were used to establish the refractive index and unit cell constants of the hydrogrossular (Table 5). It should be noted that the refractive indices suggest a wider range in composition than do the unit cell determinations, as the X-ray values represent an average

TABLE 5

*Physical constants for hydrogarnets and the composition determined from the refractive index, density, and unit cell size**

Garnet from	*Refractive index*	*Density*	*Unit cell in Å*	*Composition range*
Thomsonite–pectolite veins	1·643–1·700	2·92–3·31	11·98–12·15	$1{\cdot}5H_2O$ to $3H_2O$
Calc–silicate zone	1·67 –1·691	3·00–3·25	12·05–12·09	$2H_2O$ to $2{\cdot}5H_2O$

* Samples taken from pod-like body shown in Fig. 6.

value, whereas the lowest and highest indices are given. Using the data of Hutton (1943, p. 174), Yoder (1950*b*, p. 243), Flint *et al.* (1941), and Carlson (1956) on the grossularite–isometric tricalcium alumina hexyhydrate solid-solution series, the compositional range of the two occurrences was estimated.

To check the validity of the estimated hydrogrossular compositions, a fraction nearly free from pectolite was used by the author for a quantitative water determination. Total water was calculated as loss of weight after being heated in a platinum crucible at 900° C for 2 h in a muffle furnace. This fraction has an average refractive index of $1{\cdot}675 \pm 0{\cdot}005$ and a unit cell edge of $12{\cdot}06 \pm 0{\cdot}01$ Å, which correspond to hydrogrossular containing 2·40 moles of H_2O. The water determination gave 12·40 per cent H_2O, equivalent to 2·48 moles of H_2O in the hydrogarnet formula. Assuming, then, that the values so obtained are an estimate of the hydrogrossular composition in the series $3CaO.Al_2O_3.3SiO_2$–$3CaO.Al_2O_3.6H_2O$, the hydrogrossulars within the calc–silicate zone range in composition from $3CaO.Al_2O_3.1{\cdot}5SiO_2.3H_2O$ to $3CaO.Al_2O_3.2{\cdot}25SiO_2.1{\cdot}5H_2O$.

Using the nomenclature of Hutton (1943), these would fall in the hydrogrossular series which includes 'hibschite' (Pabst, 1942), 'plazolite' (Foshag, 1920), and 'grossularoid' (Belyankin & Petrov, 1941). According to Hutton, no natural minerals in this series more hydrous than 'plazolite' have been found. The Clear Creek material, therefore, appears to be the first recorded hydrogrossular to contain nearly 14 per cent H_2O.

Pectolite. Considerable difficulty was experienced in establishing the identity of pectolite within the Clear Creek rocks. The fibrous and fine-grained nature of

this material makes it difficult to handle by optical techniques and originally it was reported as prehnite (Coleman, 1954). The refractive indices and density are nearly identical for pectolite and iron-free prehnite, and as pectolite is elongated on the *b*-axis ($Z \wedge b = 1$–$2°$) it can easily be mistaken as having the orthorhombic symmetry of prehnite. Furthermore, the strongest lines of X-ray patterns for these two minerals coincide, particularly those at 3·08 Å. X-ray powder patterns

TABLE 6

Analyses and optical data for pectolites

	1	2	3	*Atomic ratios for No. 1*		
SiO_2	53·84	54·23	52·99	Si 2·993	3·00	
Al_2O_3	0·16	—	—	Al 0·010		
FeO	0·07	—	0·15	Fe 0·003	2·02	
MgO	0·09	—	—	Mn 0·002		
CaO	33·74	33·74	32·98	Mg 0·006		
Na_2O	8·82	9·32	8·97	Ca 2·010		
MnO	0·04	—	—	Na 0·951	0·95	
K_2O	0·019	—	—	K —		
H_2O^+	2·96	2·71	3·30	OH 1·097	1·10	
SrO	0·002	—	—			
CuO	0·004	—	—			
Others	—	—	0·56			
TOTAL	99·75	100·00	98·95			
H_2O^-	0·10	—	—			
S.G.	2·86±0·005	2·86	2·86			
α	1·598±0·003	1·595	1·595			
β	1·606 (calc.)	1·605	1·604			
γ	1·623	1·633	1·632			
Biref.	0·026	0·038	0·037			
$2V$ (+)	35°±5°	63°	60°			

1. Pectolite (6-RGC-58) from tectonic inclusion in serpentine, Myrtle Creek, Oregon. Analytical separates by Sarah T. Neil; spectrographic analysis of separates: Raymond G. Havens and Arthur A. Chodos; calculations by Rollin E. Stevens and Sarah T. Neil.
2. Theoretical pectolite from Schaller (1955).
3. Pectolite from Japan, by Harada, as taken from Schaller (1955); 0·56 per cent listed as 'others' was not specified.

of this material, obtained at a later time, were found to match very closely prehnite patterns available to the author. Unfortunately, published X-ray powder patterns of pectolite exhibited many variations in intensity or spacings and did not appear to match the Clear Creek material, and it was not until an analysis was made that the identity of the Clear Creek pectolite was established.

An excellent sample of pectolite from a tectonic inclusion within a serpentine body near Myrtle Creek, Oregon, was purified and chemically analysed (Table 6). Its composition is identical with the manganese and iron-free pectolites described by Schaller (1955); however, the gamma index, $2V$, and birefringence of the Oregon material are lower than the values given by Schaller (1955). The X-ray powder data agree fairly well with those given by Schaller (1955) and Hildebrand (1953) except that the intensities are not comparable. These differences could be explained by preferred orientation—a common problem with

fibrous minerals, as shown by Hildebrand. Comparison of the X-ray data for the Oregon pectolite and the Clear Creek material demonstrates their similarity (Table 7). Optical determinations are identical with all samples showing the anomalously low gamma index (1·623), birefringence, and $2V$. No apparent explanation can be found for the optical discrepancies between these pectolites and those described in the literature.

TABLE 7

X-ray diffraction data for pectolite

1		2		3		4	
d	*I*	*d*	*I*	*d*	*I*	*d*	*I*
7·76	10	7·76	5	7·80	10	7·83	5
6·98	10	7·14	10	7·03	10	7·03	5
5·45	10	5·45	5	5·47	10	5·50	5
3·88	50	3·88	30	3·88	40	3·90	6
3·50	40	3·50	50	3·50	50	3·52	5
3·30	70	3·30	60	3·31	60	3·33	6 B
3·26	80	3·26	75	3·27	60	3·28	
3·08	100	3·08	100	3·08	100	3·10	8
2·90	50	2·90	80	2·91	50	2·921	10
2·73	40	2·72	60	2·73	30	2·729	6
2·59	50	2·59	50	2·59	40	2·600	6
2·417	5	Not observed		Not observed		2·430	5
2·327	10	2·339	10	2·334	10	2·338	5
2·292	40	2·292	20	2·295	30	2·298	6
Not observed		Not observed		Not observed		2·227	2
2·181	10	2·176	5	2·184	10	2·191	6 B
2·161	10	Not observed		2·166	5	2·166	

1. Analysed pectolite (6-RGC-58) from tectonic inclusion in serpentine, Myrtle Creek, Oregon.
2. Pectolite (104-RGC-58 (2)) from calc–silicate zone surrounding jadeite pods (Fig. 6).
3. Pectolite (104-RGC-58 (4)) from late veins in calc–silicate zone surrounding jadeite pods (Fig. 6).
4. Pectolite from Bergen Hill, New Jersey. U.S. N.M. 82952, Schaller (1955).
Cu K_α radiation diffractometer; $I = I_{hkl}/I_{100}$; partial patterns, B-broad.

Identification of the hydrated calcium aluminum silicates such as pectolite and prehnite is difficult in fine-grained metamorphic rocks and it is suggested that such determinations be based on careful optical and X-ray determinations.

Other minerals. Within the jadeite-bearing rocks and the associated schists are various minerals whose optical and other properties are listed below.

A fibrous blue amphibole within the schist bodies forms delicate needles, aggregates of fibrous bundles, or 'whisker-like' mattes. The optical character is similar to that given for crossite: $\beta = 1{\cdot}662 \pm 0{\cdot}002$, $Y \wedge c = 30$–$40°$, $2V = 10$–$20°$ (−), X = yellow, Y = greenish blue, Z = deep blue.

Red-brown stilpnomelane is a common associate of the blue amphibole within the albite–crossite schists. Using Hutton's (1956) data for the stilpnomelane group, the optical character of the Clear Creek stilpnomelane indicates a $(Fe^{2+}, Mn, Mg)\,0 : (Al, Fe^{3+})_2O_3$ ratio of about 1:1 ($\gamma = 1{\cdot}69 \pm 0{\cdot}005$, $2V = 0°$ (−), X = dark greenish brown, $Y = Z$ = light yellow-brown).

The chlorite associated with the thomsonite–pectolite–hydrogrossular in the

calc–silicate zone of the jadeite pods has the following optical properties: $\beta = 1{\cdot}59 \pm 0{\cdot}005$, $2V = 5$–$10°$ (−) X = light yellowish brown, $Y = Z$ = dark brown, birefringence moderate.

Carbonates are present both in the albite–crossite schists and in the calc–silicate zone of the jadeite pods. The density range for most of these carbonates was found to be between 2·90 and 3·00. The optics are $\alpha = 1{\cdot}530$, $\gamma = 1{\cdot}685$, $2V$ = approx. 20° (−), and the X-ray pattern match the standard for aragonite. On the basis of this data, the carbonate associated with the Clear Creek jadeite deposits is tentatively called aragonite.

Green biotite from veinlets within the jadeite pods has the following optics: $\beta = 1{\cdot}64$, $2V$ = small (−). This is the only mica found in these deposits.

Native copper is present as small isolated blebs (less than 1 mm) within the jadeite pods; the total amount is not significant enough to warrant more than a mention of its presence.

PETROLOGY OF THE JADEITE-BEARING ROCKS

Those rock types genetically associated with the jadeite deposits will be described in detail. The fine-grained nature of these rocks precludes any statements on the modal composition. Two distinct environments have been recognized for the jadeite deposits: (1) tectonic inclusions of schist containing jadeite as an essential mineral or in cross-cutting veins, and (2) pod-like bodies characterized by a central core of jadeite surrounded by a calc–silicate rim. In the discussion to follow, these two types will be treated separately.

Tectonic inclusions. As shown earlier, the tectonic inclusions within the serpentine mass have lithologies that are similar to the units that make up the Franciscan formation. Jadeite develops only within particular types that are high in albite and contain no free quartz. The typical greenstones and graywackes present within the serpentine mass as tectonic inclusions do not contain jadeite.

A detailed sketch-map of one of these jadeite-bearing inclusions is shown in Fig. 4. This body is composed of a very fine-grained banded schist. Slaty cleavage developed parallel to the original bedding, and cross-joints normal to the bedding, contain jadeite–albite grading into albite–zeolite minerals. The banded schist is light grey-green to dark bluish green according to the minerals developed along the original bedding planes.

Under the microscope, these rocks are fine-grained (0·1–0·5 mm grain size) with the largest individual grains rarely exceeding 0·3 mm. Albite, the most abundant mineral, forms an equigranular mosaic groundmass. Polysynthetic twinning is rarely developed in the groundmass feldspar; however, larger porphyroblastic grains commonly exhibit simple albite twinning. Crossite is the dominant dark mineral (5 to 25 per cent of the schist) forming delicate needles along shear planes, aggregates of fibrous bundles, or 'whisker-like' mattes.

Acmitic pyroxene, ubiquitous in these schists, makes up to 5 per cent of some

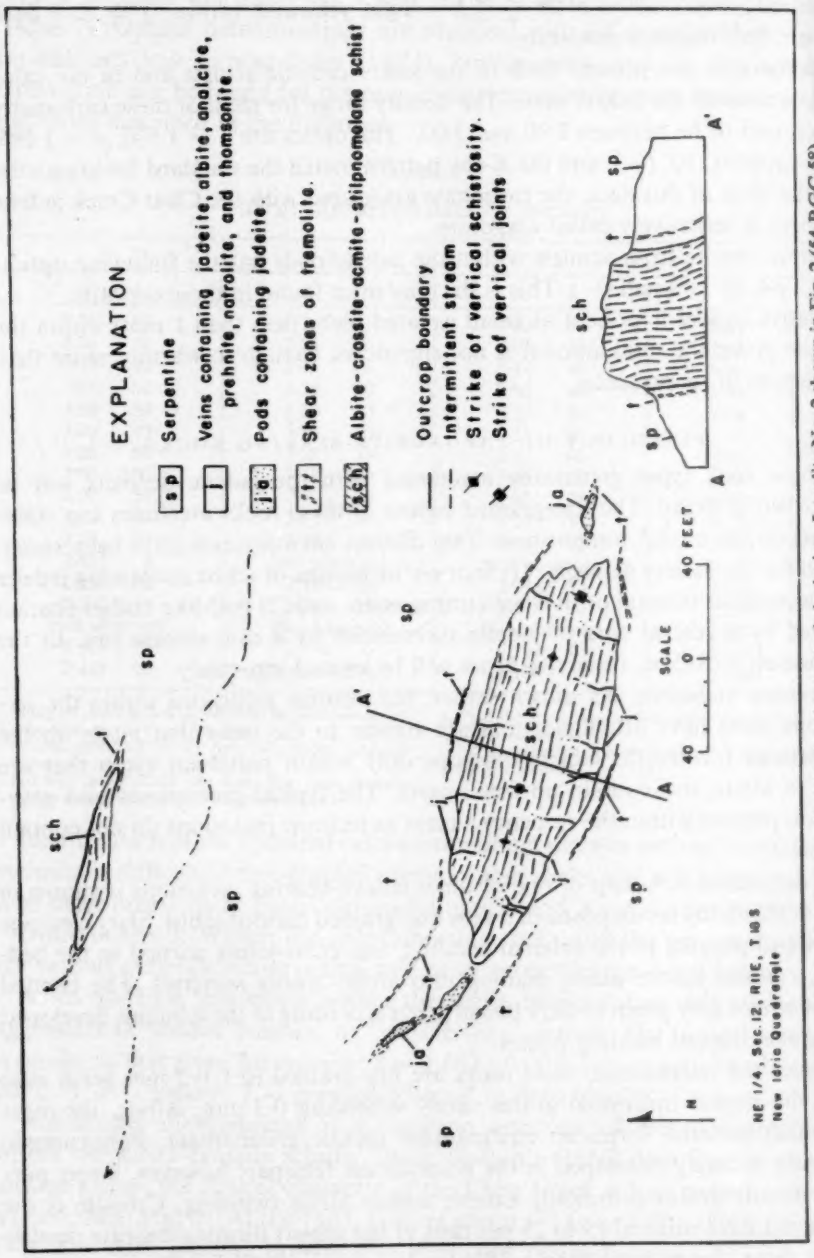

FIG. 4. Geological sketch-map of jadeite-bearing tectonic inclusion, Locality No. 2 shown in Fig. 2 (54-RGC-58).

of the darker-coloured schists. Its formation is favoured along shear planes containing abundant opaque material, and many grains characteristically contain relict opaque grains in their core. Sphene, pleochroic from pink to colourless, commonly forms in the opaque shear planes with the acmite. Stilpnomelane is a common accessory mineral of these schists, but rarely exceeds 1 or 2 per cent of the rock. Zircon was recognized in all the heavy residues (S.G. $> 2{\cdot}86$) of these schists.

Opaque material is concentrated along shear planes, forming crude segregation bands, and here blue amphibole, sphene, stilpnomelane, and acmite become concentrated. These opaque bands probably contained iron and titanium oxides that gave rise to the iron-rich silicates. Quartz was not found in any of the albite–crossite–stilpnomelane–acmite schists.

Folia paralleling the schistosity, within the lighter-coloured rocks, contain pectolite, albite, and carbonate. The minerals within the folia are late as they extend outward and partially replace the fine-grained schist.

In limited areas, along the margins of the tectonic inclusions, the albite–crossite schist grades into a much denser rock (S.G. $= 3{\cdot}10$) containing essentially fibrous, green, Jd-rich pyroxene intergrown with albite and banded by opaque stringers containing sphene. X-ray and optical determinations on this fibrous pyroxene suggest a composition similar to the analysis No. 3 in Table 1 (approximately 75 per cent Jd+25 per cent Ac, Di, He). Cross-joints developed in the green jadeite–albite schists are filled with white jadeite (Pl. 1). The joints form in the '*a*–*c*' plane of deformation and show no differential movement. The jadeite crystallized inward from the joints and in the central portions may be intergrown with low albite. Later shearing movements have offset the veins in some areas and albite is found healing shears and replacing the jadeite. Analcime is found replacing both the jadeite and albite in restricted areas within the veins (Fig. 5). The contacts between the jadeite–albite veins and the schist are sharp and replacement of schist by the vein material was not observed.

Tracing the jadeite–albite-filled '*a*–*c*' joints from the edge of the tectonic inclusion inward, jadeite is replaced by albite and zeolites. Natrolite and thomsonite predominate inward and form radial crystals that grow outward from the vein walls. Fibrous pectolite infills the interstices between the larger zeolite crystals.

Other tectonic inclusions within the area containing jadeite reveal the same pattern of jadeite deposition. These inclusions are also dominantly albite-rich schists lacking in free quartz and with greater or lesser amounts of stilpnomelane, crossite, and acmite. In the large inclusion (Fig. 2, Locality No. 1) small jadeite masses are present within the centre of the mass as well as along its margins. These all show transition from albite–crossite–stilpnomelane schists into green jadeite–albite rocks and there can be little doubt that this transformation took place with minor metasomatism.

Pod-like jadeite deposits. These bodies form bold resistant outcrops and have

a very indistinct contact with the serpentine country rock (Fig. 2, Locality No. 3; Fig. 6). Following the usage of Brothers (1954) these bodies could also be classed as tectonic inclusions; however, their small size and peculiar zonation place them in a different category from the schist inclusions previously described.

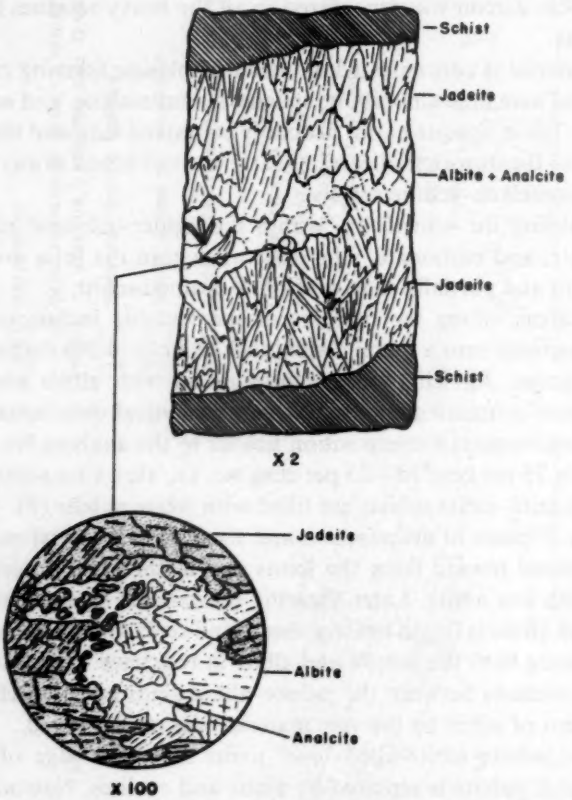

FIG. 5. Sketch of jadeite vein showing relations between jadeite, albite, and analcite. The enclosing schist contains green jadeite and albite. Locality No. 2 shown in Fig. 2.

Near the contact, the serpentine is sheared into ellipsoidal fragments that are veneered by a thin film of black, glassy antigorite completely surrounding bodies of chrysotile. This gives way to an earthy, weathered, chloritic material at the contact, showing extreme cataclastic movement. The outer rim of the pod is a tough, greenish to brown, fine-grained rock composed essentially of fibrous pectolite, hydrogarnet, thomsonite, and sphene. The sphene is concentrated in distinct bands reminiscent of bedding or schistosity, although the other minerals within the rock form an extremely fine matte of interlocking grains.

This outer zone grades imperceptibly into a similar rock that is brownish,

with a cavernous weathered surface. It also is composed of an interlocking matte of thomsonite, pectolite, and hydrogarnet, with late veins of hydrogarnet. Irregular patches of carbonate, showing a peculiar sieve-texture, are common throughout the rock. Again, sphene forms segregated bands that appear to be

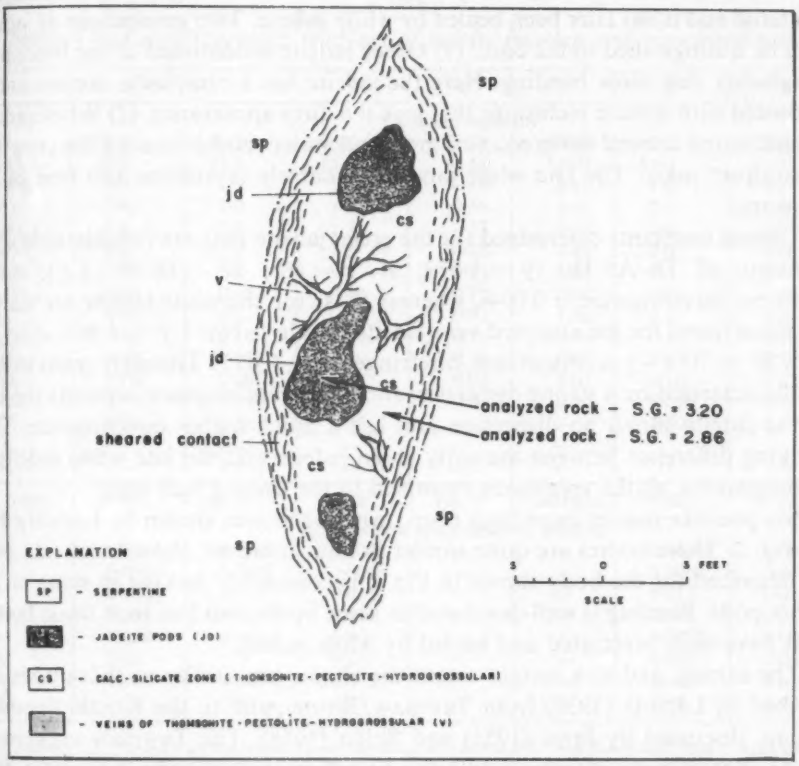

FIG. 6. Geological sketch-map of pod-like jadeite body, Locality No. 3, Fig. 2 (105-RGC-58).

relicts of original bedding. Pale greenish-brown chlorite is concentrated along shear planes. Within this calc–silicate zone, irregular white veins and pockets permeate and replace the greenish-brown rock (Fig. 6). These late veins contain mostly thomsonite with small blebs of natrolite as a mosaic aggregate. Pectolite crystallizes in isolated fibrous bundles associated with irregular patches of hydrogarnet. The compositions of the hydrogrossular from this rock were given in Table 5. The zone of hydrated calcium–aluminium silicates grades into a central pod of jadeite. Where the two zones meet, there is an area, several inches wide, of interpenetrating jadeite and calc–silicates. Although some replacement of jadeite is noted within an inch of this contact, no replacement of jadeite was found extending into the jadeite core.

The core is almost monomineralic, except for small veinlets of zeolites and

biotite. Small but persistent clots of native copper are present throughout the jadeite core. No apparent structures can be observed in this core; however, when large slabs are cut, a crude banding or schistosity is revealed. This banding is crumpled and tightly folded, similar to that observed in the albite–crossite-acmite schist. The banding is not continuous, as fracturing has brecciated this material and it has later been healed by white jadeite. Two generations of jadeite can be distinguished in the core: (1) Green jadeite is dominant in the brecciated fragments that show banding. Here the jadeite has a cataclastic texture and is crowded with minute inclusions that give it a dirty appearance. (2) White jadeite forms in and around the brecciated green jadeite as veinlets healing the core into a compact mass. The late white jadeite is coarsely crystalline and free of inclusions.

Optical constants determined for the green jadeite indicate considerable solid solution of Di–Ac–He ($\gamma = 1{\cdot}679$, $Z \wedge c = 40°$, $2V = 66$–$86°$ (+), $r > v$ extreme, birefringence = 0·004), whereas those for the white jadeite are similar to those found for the analysed vein jadeite (Table 1, No. 1 $\gamma = 1{\cdot}666$, $Z \wedge c = 34°$, $2V = 70°$ (+), no dispersion, birefringence = 0·012). The early green jadeite is characterized by a strong dispersion and lower birefringence, whereas the late white jadeite shows no dispersion and has a much higher birefringence. This striking difference between the early green jadeite and the late white jadeite is consistent for all the specimens examined in the Clear Creek area.

Six pod-like masses have been found within the area shown by Locality No. 3, Fig. 2. These bodies are quite similar in size; however, the calc–silicate zone as described for the body shown in Fig. 6 is completely lacking in some of the other pods. Banding is well-developed in some bodies but less so in those bodies that have been brecciated and healed by white jadeite.

The zoning, and to a certain extent the shape, are similar to those pods described by Lacroix (1930) from Tawmaw, Burma, and to the Kotaki deposits, Japan, discussed by Iawo (1953) and Shido (1958). The Tawmaw occurrence has a central zone of jadeite followed by albite–jadeite and albite zones that grade outward into amphibolite at the serpentine contact. The Kotaki bodies exhibit similar zoning, with a central core of albite and some free quartz followed by a thin rim of jadeite which in turn gives way to an amphibolite zone at the serpentine contact.

The association of pods with larger tectonic inclusions and the relict banding of these bodies indicate a probable common source rock for all the jadeite-bearing rocks in the Clear Creek area. The chemical composition, as discussed next, provides further evidence of this relationship.

CHEMISTRY OF THE JADEITE-BEARING ROCKS

From the previous discussions concerning the mineralogy of the jadeite-bearing rocks and the associated rocks, it is apparent that their chemical composition is indeed unusual. Table 8 presents analyses of three selected rocks

representative of the Clear Creek area, two graywackes of the Franciscan formation, and two quartz keratophyres from the Del Puerto volcanics Franciscan formation of Maddock (1955). The schists characteristic of the tectonic inclusions are represented by the albite–crossite schist (No. 3). The variation between the

TABLE 8

*Chemical and spectrographic analyses of jadeite-bearing and associated rocks**

	1	2	3	4	5	6	7
	Chemical analysis						
SiO_2	57·1	37·2	64·8	77·08	68·04	68·2	72·9
Al_2O_3	20·9	13·8	15·8	12·43	12·09	13·0	11·3
Fe_2O_3	2·3	1·3	1·6	1·48	3·81	1·6	1·1
FeO	0·63	3·6	1·8	0·55	3·21	2·7	2·8
MgO	1·4	2·6	1·7	0·23	1·97	2·4	2·7
CaO	2·6	25·9	2·3	0·88	3·41	2·0	0·60
Na_2O	13·3	2·8	9·8	6·13	5·04	2·2	3·8
K_2O	0·09	0·48	0·40	0·15	0·00	2·2	0·90
H_2O^+	0·35	6·3	0·52	0·92	1·89	3·2	2·2
H_2O-	0·12	0·38	0·12	0·31	0·54	0·50	0·39
TiO_2	0·46	0·90	0·49	0·22	0·46	0·62	0·56
P_2O_5	0·04	0·00	0·07	0·02	0·05	0·10	0·12
MnO	0·07	0·14	0·10	0·07	0·10	0·08	0·20
CO_2	0·25	0·59	0·36	—	—	1·00	0·15
SO_3	—	< 0·05	—	—	—	—	—
BaO	—	3·4	—	—	—	—	—
TOTAL	99·61	99·39	99·86	100·47	100·61	99·80	99·72
	Quantitative spectrographic analysis						
Co	0·0008	0·0009	0·0008	—	—	0·0008	0·0010
Ni	0·0026	0·0037	0·0026	—	—	0·0069	0·0082
Cr	0·0066	0·010	0·0066	—	—	0·012	0·014
Zr	0·013	0·022	0·013	—	—	0·016	0·014
Sr	0·030	0·045	0·030	—	—	0·0072	0·0029
Ba	0·25	†	0·25	—	—	0·062	0·086
B	0·002	0·31	0·002	—	—	0·008	0·007
S.G.	3·20	2·86	2·75	—	—	2·75	2·62

* Analyses 1, 2, 3, 6, and 7 are Rapid rock determinations as described in U.S. Geol. Survey Bull. 1036-C. Analysts: Paul L. D. Elmore, Ivan H. Barlow, Samuel D. Botts, Marvin D. Mack. Quantitative spectrographic analyses by Harry Bastron.
† Ba determined gravimetrically.

1. Jadeite core from pod (105-RGC-58-3) (Fig. 6).
2. Pectolite–thomsonite–hydrogrossular rock from jadeite-bearing pod (105-RGC-58-2) (Fig. 6).
3. Albite–crossite schist from jadeite-bearing tectonic inclusion (54-RGC-58-6) (Fig. 4).
4. Quartz keratophyre, Franciscan formation Del Puerto volcanics of Maddock (1955), Mt. Boardman quadrangle, California (analysis from Dr. Maddock, 88-I-1; R. Klemen, analyst).
5. Quartz keratophyre, Franciscan formation Del Puerto volcanics of Maddock (1955), Mt. Boardman quadrangle, California (analysis from Dr. Maddock, 88-I-2; R. Klemen, analyst).
6. Quartz–jadeite–lawsonite–sericite schist (metagraywacke) from Franciscan formation, Angel Island, San Francisco Bay, California (80-RGC-58).
7. Graywacke from Franciscan formation, Angel Island, San Francisco Bay, California (80-RGC-58-1).

jadeite core (No. 1), and the calc–silicate rim (No. 2) are clearly shown by these analyses. For comparison, a normal graywacke (No. 7) and a metagraywacke (quartz–jadeite–lawsonite–sericite schist, No. 6) from the same locality in the Franciscan formation are included.

Rocks from the Clear Creek area are distinctly low in silica and enriched in sodium. The albite–crossite schist is similar to the monomineralic jadeite core, each showing approximately a 1 : 1 molecular ratio of Na_2O to Al_2O_3. In contrast,

the calc–silicate zone surrounding the jadeite pods is enriched in CaO and low in Na_2O.

The relations between the Clear Creek rocks, those characteristic of the Franciscan, and those from other jadeite localities must be made clear before an ultimate source rock can be established. Fig. 7 presents a triangular diagram of

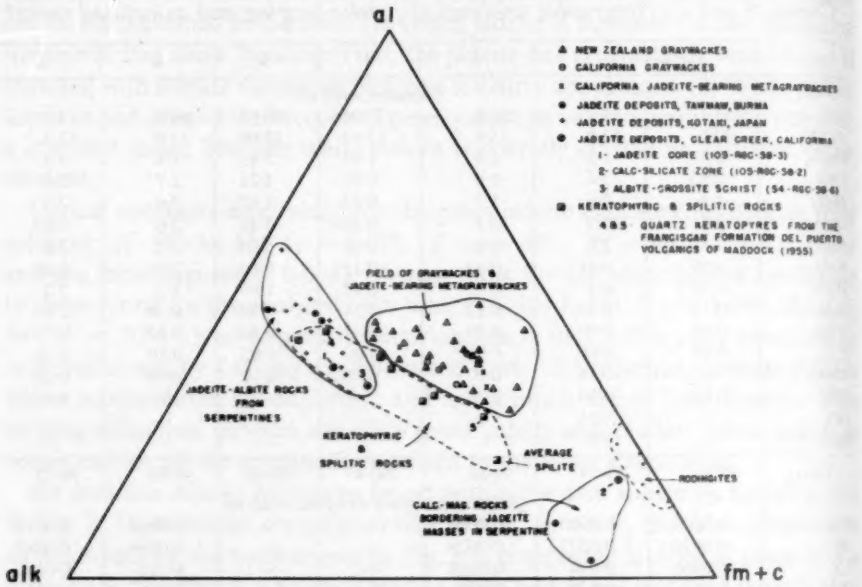
al
alk
fm+c
NEW ZEALAND GRAYWACKES
CALIFORNIA GRAYWACKES
CALIFORNIA JADEITE-BEARING METAGRAYWACKES
JADEITE DEPOSITS, TAWMAW, BURMA
JADEITE DEPOSITS, KOTAKI, JAPAN
JADEITE DEPOSITS, CLEAR CREEK, CALIFORNIA
1- JADEITE CORE (105-R6C-58-3)
2- CALC-SILICATE ZONE (105-R6C-58-2)
3- ALBITE-CROSSITE SCHIST (54-R6C-58-6)
KERATOPHYRIC & SPILITIC ROCKS
4 & 5 QUARTZ KERATOPYRES FROM THE FRANCISCAN FORMATION DEL PUERTO VOLCANICS OF MADDOCK (1955)
FIELD OF GRAYWACKES & JADEITE-BEARING METAGRAYWACKES
JADEITE-ALBITE ROCKS FROM SERPENTINES
KERATOPHYRIC & SPILITIC ROCKS
AVERAGE SPILITE
RODINGITES
CALC-MAG ROCKS BORDERING JADEITE MASSES IN SERPENTINE

FIG. 7. Triangular diagram of Niggli values for jadeite-bearing and associated rocks $\Sigma\,[al+alk+(fm+c)] = 100$.

Descriptions and sources of plotted rock analyses:

New Zealand graywackes. Twenty-eight analyses of lower Mesozoic, Palaeozoic, and Precambrian graywackes (Reed, 1957).

California graywackes and metagraywackes. Seven analyses. (Davis, 1918; Taliaferro, 1943; Bloxam, 1956; two analyses, Table 8).

Jadeite deposits, Tawmaw, Burma. Five analyses representative of the zones in the Tawmaw Dike (Lacroix, 1930).

Jadeite deposits, Kotaki, Japan. Thirteen analyses of albitites associated with jadeite-bearing rocks (Iwao, 1953).

Keratophyric and spilitic rocks. Five selected analyses representing highly sodic varieties (Benson, 1915; Park, 1946; Dewey and Flett, 1911; Sundius, 1930; Norin, 1937; two analyses, Table 8).

Rodingites. Analyses taken from Bloxam (1954), Baker (1959), Marshall (1911), Grange (1927), and Miles (1950).

Jadeite deposits, Clear Creek, California (three analyses, Table 8).

The field boundaries are arbitrary and are not meant to be restrictive in a chemical sense.

Niggli values determined for these rock types. Here the values *al*, *alk*, *fm*, and *c* are used to characterize each analysed rock. The values *fm* and *c* are combined so that $\Sigma[al+alk+(fm+c)] = 100$.

Graywackes from New Zealand (Reed, 1957) and California (Taliaferro, 1943; Bloxam, 1956) are plotted along with three California jadeite-bearing metagraywackes (Bloxam, 1956) to establish the apparent homogeneity of this group of rocks. Available and reliable rock analyses of jadeite-bearing and associated rocks from the Tawmaw, Burma, occurrence (Lacroix, 1930) and the Kotaki District, Japan (Iwao, 1953), are also plotted. To complete the picture, two quartz keratophyres from the Franciscan formation Del Puerto volcanics

of Maddock (1955) in the Mt. Boardman quadrangle, California, are included with other spilitic and keratophyric rocks typical of these orogenic zones.

The comparison of Niggli values for the jadeite-bearing rocks, when plotted in this fashion, reveals three distinct groups that are related to their mode of occurrence. Jadeite deposits within serpentine masses from Burma, Japan, and California are characterized by nearly equal amounts of *al* and *alk* with very low $fm+c$. These are considered as comprising a distinct group. A second group is formed by the peculiar Ca–Mg silicate zones surrounding the jadeite–albite masses in serpentine. Jadeite is not reported in these zones from Burma (Lacroix, 1930) or Japan (Iwao, 1953); however, these rocks represent intermediate reaction zones between the jadeite masses and the enclosing serpentine. Most of the rocks from the Kotaki District, Japan, are described as albitites and none of those analysed is truly representative of the jadeite masses. Analysed rocks from Tawmaw, Burma, however, include both the jadeite and albitite zones.

A third group is formed by the California and New Zealand graywackes, and the jadeite-bearing metagraywackes of California. Metamorphism of California graywackes to quartz–jadeite–lawsonite schists produces no apparent change in bulk composition, as shown by the coherence of this third group on the diagram. It seems clear, then, that jadeitic metagraywackes represent a distinct metamorphic facies. Reed (1958) has shown very clearly that regional metamorphism of the New Zealand graywackes, similar in composition to California graywackes, gives rise to schists typical of the greenschist and amphibolite facies. These same graywackes of the New Zealand geosyncline are characterized by the zeolite facies in less intensely metamorphosed areas (Coombs *et al.*, 1959).

In contrast, the albite–crossite schist within the New Idria serpentine mass has an unusual composition. Extensive metasomatism of these schists is not supported by field and petrographic evidence. Preservation of original bedding planes attests to their sedimentary origin; however, almost complete reconstitution of the minerals precludes a possible clue as to whether the source-material was detrital and/or volcanic. Close similarity in composition between the Franciscan Del Puerto keratophyres and other keratophyres described by Benson (1915), Norin (1937), and Park (1946), and the albite–crossite schist suggests that they may have been derived from keratophyric pyroclastic marine sediments. The extremely low K_2O content of the Clear Creek schists sets them apart from other Na_2O-rich sediments such as the Gowganda Precambrian argillites (Pettijohn & Bastron, 1959) or the Tibet hornstones (Norin, 1937). Even though these argillites and hornstones are exceptional for their high Na_2O/K_2O ratio, the total K_2O content is much greater than that found in the schist of the Clear Creek area.

It is difficult to establish a direct connexion between the pod-like jadeite occurrences and their pre-metamorphic precursors. However, a plot of the SiO_2-Al_2O_3–Na_2O molecular ratios for the Franciscan Del Puerto quartz keratophyres, the albite–crossite schist, and the jadeite cores (from Table 8) illustrates

a possible relation between these rocks (Fig. 8). By progressive loss of SiO_2, the keratophyric rocks could easily attain a composition favourable for the formation of jadeite. Desilication could be effected during and after tectonic emplacement of keratophyric material within serpentine. The unusual zoning suggests this possibility, as these small bodies may have differentiated during metamorphism of keratophyric tuff. The striking resemblance in composition between the jadeite core and albite–crossite schist gives further credence to this possibility.

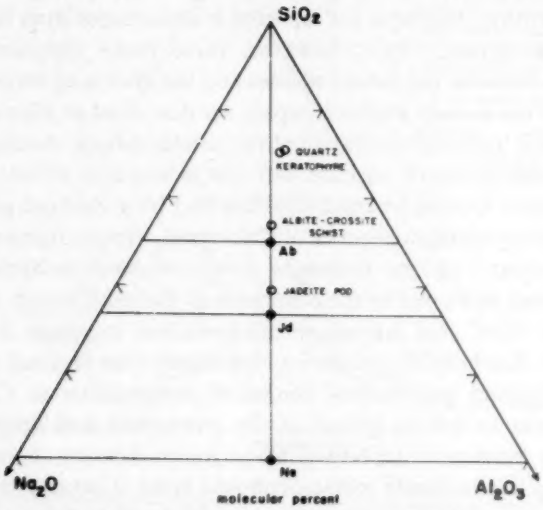

FIG. 8. Plot showing the relations between the phases Ab (albite), Jd (jadeite), and Ne (nepheline) and the molecular ratios of SiO_2–Na_2O–Al_2O_3 in the Franciscan formation Del Puerto keratophyres of Maddock (1955) and the Clear Creek rocks.

The outer calc–silicate zone in many respects resembles (Fig. 7) the mineralogy of rodingites (Grange, 1927; Bloxam, 1954; Baker, 1959; Miles, 1950). It is generally considered that hydrothermal calcium-rich solutions within serpentines alter gabbroid rocks into calc–silicate masses of hydrogarnet, idocrase, and diopside (rodingites) during the process of serpentinization (Benson, 1915; Bloxam, 1954). The outer margins of jadeite pods may well have developed in a similar manner during the period of metamorphism of the keratophyric inclusions to jadeite. The high boron content and increase in chromium over that in the jadeite core are interpreted as evidence for this reaction (Table 8). Enrichment of boron in serpentines has been demonstrated by Faust *et al.* (1956) and they consider that this enrichment takes place during serpentinization. The boron content of six serpentine samples from the New Idria mass ranges from 0·01 to 0·05 per cent boron by spectrographic analyses, whereas the jadeite core shows 0·002 per cent and the albite–crossite schist contains less than 0·002 per cent boron. This boron concentration demonstrates that formation of the jadeite

core and calc–silicate border may have been contemporaneous with, or later than, the process of serpentinization.

The clustering of the larger tectonic inclusions and pods in the Clear Creek area indicates that during serpentinization or shortly thereafter, keratophyric tuff blocks of varying sizes were emplaced tectonically. The smaller bodies undergoing more intense metamorphic reaction with serpentine have become zoned, whereas the larger bodies show only local reaction with the enclosing serpentine.

In considering the Burmese, Japanese, and Californian occurrences, a striking parallelism is observed in their chemical composition and zoning. All these occurrences show a zoning which, in a general way, follows the same pattern. The central core is usually albite and/or jadeite intergrown or as distinct bands. This central core is surrounded by a rim which is characteristically enriched in Ca–Mg silicates. The mineralogy for these three occurrences varies considerably from one to the other; however, the bulk composition of each zone demonstrates a remarkable consistency, i.e. Na–Al-rich cores and Ca–Mg-rich borders. Rather than call on exotic intrusives or desilicification of granitic intrusives (cf. Lacroix, 1930; Chhibber, 1934; Bleeck, 1907) to explain these deposits, it seems much more reasonable to assume an original composition in keeping with the common associates of these orogenic zones; i.e. serpentine–graywackes, spilites–keratophyres.

The mutual chemical and geological conformity between the Californian, Japanese, and Burmese jadeite deposits manifests a common genesis. It is proposed that these deposits developed from keratophyric or spilitic inclusions tectonically emplaced within serpentine. Following emplacement, metamorphic reaction at depth, between serpentine and inclusions, provided an environment that allowed the stable formation of jadeite.

MINERAL FACIES AND THEIR RELATION TO THE FORMATION OF JADEITE

Important to a discussion regarding the origin of jadeite in these deposits is a clear description of the associated minerals that appear to be in equilibrium with jadeite, and of those that have formed either earlier or later than the jadeite. It is apparent from the textural relations in many thin sections studied that equilibrium may never have been attained during the period of jadeite crystallization; however, where jadeite coexists with other minerals and replacement one by the other was not suggested by their textures, it is assumed that the coexisting minerals closely approached equilibrium.

As shown in a previous section, jadeite is found in two distinct environments: (1) small areas in albite–crossite schist inclusions, and (2) pod-like bodies associated with calc–silicates.

Within the schist, green jadeite was not replaced by albite, nor was it found replacing acmite or glaucophane. The stable assemblage is:

Green jadeite (5–25 per cent Ac–Di–He)+low albite (An_{0-2})

As the small areas of green jadeite–albite schists can be traced into albite–crossite schists, it is assumed that the formation of jadeite was accomplished by metamorphism of the albite–crossite schist. Veins of white jadeite (98 per cent Jd) cutting the green jadeite–albite schist are clearly later, and again show the following stable assemblage:

White jadeite (98 per cent Jd)+low albite (An_{0-2})

Within the veins, low albite (An_{0-2}), analcime, and zeolites are found replacing the jadeite–albite assemblage. These joints may represent low-pressure zones similar to those developed in boudins (Ramberg, 1955) and contain 'sweated out' silicates and hydrous phases representing an accumulation of available liquid within the low-pressure zone.

Experimental studies on the stability of the mineral assemblages present in the Clear Creek area have been under intensive study during recent years, and therefore a discussion of the natural assemblages, in the light of the experimental findings, is necessary. The reactions previously studied, together with the relevant references to some of the experimental work and thermodynamic relations, are given below:

$$\text{nepheline}+\text{albite} = 2\ \text{jadeite} \qquad (1)$$

(Robertson *et al.*, 1957; Adams, 1953; Yoder & Weir, 1951)

$$\text{analcime} = \text{jadeite}+\text{water} \qquad (2)$$

(Griggs & Kennedy, 1956; Fyfe & Valpy, 1959)

$$\text{albite} = \text{jadeite}+\text{quartz} \qquad (3)$$

(Robertson *et al.*, 1957; Fyfe & Valpy, 1959; Birch & LeComte, 1960)

$$\text{analcime} = \text{nepheline}+\text{albite}+\text{water} \qquad (4)$$

(Yoder, 1954, 1950*a*; Fyfe & Valpy, 1959)

The complete absence of quartz from the Clear Creek jadeite deposits eliminates reaction (3) from this discussion or it would have to be assumed that silica was removed from the system during jadeite formation. Kracek *et al.* (1951) have determined the thermodynamic properties of jadeite and the other minerals involved in reactions (1) and (2). As shown by their data, the formation of jadeite is favoured by a silica-deficient environment because the free energy change for reaction (3) is positive ($\Delta F = +1{\cdot}60$ K cal at 298° K), whereas for reaction (1) it is negative ($\Delta F = -1{\cdot}15$ K cal at 298° K). Considering the composition of the albite–crossite schist, and the lack of quartz both during the formation of jadeite and during its inversion to albite and/or analcime, reactions (1) and (2) more nearly represent the composition during the Clear Creek jadeite formation. It must be stated that nepheline was not identified in any of the specimens from the area, but for this discussion the nepheline molecule could be contained within natrolite.

Assuming that the bulk composition of the jadeite-bearing rocks was derived

by desilicification of keratophyric material within the serpentine mass, a diagram can be constructed to demonstrate the sequence (Fig. 9). All bulk compositions of the rocks plotted on the diagram include SiO_2, Al_2O_3, Na_2O, and H_2O. These oxides make up 87 to 90 per cent (by weight) of the total rock composition with Na_2O:Al_2O_3 (molecular per cent) very nearly 1:1 in each case (see Fig. 8). The

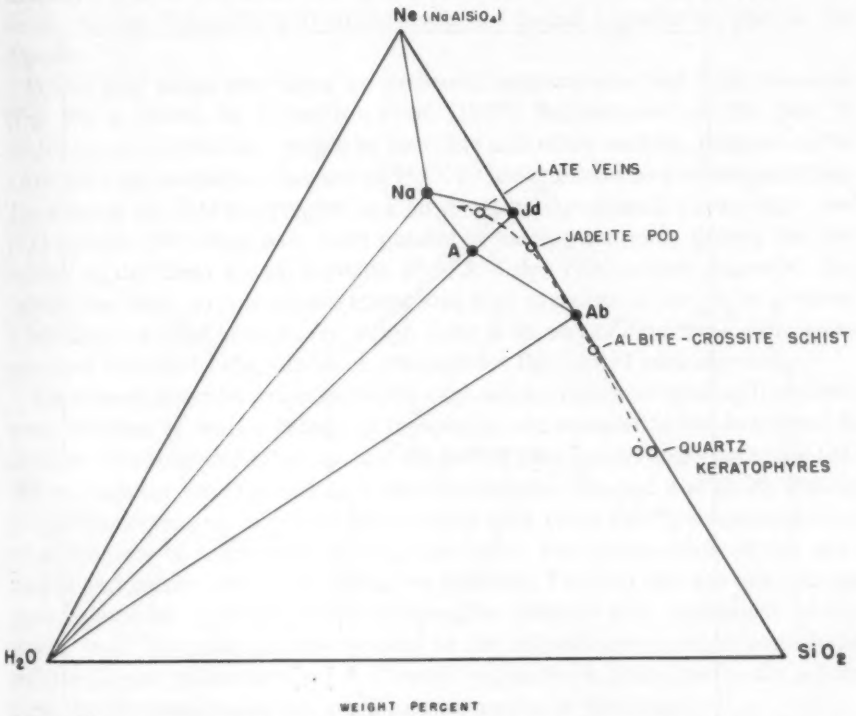

FIG. 9. Triangular plot illustrating the relations between bulk compositions of the jadeite-bearing rocks and the stable assemblages. Ne (nepheline), Na (natrolite), A (analcime), Jd (jadeite), Ab (albite). Weight per cent.

phases expected with each compositional type are included on the diagram. The keratophyres, albite–crossite schists, and jadeite pod all fall on or near the SiO_2–Ab–Jd–Ne line. An estimated composition of the zeolite–jadeite veins in the schist bodies is plotted to illustrate their high water and low silica content. Modal analysis of the keratophyres shows 53–58 per cent albite and 35–38 per cent quartz (?); the remainder consists of varying amounts of chlorite, augite, and opaque minerals (Maddock, 1955).

The phases Ab ($Na_2O.Al_2O_3.6SiO_2$), Jd ($Na_2O.Al_2O_3.4SiO_2$), A ($Na_2O.Al_2O_3.4SiO_2.H_2O$), Na ($Na_2O.Al_2O_3.3SiO_2.2H_2O$), and H_2O gas, all lie within a plane of the system SiO_2–Al_2O_3–Na_2O–H_2O where Na_2O:Al_2O_3 is 1:1. Morey (1957) has discussed in detail, on a theoretical basis, possible univariant *P–T*

curves and invariant points within this same system. Following his reasoning, the mineral assemblages associated with the Clear Creek jadeite are plotted in the triangular diagram of Fig. 9. The coexisting mineral phases most commonly observed are as follows; these may be stable or metastable assemblages:

(1) Jd; (2) Jd+Ab; (3) Ab; (4) Ab+Jd+A; (5) Jd+A+Na.

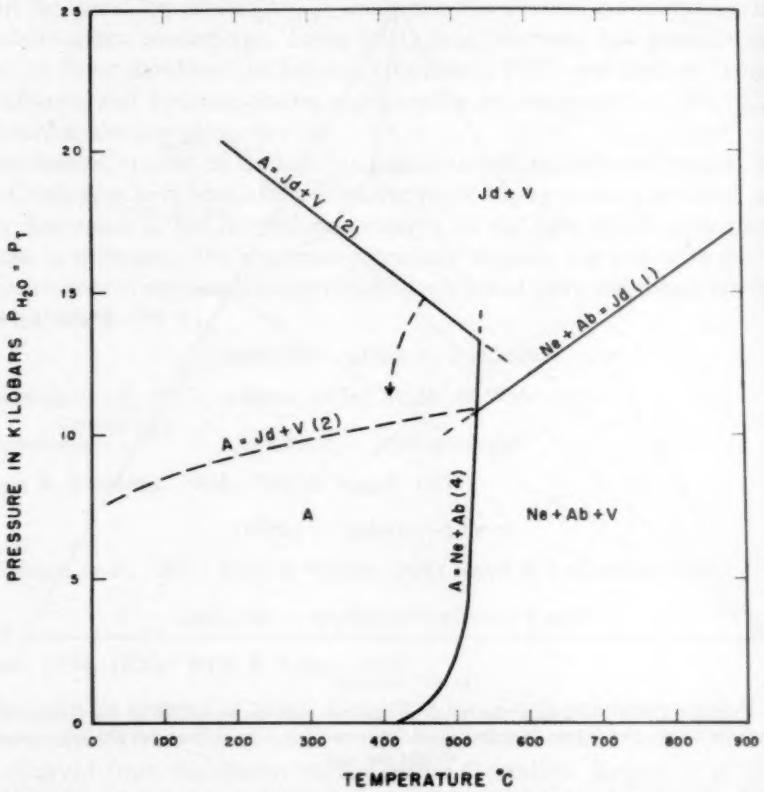

FIG. 10. Equilibrium lines for reactions (1) Robertson *et al.* (1957), (2) Griggs & Kennedy (1956), Fyfe & Valpy (1959), (4) Yoder (1954).

Jd+Ab coexisted, in the early stages, and as crystallization continued Jd became the dominant phase with a minor development of Jd+Ab+A. At this time the bulk composition could have been within the triangle Jd–Ab–A and near the Jd–Ab tie-line. The appearance of A suggests local variations in water pressures or temperatures. The experimental stability of analcime, as shown in Fig. 10, indicates that it is stable up to 500° C when $P_{H_2O} = P_{total}$. Yoder (1954) has shown that this stability limit of analcime is reduced to 400° C when $P_{H_2O} = 1$ atm. For reaction (2), Fyfe & Valpy (1959) have suggested that the equilibrium curve (Fig. 10) may assume a positive slope at low temperatures.

Therefore at low temperatures, when $P_{H_2O} < P_{total}$, jadeite may form more readily as the analcime field of stability becomes restricted. Nepheline is not found in the Clear Creek deposits; however, natrolite is found sparingly replacing jadeite and analcime or coexisting with analcime. Na+Jd+A could coexist when the bulk composition lies within the triangle Na–Jd–A. By changing this composition to lie within the triangle A–Jd–Ab, Na would not be stable and Ab would appear. Natrolite and albite were not found together in any of the deposits.

Jadeite and albite may exist at moderate temperatures and high pressures (Fig. 10), as shown by Robertson *et al.* (1957). Replacement of this pair by analcime, and in the later stages by natrolite and other zeolites, suggests either a low silica environment, increase of H_2O, or lower pressures and temperatures. The amount of H_2O determines to a large extent the mineral assemblages and H_2O undoubtedly must have been present in varying amounts during the formation of the Clear Creek deposits. Fyfe & Valpy (1959) have suggested that jadeite may form at low temperatures and high pressures if the water pressure is less than the total pressure; however, there is no way of determining the water pressures relative to the total rock pressure for the Clear Creek deposits.

The mineral assemblage formed in the calc–silicate zone surrounding the jadeite pods provides us with a means of comparing the mineral facies developed in calcium–aluminium silicate rock and the jadeite core facies. It has been said that the calc–silicate zone formed as a reaction between the pod and fluids present within the serpentine. Whether this reaction took place during serpentinization or at the time of jadeite formation is not clear. The composition of the calc–silicate and jadeite zones is so distinctly different (Table 8) that the calc–silicate zone cannot be regarded as a retrogressive metamorphic equivalent of the jadeite core. The minerals now present in the calc–silicate zone are considered to have formed under the same *P–T* conditions as those giving rise to the jadeite core. The following minerals are found to coexist in this zone:

pectolite–thomsonite–hydrogarnet–carbonate

The mineral phases have been plotted on a triangular diagram with CaO–SiO_2–Al_2O_3 at the apexes, together with a point representing the approximate composition of the rock containing these minerals (Fig. 11). Experimental work on the stability of grossularite–hydrogrossular by Flint *et al.* (1941), Yoder (1950*b*), and Carlson (1956) allows for some speculation on the conditions for formation of hydrogrossular in this rock. Yoder has shown that grossularite in the presence of water at elevated temperatures is unstable and inverts to hydrogrossular. Above 750° C grossularite–hydrogrossular solid solutions are unstable and invert to gehlenite–wollastonite–anorthite in the absence of quartz. Carlson (1956) extended Yoder's curve and has defined the relationships between temperature of formation and composition, for the hydrogarnets. The silica content of hydrogrossular increases with temperature up to 800° C, 1,020 atm, at which

point grossularite becomes stable, whereas fully-hydrated hydrogrossular is stable at 220°–226° C, 1,020 atm. Assuming that the hydrogarnets associated in the calc–silicate zone formed contemporaneously with the jadeite core, a minimum temperature of formation can be estimated. To make such an assumption,

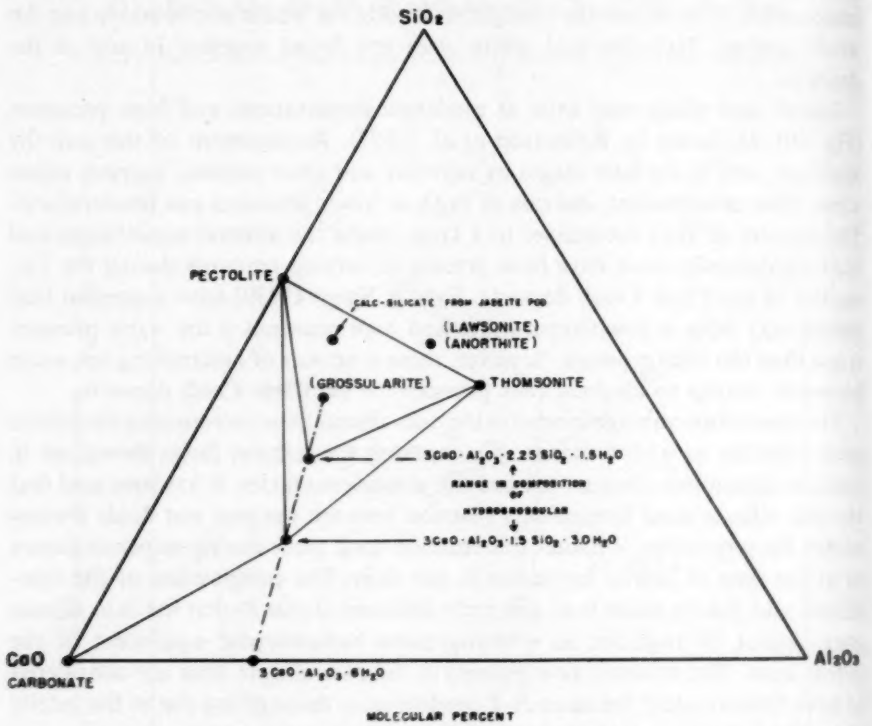

FIG. 11. Triangular diagram of CaO, Al_2O_3, SiO_2 system illustrating the relations of the minerals present in the calc–silicate rock of the jadeite pods. The composition of the calc–silicate rock plotted is from Table 8 and the minerals contained are pectolite–hydrogrossular–thomsonite–carbonate. Only a few tie-lines are shown.

it would be necessary to exclude the possibility of silica loss during the hydrogarnet formation. Pistorius & Kennedy (1960) have shown experimentally that the presence of quartz might affect the stability of grossularite–hydrogrossular; however, it is doubtful that equilibrium conditions were obtained, because the unit cell variations of their synthesized hydrogarnets suggest strong compositional variation. With these restrictions in mind, hydrogarnets from the calc-silicate zone may have formed at temperatures ranging from 240°–360° C, and hydrogarnets in late veins suggest temperatures between 260° and 300° C. These reactions are not necessarily pressure-dependent, as demonstrated by Yoder (1950*b*) and Carlson (1956).

Further evidence on temperature and pressure conditions within the calc–silicate zone may be obtained by considering Fyfe's work (Ellis & Fyfe, 1957; Fyfe, Turner, & Verhoogen, 1958; Fyfe & Valpy, 1959; Coombs *et al.*, 1959) on the stability of thomsonite–lawsonite–anorthite. As shown in Fig. 11, lawsonite or anorthite could be expected to form within the calc–silicate rock with a slight increase of silica content. Fyfe has suggested that thomsonite is stable below 300° C with low water pressures; with an increase in water pressure above 5,000 bars, thomsonite may invert to lawsonite. Anorthite is stable above 300° C at low water pressures and might also invert to lawsonite by a large increase in the partial pressure of water. Assuming that the bulk composition would allow the formation of lawsonite, the presence of hydrogarnet and thomsonite within the calc-silicate zone suggests that the temperatures were less than 300° C and that the pressures ranged from 5,000 to 8,000 bars.

Additional indirect evidence on the *P–T* conditions prevailing during the formation of jadeite in the Clear Creek area may be obtained by considering the reaction:

$$\text{serpentine} \rightarrow \text{forsterite} + \text{talc} + \text{vapour}$$

All the jadeite-bearing rocks lie within the serpentine and, as discussed earlier, the period of jadeite mineralization is considered to be later than, or contemporaneous with, the period of serpentinization. Bowen & Tuttle (1949, p. 459) state: 'serpentine cannot be present in any layer of the earth's crust whose temperature is normally above the decomposition temperature (500° C) under the pressure prevaling'. The serpentine, then, fixes the maximum temperature as there is no evidence for the decomposition of serpentine to forsterite+talc in the Clear Creek area.

The schists from the tectonic inclusions are classified as belonging to the greenschist or glaucophane schist facies as defined by Turner (Fyfe, Turner, & Verhoogen, 1958). As lawsonite has not been identified in these rocks and the jadeite is restricted to local areas within albite–crossite–stilpnomelane schists, it seems appropriate to place the schists in the chlorite zone of metamorphism as defined by Hutton (1940). Turner has suggested that the greenschist facies probably does not form below 300° C with P_{H_2O} between 5,000 and 10,000 bars.

If the interpretation of the mineral facies is correct in the light of experimental data, and if the observed geological relations are correct, it is suggested that these jadeite deposits developed at temperatures less than 300° C and at pressures near 5,000 bars with $P_{load} > P_{H_2O}$.

These *P–T* values are much less than have been recorded experimentally for reactions (1), (2), and (3). However, several points of difference can be cited between the experimental conditions and the reconstructed conditions found for the Clear Creek jadeite deposits; these differences may explain why jadeite develops at low temperatures and moderate pressures.

(1) The jadeite composition varies from almost pure material to as much as 25 per cent Di–Ac–He. The effect of diopside–acmite solid solution has not

been investigated for reactions (1), (2), and (3). It would seem probable that Ac solid solution in the Jd molecule could strongly affect the stability curve of jadeite and would certainly lower its stability pressure, as Ac is stable at 1 atm.

(2) As a low silica environment favours the formation of jadeite, it may be that the serpentine mass continuously captured silica during the period of jadeite mineralization. Leaching of silica from tectonic inclusions may be simultaneous with the formation of serpentine if we assume the reaction forsterite+SiO_2+H_2O = serpentine. Removal of silica during experimental synthesis of jadeite is not easily accomplished.

(3) The partial pressure of water may have been profoundly affected by the serpentine mass. If it is assumed that the formation of jadeite took place during or shortly after the period of serpentinization, the water content may have been reduced by the conversion of the ultramafic to serpentine. Thus, vein jadeite may have formed where the water phase was nonexistent or greatly reduced in quantity. As shown by Adams (1953) and Fyfe & Valpy (1959), a dry environment favours the formation of jadeite.

(4) Excluding the vein-type jadeite, the localized distribution of the other jadeite bodies and zones gives some credence to the possibility that shearing or directed pressures may be effective catalysts in causing jadeite to form. All the equilibrium studies on jadeite were made under hydrostatic pressures.

CONCLUSIONS

Formation of jadeite within the New Idria serpentine mass was restricted to large tectonic inclusions of albite–crossite schist and smaller zoned pods situated near these inclusions. Assuming that sodium was not introduced, the composition of these schists is similar to keratophyric lavas. Emplacement of the keratophyric blocks within the serpentine was accomplished during the period of orogeny when the serpentine invaded the geosynclinal sediments and volcanics of the Franciscan, at depth. Metamorphism of the keratophyric rocks developed, mainly, albite–crossite–stilpnomelane–acmite schists. Localized areas of high confining pressures along the margins of the tectonic inclusions gave rise to green jadeite–albite schists. Continuing tectonic movement and possible mobilization of a liquid rich in the jadeite molecule and low in H_2O produced cross-cutting veins of white jadeite+albite. A lowering of the water pressure could have resulted in the later replacement of albite–jadeite by zeolites. The smaller pod-like bodies may have been keratophyric blocks that reacted to a greater extent with fluids within the serpentine, giving rise to a rodingite-like calc-silicate zone surrounding the jadeite core. The Californian, Burmese, and Japanese bodies all follow the same pattern; that is, a central Na–Al silicate core grading into border zones of lower silica and sodium content and increasing in Ca–Mg silicates. It seems apparent that these bodies have reacted with fluids within the serpentine and, in so doing, a typical metamorphic differentiation

trend was developed. Similar zoning has been recognized in serpentines both at their contacts (Phillips & Hess, 1936; Read, 1934) with siliceous country rock and for bodies within serpentine (Watson, 1953; Francis, 1955). The metamorphic reaction between serpentines and siliceous rocks is characterized by enrichment of Na–Al silicates in the central zone and outward decrease in silica and enrichment in Ca–Mg. This environment, apparently common to serpentines, favours the formation of jadeite because of the low silica and enrichment of Na and Al.

Extremely high pressures are needed to form jadeite experimentally. Robertson *et al.* (1957) suggest a pressure of 15,000 bars and temperatures between 500° and 700° C to allow the ready formation of a jadeite–albite assemblage. If the assumption is made that these pressures and temperatures are attained only by depth of burial, it is necessary to allow 37 km of depth before these *P–T* conditions are satisfied (ibid., 1957). In reconstructing the hypothetical depth of burial for the serpentine and contained jadeite deposits in the New Idria area, from stratigraphic data given by Reed (1951), it is found that a range from 9 to 12 km appears feasible.

This reconstruction is based on the assumption that the emplacement of the serpentine into the geosynclinal sediments and volcanics of the Franciscan coincided with the Nevadan Orogeny and that during this emplacement, tectonic inclusions derived from the geosynclinal sediments and volcanics became immersed in the serpentine. The presence of serpentine debris in Miocene sediments derived from the New Idria mass indicates that the serpentine reached the surface during this time; therefore, to attain a depth of 12 km, it has to be assumed that the serpentine was covered by the total thickness of sediments making up the Jurassic to Miocene section in the New Idria area. It therefore seems impossible that these rocks could ever have been at depths up to 37 km.

Thus one is forced to call upon a unique situation to allow the stable formation of jadeite in the upper portions of the earth's crust. Based on thermodynamic calculations of Adams (1953), it is possible to form jadeite in anhydrous conditions by the reaction nepheline + albite = 2 jadeite at approximately 240° C and 2,000 bars. The stability of crystalline OH-bearing minerals under varying *P–T* conditions dictates the P_{H_2O} to a great extent (Yoder, 1955). In a serpentine mass, almost all the water may be effectively held in the structure of the serpentine minerals. Thus at great depths, the partial pressure of water in a serpentine mass could have been small compared to the total rock pressure. The tectonic inclusions, being small in mass compared to the serpentine body, are in essence affected by this same pressure as any residual interstitial water could migrate to the serpentine and be used in the process of further serpentinization. This effective mechanism would provide an anhydrous environment and also produce very low partial water pressures, both of which favour the formation of jadeite at low temperatures and somewhat reduced total pressure.

The localized nature of jadeite in the tectonic inclusions and pod-like bodies

may be indicative of local shearing stress which could give rise to high enough pressures within these small areas to favour the formation of jadeite. However, the unique situation within the serpentine body which has produced a silica gradient away from the tectonic inclusions, combined with a dry environment, seems to be the important factor in the formation of jadeite.

Further experimental work is needed to elucidate the role of diopside–acmite solid solution and its effect on the stability of jadeite. As yet we are not able to suggest a field of stability at high pressures and low temperatures for the reactions (1) and (3). Another problem regarding the stability of jadeite is its extensive development in metagraywackes in equilibrium with quartz and lawsonite (McKee, 1958; Bloxam, 1956), within the Franciscan formation. The association of quartz with jadeite in these rocks moves us to reaction (3) where even greater pressures are needed to allow the stable formation of jadeite. Here again there is no evidence that these rocks attained depths greater than 12 km.

ACKNOWLEDGEMENTS

This problem was initiated while the author was pursuing graduate studies at Stanford University, where much of the preliminary work was completed under the guidance of Professor C. O. Hutton, to whom I am grateful for advice and counsel. Reviews by David B. Stewart and George Phair, U.S. Geological Survey, have enhanced the petrological interpretations. Hatten S. Yoder, Jr., Geophysical Laboratory, has allowed free use of his preliminary data on these deposits and ensuing discussions on the problem were of value to the author. Further discussions with Professor William S. Fyfe, University of California, on the experimental aspects of the problem, assisted in the interpretation. George S. Switzer, U.S. National Museum, kindly provided chemical analyses and specimen material for two jadeites from the Clear Creek deposits. Professor Marshall E. Maddock, San Jose State College, has allowed the writer the use of two unpublished analyses of the Del Puerto quartz keratophyres.

REFERENCES

Adams, L. H., 1953. A note on the stability of jadeite. *Amer. J. Sci.* **251**, 299–308.

Alderman, A. R., 1936. Eclogites in the neighbourhood of Glenelg, Inverness-shire. *Quart. J. geol. Soc. Lond.* **92**, 488–530.

Anderson, R., & Pack, R. W., 1915. Geology and oil resources of the west border of the San Joaquin Valley north of Coalinga, California. *Bull. U.S. geol. Surv.* **603**, 220 pp.

Baker, George, 1959. Rodingite in nickeliferous serpentinite, near Beaconsfield, Northern Tasmania. *J. geol. Soc. Aust.* **6**, Pt. 1, 21–35.

Banno, Shohei, 1959. Aegirinaugites from crystalline schists in Sikoku. *J. geol. Soc. Japan*, **65**, 652–7.

Belyankin, D. S., & Petrov, V. P., 1941. The grossularoid group (hibschite and plazolite). *Amer. Min.* **25**, 450–3.

Benson, W. N., 1915. The geology and petrology of the great serpentine belt of New South Wales. Part IV. The dolerites, spilites, and keratophyres of the Nundle District. Part V. The Geology of the Tamworth District. *Proc. Linn. Soc. N.S.W.* **40**, 121–73, 540–624.

Birch, F., & LeComte, P., 1960. Temperature–pressure plane for albite composition. *Amer. J. Sci.* **258**, 209–17.

Bleeck, A. W. G., 1907. Die Jadeitlagerstätten in Upper Burma. *Z. Prakt. Geol.* **15**, 341–65.

Bloxam, T. W., 1954. Rodingite from the Girvan–Ballantrae complex, Ayrshire. *Miner. Mag.* **30**, 525–8.

BLOXAM, T. W., 1956. Jadeite-bearing metagraywackes in California. *Amer. Min.* **41,** 488–96.
—— 1959. Glaucophane-schists and associated rocks near Valley Ford, California. *Amer. J. Sci.* **257,** 95–112.
BOLANDER, L. PH., 1950. First jadeite discovery in America. *Mineralogist,* **18,** 186, 188.
BOWEN, N. L., & TUTTLE, O. F., 1949. The system MgO–SiO_2–H_2O. *Bull. geol. Soc. Amer.* **60,** 439–60.
BRIÈRE, Y., 1920. Les Eclogites françaises — leur composition minéralogique et chimique; leur origine. *Bull. Soc. franç. Minér.* **43,** 72–222.
BROTHERS, R. N., 1954. Glaucophane schists from the North Berkeley Hills, California. *Amer. J. Sci.* **252,** 614–26.
CARLSON, E. T., 1956. Hydrogarnet formation in the system lime–alumina–silica–water. *U.S. Nat. Bur. Standards, J. of Res.* **56,** 327–35.
CHIBBER, H. L., 1934. *Mineral resources of Burma.* London: Macmillan & Co. Ltd.
COLEMAN, R. G., 1954. Optical and chemical study of jadeite from California (abst). *Bull. geol. Soc. Amer.* **65,** 1241.
—— 1956. Jadeite from San Benito County, California. *Gems & Gemology,* **Fall 1956,** 331–4.
—— 1957. Mineralogy and petrology of the New Idria District, California. Unpublished thesis for D.Ph. degree. *Dissertation Abstracts,* **17,** No. 7, 1533.
COOMBS, D. S., ELLIS, A. J., FYFE, W. S., & TAYLOR, A. M., 1959. The zeolite facies; with comments on the interpretation of hydrothermal syntheses. *Geochim. et Cosmochim. Acta,* **17,** 53–107.
DAVIS, E. F., 1918. The Franciscan Sandstone. *Bull. Univ. Calif. Pub. Dept. Geol.* **11,** 22 pp.
DE ROEVER, W. R., 1955. Genesis of Jadeite by low-grade metamorphism. *Amer. J. Sci.* **253,** 283–98.
DEWEY, H., & FLETT, J. S., 1911. Some British pillow lavas and the rocks associated with them. *Geol. Mag. Lond.* **8,** 202–9, 241–8.
ECKEL, E. B., & MYERS, W. B., 1946. Quicksilver deposits of the New Idria District, San Benito and Fresno Counties, California. *Calif. J. Min.* **42,** Pt. 2, 81–124.
ELLIS, A. J., & FYFE, W. S., 1957. Hydrothermal chemistry. *Rev. Pure and Appl. Chem.* (Aust.), **7,** 261–316.
ESKOLA, P., 1921. On the eclogites of Norway. *Skr. Norske Vidensk Akad.,* I Mat.-naturv., Kl., No. **8,** 1–118.
FAUST, G. T., MURATA, K. J., & FAHEY, J. J., 1956. Relation of minor element content of serpentines to their geological origin. *Geochim. et Cosmochim. Acta,* **10,** 316–20.
FLINT, E. F., MCMURDIE, H. F., & WELLS, L. S., 1941. Hydrothermal and X-ray studies of the garnet–hydrogarnet series and the relationship of the series to hydration products of Portland cement. *U.S. Nat. Bur. Standards, J. of Res.* **26,** 13–33.
FOSHAG, W. F., 1920. Plazolite, a new mineral. *Amer. Min.* **5,** 183–5.
—— 1955. Chalchihuitl—a study in jade. Ibid. **40,** 1062–70.
—— 1957. Mineralogical studies on Guatemalan Jade. *Smithsonian Misc. Collection,* **135,** No. 5, 1–60.
FRANCIS, G. H., 1955. Zoned hydrothermal bodies in the serpentinite mass of Glen Urquhart (Inverness-shire). *Geol. Mag. Lond.* **92,** 433–47.
FYFE, W. S., TURNER, F. J., & VERHOOGEN, J., 1958. Metamorphic reactions and metamorphic facies. *Mem. geol. Soc. Amer.* **73,** 259 pp.
—— & VALPY, G. W., 1959. The analcime–jadeite phase boundary: some indirect deductions. *Amer. J. Sci.* **257,** 316–20.
GRANGE, L. I., 1927. On the 'rodingite' of Nelson. *Trans. Proc. N.Z. Inst.* **58,** 160–6.
GRIGGS, D. T., & KENNEDY, G. C., 1956. A simple apparatus for high pressures and temperatures. *Amer. J. Sci.* **254,** 722–35.
HESS, H. H., 1949. Chemical composition and optical properties of common clinopyroxenes, Part I. *Amer. Min.* **34,** 621–66.
HEY, M., 1932. Studies on the zeolites. Part II. Thomsonite (including faroelite) and gonnardite. *Miner. Mag.* **23,** 51–125.
HILDEBRAND, F. A., 1953. Minimizing the effects of preferred orientation in X-ray powder diffraction patterns. *Amer. Min.* **38,** 1051–6.
HUTTON, C. O., 1940. Metamorphism in the Lake Wakatipu region, western Otago, New Zealand. *Mem. geol. Surv. N.Z.* **5,** 90 pp.
—— 1943. Hydrogrossular, a new mineral of the garnet–hydrogarnet series. *Trans. Proc. N.Z. Inst.* **73,** 174–80.
—— 1956. Further data on the stilpnomelane mineral group. *Amer. Min.* **41,** 608–15.
IWAO, S., 1953. Albitite and associated jadeite rock from Kotaki District, Japan: a study in ceramic raw material. *Geol. Surv. Japan Report,* **No. 153,** 25 pp.
JENNINGS, C. W., & STRAND, R. G., 1958. Geologic Map of California, Olaf P. Jenkins ed., *Santa Cruz sheet, California Div. Mines.*

KAWANO, Y., 1939. A new occurrence of jade (jadeite) in Japan and its chemical properties. *J. Jap. Ass. Mineralog.* **22**, 219–25 (in Japanese).

KNORRING, O. VON, & KENNEDY, W. Q., 1958. The mineral paragenesis and metamorphic status of garnet–hornblende–pyroxene–scapolite gneiss from Ghana (Gold Coast). *Miner. Mag.* **31**, 846–59.

KRACEK, F. C., NEUVONEN, K. J., & BARLEY, G., 1951. Thermochemistry of mineral substances. I. A thermodynamic study of the stability of jadeite. *J. Wash. Acad. Sci.* **41**, 373–83.

LACROIX, M. A., 1930. La Jadeite de Birmanie: les roches qu'elle constitue ou qui'l accompagnent. Composition et origin. *Bull. Soc. franç. Minér.* **53**, 216–54.

MCKEE, BATES, 1958. Jadeite alteration of sedimentary and igneous rocks (abst). *Bull. geol. Soc. Amer.* **69**, 1612.

MACKENZIE, W. S., 1957. The crystalline modifications of $NaAlSi_3O_8$. *Amer. J. Sci.* **255**, 481–516.

MADDOCK, M. E., 1955. Geology of the Mt. Boardman quadrangle. Unpublished thesis for D.Ph. degree, Univ. of Calif.

MARSHALL, P., 1911. The geology of the Dun Mountain Subdivision, Nelson. *Bull. geol. Surv. N.Z.* **12**, 29–40.

MIELENZ, R. C., 1939. The geology of the southwestern part of San Benito County, California. Unpublished thesis for D.Ph. degree, Univ. of Calif., 295 pp.

MILES, K. R., 1950. Garnetized Gabbros from the Eulaminna District, Mt. Margaret Gold field. *Bull. geol. Surv. W. Austral.* **103**, Pt. 2, 108–30.

MOREY, GEORGE W., 1957. The system water–nepheline–albite: a theoretical discussion. *Amer. J. Sci.* **255**, 461–80.

NORIN, ERIK, 1937. Reports from the Scientific Expedition to the northwestern provinces of China under leadership of Dr. Sven Hedin—The Sino-Swedish expedition—III. Geology; I, Geology of Western Qurug tagh, Eastern T'ien-shan. Stockholm: Thule. 195 pp.

OMORI, K., 1939. Optical properties of Japanese jade. *J. Jap. Ass. Mineralog.* **22**, 201–12 (in Japanese).

PABST, A., 1942. Re-examination of hibschite. *Amer. Min.* **27**, 783–92.

PALACHE, CHARLES, 1894. On a rock from the vicinity of Berkeley containing a new soda amphibole. *Bull. Univ. Calif. Dept. Geol. Sci.* **1**, 181–92.

PARK, C. F., 1946. The spilite and manganese problems of the Olympic Peninsula, Washington. *Amer. J. Sci.* **244**, 305–23.

PETTIJOHN, F. J., & BASTRON, H., 1959. Chemical composition of argillites of the Cobalt Series (Precambrian) and the problem of soda-rich sediments. *Bull. geol. Soc. Amer.* **70**, 593–600.

PHILLIPS, A. H., & HESS, H. H., 1936. Metamorphic differentiation at contacts between serpentine and siliceous country rocks. *Amer. Min.* **21**, 333–62.

PHILLIPS, R. M., 1939. The general geology of a part of San Benito County, California. Unpublished thesis for D.Ph. degree, Univ. of Calif., 76 pp.

PISTORIUS, C. W. F. T., & KENNEDY, G. C., 1960. Stability relations of grossularite and hydrogrossularite at high temperatures and pressures. *Amer. J. Sci.* **258**, 247–57.

RAMBERG, HANS, 1955. Natural and experimental boudinage and pinch-and-swell structures. *J. Geol.* **63**, 512–26.

READ, H. H., 1934. On zoned associations of antigorite, talc, actinolite, chlorite, and biotite in Unst, Shetland Islands. *Miner. Mag.* **23**, 519–40.

REED, J. J., 1957. Petrology of the Lower Mesozoic rocks of the Wellington District. *Bull. Geol. Surv. N.Z.* **57** (new series), 53 pp.

—— 1958. Regional metamorphism in southeast Nelson. Ibid. **58** (new series), 60 pp.

REED, R. D., 1951. Geology of California. *Am. Ass. Petrol. Geol.*, Tulsa, Oklahoma.

ROBERTSON, E. C., BIRCH, F., & MACDONALD, G. J. F., 1957. Experimental determination of jadeite stability relations to 25,000 bars. *Amer. J. Sci.* **255**, 115–37.

SAHA, P., 1959. Geochemical and X-ray investigation of natural and synthetic analcite. *Amer. Min.* **44**, 300–13.

SCHALLER, W. T., 1955. The pectolite–schizolite–serandite series. Ibid. **40**, 1022–31.

SCHÜLLER, K. H., 1958. Das Problem Akmit-Ägirin. *Heidelberg. Beitr. Min.* **6**, 112–38.

SEKI, Y., & SHIDO, F., 1959. Finding of jadeite from the Sanbagawa and Kamuikotan Metamorphic belts, Japan. *Proc. Japan Acad.* **35**, 137–8.

SHIDO, F., 1958. Calciferous amphibole rich in sodium from jadeite-bearing albitite of Kotaki, Niigata Prefecture. *J. geol. Soc. Japan*, **64**, 595–600.

—— & SEKI, YOTARO, 1959. Notes on rock-forming minerals. II. Jadeite and hornblende from the Kamuikotan metamorphic belt. *J. geol. Soc. Japan*, **65**, 673–7.

SMITH, J. R., & YODER, H. S., 1956. Variations in X-ray powder diffraction patterns of plagioclase feldspars. *Amer. Min.* **41**, 632–47.

SMITH, J. V., 1956. The powder patterns and lattice parameters of plagioclase feldspars. I. The soda-rich plagioclases. *Miner. Mag.* **31**, 47–68.

A

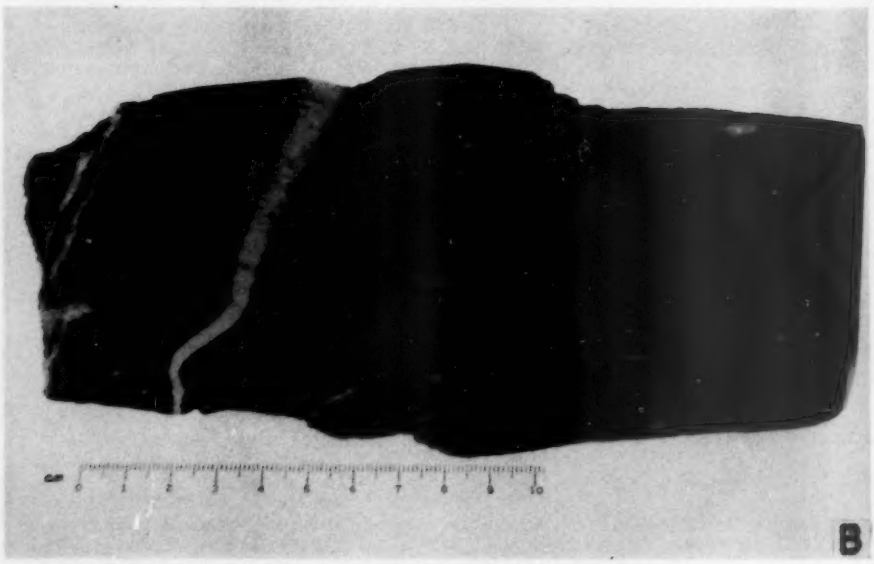
B

SUNDIUS, N., 1930. On the spilitic rocks. *Geol. Mag. Lond.* **67**, 1–17.
SWITZER, G., 1945. Eclogite from the California glaucophane schists. *Amer. J. Sci.* **243**, 1–8.
TALIAFERRO, N. L., 1943. Franciscan–Knoxville problem. *Bull. Amer. Ass. Petrol. Geol.* **27**, 109–219.
WARREN, B. E., & BISCOE, J., 1931. The crystal structure of the mono-clinic pyroxenes. *Z. Kristallogr.* **69**, 391–401.
WATSON, K. D., 1953. Prehnitization of albitite. *Amer. Min.* **38**, 197–206.
WOLFE, C. W., 1955. Crystallography of jadeite crystals from near Cloverdale, California. *Amer. Min.* **40**, 248–60.
YODER, H. S., 1950*a*. The jadeite problem: Parts I and II. *Amer. J. Sci.* **248**, 225–48, 312–34.
—— 1950*b*. Stability relations of grossularite. *J. Geol.* **58**, 221–53.
—— 1954. *Ann. Rep. geophys. Lab.*, Year Book No. **53**, 121–2.
—— 1955. Role of water in metamorphism. *Geol. Soc. Amer. Special Paper*, No. **62**, 505–24.
—— & CHESTERMAN, C. W., 1951. Jadeite of San Benito County, California. *Calif. Div. Mines Special Report*, **10-C**, 8 pp.
—— & TILLEY, C. E., 1959. *Ann. Rep. geophys. Lab.*, Year Book No. **58**, 90–91.
—— & WEIR, C. E., 1951. Change of free energy with pressure of the reaction nepheline + albite = 2 jadeite. *Amer. J. Sci.* **249**, 683–94.

EXPLANATION OF PLATE

FIG. A. Exposure of green jadeite–albite schist cut by white jadeite veins.

FIG. B. Polished slab of green jadeite–albite schist cut by veins of white jadeite. Original bedding planes are still preserved in the schist.

Zoned Ultrabasic and Basic Gneiss Masses in the Early Lewisian Metamorphic Complex at Scourie, Sutherland

by M. J. O'HARA

Grant Institute of Geology, University of Edinburgh, Scotland

ABSTRACT

The field relations and petrography of ultrabasic and basic gneisses which occur associated in small masses among banded granulite facies gneisses are described. The rocks are ascribed to reaction between ultrabasic intrusive bodies and country rock under granulite facies conditions.

INTRODUCTION

THE first account of these ultrabasic and basic masses in the Lewisian of the Scourie district is contained in the Geological Survey Memoir by Clough, Teall, *et al.* (1907). The masses were not mapped in detail. The account of the field relations given here agrees with the majority of their observations, and includes some additional data.

The gneisses were referred to by Davidson (1943), who observed that they were of granulite facies but correlated some of the rocks with true eclogites.

An account by Watson (Sutton & Watson, 1951) mentions these rocks briefly in the course of describing the Lewisian history of the region, which may be summarized as follows:

(1) Early regional metamorphism, producing a granulite facies complex.
(2) Intrusion of a swarm of NW.–SE. dolerite dykes, and other dykes of slightly different ages.
(3) Late regional metamorphism which affected the rocks to the north of Scourie.
(4) Pre-Torridonian erosion.

The recognition of two periods of metamorphism rests upon the identification of remetamorphosed early complex gneisses, cut by metamorphosed dolerite dykes, within the region affected by the late metamorphism.

A discussion of the origin of the masses, and of the views of previous workers, is given later.

FIELD RELATIONS

The ultrabasic and basic gneisses occur among banded granulite facies gneisses of the early Lewisian metamorphic complex. The masses in which the ultrabasic and other gneisses are associated are well exposed in the neighbourhood of Scourie Bay (Fig. 1).

[Journal of Petrology, Vol. 2, Part 2, pp. 248–276, 1961]

The *ultrabasic gneisses* are dark, medium- to coarse-grained compact rocks with specific gravities ranging from 2·9 to 3·4. They are occasionally pale weathering, and are of a massive, irregularly jointed aspect. There is little evidence of foliation; where this is recognizable it is picked out by bands of serpentinous alteration following olivine-rich layers, or by amphibole-rich,

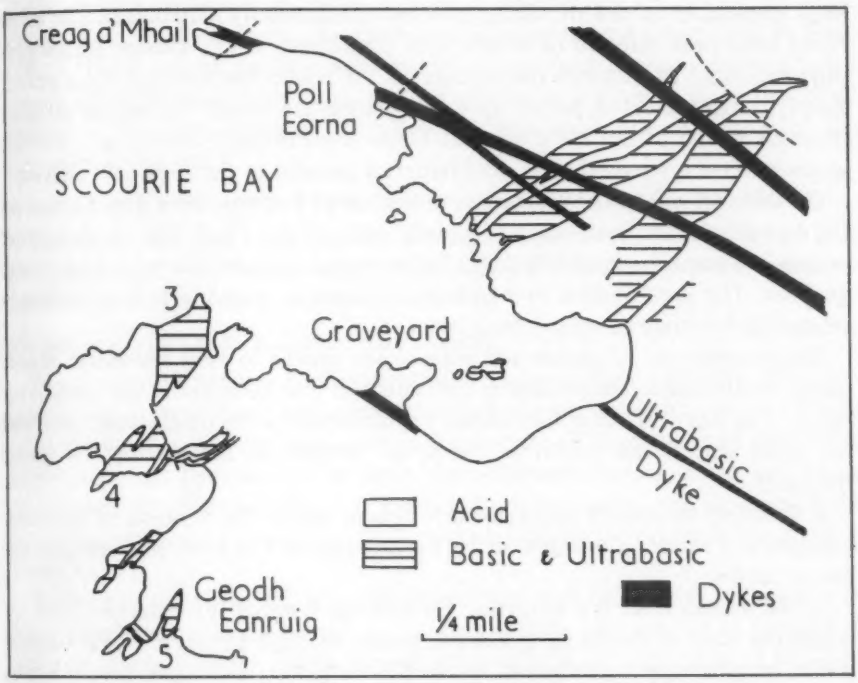

FIG. 1. Sketch-map of the outcrops of basic and ultrabasic gneisses near Scourie.

coarse-grained layers. The foliation is parallel to the margins of the ultrabasic rock, and to the regional foliation, but the amphibole-rich bands also follow planes perpendicular to the foliation (Sutton & Watson, 1951, p. 269). No chromite-rich layers have been observed. Rocks referred to as dunite gneiss, peridotite gneiss, and pyroxenite gneiss may be distinguished by their olivine content.

The *contact gneisses* form a poorly exposed group of rocks, found only at the contacts between ultrabasic and garnetiferous basic gneisses. They occur as bands up to one foot thick, which are readily eroded. The best exposure is in a mass at Loch an Daimh Mhor, 15 yds from the Badcall road, and 30 yds south of the loch (locality not shown on Fig. 1; map reference 29/159428). Rocks of this group contain varying proportions of garnet, augite, hypersthene, amphibole, spinel, plagioclase, and ore minerals. The composition appears to vary rapidly perpendicular to the foliation.

The *basic* and *garnetiferous basic gneisses* are pale grey to dark red-brown rocks, medium- to coarse-grained, and weathering to a pale-brown crust. The darker varieties are rich in deep-red, anhedral garnets, occurring as rounded or oval porphyroblasts. The specific gravity ranges from 2·85 in the garnet-free types to 3·65 in the most garnetiferous. All intermediate stages exist between a plagioclase–pyroxene gneiss, referred to as basic gneiss, through garnetiferous basic gneisses to garnet–pyroxene gneisses with accessory plagioclase. The latter rocks have been referred to as eclogites (Davidson, 1943). Garnet forms porphyroblasts up to ten times the diameter of the plagioclase and pyroxene grains. Rarely, large masses of garnet up to 3 ft across are found. Inclusions of other minerals in the garnet are common. There is no mineral orientation, but the larger garnets are lens-shaped, and flattened parallel to the regional foliation.

On the west side of the basic mass at Camas an Lochain, (4 of Fig. 1), and on the east side of the basic mass at Geodh' nam Cliabh (3 of Fig. 1), the garnet occurs in a manner suggesting that it has grown along joint fractures in the basic gneisses. The joint system to which it is related is sealed, and not obviously related to the existing open-joint system.

The proportions of garnet and plagioclase appear to vary inversely. Where garnet is abundant, plagioclase is concentrated into rims about the porphyroblasts. The size of the porphyroblasts, the definition of the plagioclase rims, and the grain size of the pyroxene matrix all increase as the amount of garnet increases.

A foliation parallel to the regional foliation, and to the contacts of the basic gneisses as a whole, is brought out by the arrangement of more and less garnetiferous layers.

In the masses there is a sequence, on passing towards the exterior, from an ultrabasic core of dunite or peridotite gneiss through pyroxenite and contact gneiss to garnet–pyroxene gneiss, garnetiferous gneiss, and basic gneiss. Ultrabasic rocks may occur at more than one horizon in the mass.

Externally, the basic gneisses are enveloped by plagioclase gneisses, which are transitional from the basic gneisses and are themselves transitional outwards into quartzo–feldspathic gneisses which are only rarely potash-rich. Leucocratic gneiss bands within the basic series pass out into basic gneiss on both sides through plagioclase gneiss, but internally they frequently contain potash-rich types such as quartz–perthite gneiss or pegmatite. The enveloping quartz–plagioclase gneiss passes gradually outwards into a finer-grained, banded acid gneiss.

On the west side of the basic rocks at both masses west of Pairc a Cladaich (map reference 29/153452), and on the west side of the mass at Geodh' Eanruig, leucocratic and basic gneisses are coarsely interbanded without the development of plagioclase gneisses or potash-rich types. Patches and strips of mafic material occur in these strongly banded rocks, and resemble xenoliths torn off the ultrabasic mass; in a few cases a rotated foliation is apparent within them.

With the exception of the basic gneiss itself, none of the rock types is found as an isolated component of the banded acid gneisses of the early Lewisian complex. The ultrabasic and basic gneisses occur as elongated masses up to half a mile in length, and 100 yds in breadth, which are concordant with the foliation of the banded gneisses. The volume of ultrabasic material is exceeded by that of the basic and garnetiferous basic gneiss.

The masses occurring on the north side of Scourie Bay are cut by two large dykes of the Scourie swarm, the southern one being the dyke described by Teall (1885). These are of pre-late metamorphism age, and are unmetamorphosed except locally within shear belts, and marginally in a manner to be described elsewhere. The formation of the ultrabasic and basic gneisses preceded the intrusion of the dykes.

PETROGRAPHY AND CHEMISTRY OF THE ROCKS AND MINERALS

The ultrabasic and basic gneisses are illustrated by the description of four rocks and brief reference to others. It is believed that these are representative of all fresh material from this group of rocks.

Peridotite gneiss (*X 282*), *Geodh' nam Cliabh*

The greater part of this rock is a granular coarse-grained aggregate of hypersthene, augite, amphibole, and accessory spinel intergrown with iron ore. Olivine occurs as smaller, rounded grains set in the margins of larger plates of amphibole or hypersthene. The chemical analysis, trace-element content, norm, and mode of this rock are given in Table 7, column 2. Both pyroxenes, and the amphibole, have been analysed (Tables 4, 5), and optical data for the minerals are given in Table 6.

The augite is pale-green, non-pleochroic, and well cleaved. Fine lamellae of hypersthene occur in the augite, but none has been observed to lie parallel to (001) (cf. Muir & Tilley, 1958). Fine lamellae of iron ore also occur in two sets, one of which is parallel to (001) and picked out by later alteration to blue-green amphibole.

The hypersthene is feebly pleochroic, the colour scheme being X = pale red; Y = pale yellow; Z = apple-green, as in all rocks of the basic series. Fine lamellae of augite are present parallel to (100) of the hypersthene. The hypersthene is altered to chlorite along cracks, the latter mineral being feebly pleochroic from pale green to pale yellow-brown. A similar, but finer-grained chlorite appears to be the principal component of the serpentinous alteration which affects the olivine.

The amphibole appears to be primary, and is pleochroic with X = yellow-green; Y = olive-green; Z = green. Iron-ore plates and rods are present as inclusions in the amphibole, and small granules of ore commonly occur at the grain boundaries.

A deep-green, isotropic spinel forms small, rounded grains and is intergrown with magnetite which may exceed 30 per cent by volume of the grains.

The olivine is free from inclusions of other minerals, but some of the grains, especially where they are adjacent to amphibole, have a narrow mantle of hypersthene (Fig. 2). The olivine grains are set in the margins of larger crystals

FIG. 2. Narrow rim of orthopyroxene (dark) between olivine and amphibole (pale) in peridotite (X 282). Crossed nicols, × 50 approx.

of amphibole, orthopyroxene, and occasionally of augite and appears to be at the margins of these other minerals rather than included within them. The olivine is partially altered to chlorite, magnetite, and small patches of carbonate. A preferred orientation of the olivine was detected by universal stage work.

On the one hand, the peridotite gneiss is transitional into olivine-rich types, i.e. dunite gneisses, and, on the other hand, into pyroxenites. The olivine-rich types are represented by rocks such as (Z 135) from Camas an Lochain (analysis in Table 7, column 1; mineralogical data in Table 6). Mineralogical data for

another dunite gneiss (X 191) from Loch an Daimh Mhor, and for three olivine-rich peridotites (Z 111, Z 140, X 593), the first two from Camas an Lochain and the other from the Allt Mor Geisgil, are given in Table 6. The dunite gneisses are poor in augite, amphibole, and spinel, and contain an olivine of higher iron to magnesium ratio (according to R.I.) than the associated orthopyroxene. In the presence of increased amounts of augite, amphibole, and spinel, the iron to magnesium ratio of olivine is less than that of the hypersthene, as is the case in (X 282) described above, and in (37,310) (see Table 6 and Muir & Tilley, 1958). The hypersthene rims about the olivine in (X 282) are of lower iron to magnesium ratio than the majority of the pyroxene, but higher than that of the olivine (Table 6).

The pyroxenites are represented by rocks such as (X 284) from Geodh' nam Cliabh, which has the composition: augite 19·4 per cent; hypersthene 56·2 per cent; amphibole 17·8 per cent; spinel and ore 5·9 per cent; olivine 0·7 per cent. The texture of this rock is granular throughout, and there is little alteration. The hypersthene is more strongly pleochroic than in (X 282). An analysis of hypersthene from a similar pyroxenite is given in Table 4, V.

Contact of the ultrabasic rock at Loch an Daimh Mhor, Samples UA 1–13

The material described comes from the lower contact of a layer of ultrabasic gneiss near the south shore of Loch an Daimh Mhor, as noted in the account of field relations (p. 249).

Two contiguous blocks afforded a continuous section of 19 cm perpendicular to the strike, in ultrabasic and ultramafic gneisses. Considerable variation in composition is evident in the hand specimens but there is transition between each of the zones and no sharp contact is apparent. The results of petrographic observations on this specimen are given in Fig. 3, and further mineral data determined on two specimens (X 819, X 192) from the same locality are given in Tables 1 and 2. The terms 'harzburgite', 'lherzolite', and 'ariegite' are used in accordance with the mineralogical composition (Johannsen, 1938) and are not intended to imply similarity of genesis between these rocks and the same rock types found elsewhere. In Fig. 3, modal estimates and refractive indices are arranged in their correct positions relative to the centimetre scale.

The spinels are variable in composition and appearance, the most iron-rich apparently occurring in the lherzolite and hypersthene–pyroxenite, and again in the ariegites at distances greater than 10 cm from the ultrabasic end of the specimen. The intervening ariegites (4–10 cm from the ultrabasic end of the specimen) contain a blue-green spinel which is not intergrown with iron ore and which appears to be relatively rich in magnesia. The iron-rich spinels are dark green and crowded with minute inclusions of opaque ore, possibly magnetite, and intergrown with ilmenite and pyrrhotite. Pyrrhotite frequently contains subhedral inclusions of pyrite and chalcopyrite. Independent primary magnetite has not been observed in this specimen.

The garnet is anhedral, occurring as irregular masses and in one variety of ariegite (the 'contact gneiss' of Fig. 3) garnet forms a network which binds the other constituents.

The amphibole is a variety pleochroic in shades of brown and yellow. It occurs as large crystals which frequently enclose pyroxene and spinel. Small granules of iron ore occur at the margins of the amphibole and there are abundant rod-shaped inclusions (0·03 by 0·001 mm) of a material with high relief and high birefringence. These are oriented parallel to three directions in the host. The amphibole of the ariegite nearest the ultrabasic rock is oriented so that all the grains have [001] lying close to the plane of foliation.

TABLE 1

Further data for contact gneisses

Data of Table 1 determined by cutting grains from selected parts of the respective thin sections. The cell sizes given in Table 2 represent mean values for samples the composition of which varied within narrow limits.

Specimen	*Clinopyroxene* (+)2*V*	*R.I.*	*Orthopyroxene* (−)2*V*	*R.I.*	*Garnet R.I.*	*Spinel R.I.*	*Plagioclase R.I.*
X 819 (*a*)	n.d.			$\gamma = 1{\cdot}694$	1·770	1·770	n.d.
(*b*)		$\gamma = 1{\cdot}702$		$\beta = 1{\cdot}687$	1·768	1·742	n.d.
(*c*)	n.d.			$\beta = 1{\cdot}680$	1·752	1·761	n.d.
X 192 (*a*)	53°	$\beta = 1{\cdot}684$	75°	$\gamma = 1{\cdot}690$	1·760	n.d.	n.d.
Z 116 (*a*)		$\beta = 1{\cdot}695$		$\beta = 1{\cdot}690$	n.d.	1·786	$\beta = 1{\cdot}564$
(*b*)	n.d.			$\beta = 1{\cdot}697$	1·782	n.d.	n.d.
(*c*)	n.d.			$\gamma = 1{\cdot}699$	1·778	1·803	n.d.

TABLE 2

Data for analysed or partially analysed samples of garnet

Specimen	a_0 (Å)	*R.I.*
X 192	11·550	1·760
X 819L_1	11·548	1·757
X 819L_2	11·545	1·756
X 819H_1	11·550	1·760
X 819H_2	11·552	1·766

Only one plagioclase composition has been determined, falling in the bytownite range. The majority of the plagioclase is partly or completely altered to prehnite. Alteration of the other minerals is slight except for some serpentinization of the harzburgite and lherzolite zones and the formation of a mineral, which may be diaspore, from the spinel.

Chemical analyses of ten samples from this sequence are presented in Table 3, together with the atomic percentages of the main constituents and various atomic ratios. Each analysis gives the mean composition of a narrow zone parallel to the foliation. Distribution curves for the main constituents obtained from the average results of the samples are shown in Fig. 4; Ca–Mg–Fe ratios for the rocks are compared in Fig. 5.

TABLE 3

Wt. per cent	*Sample nos. UA*									
	1	2	3	4	5	6	7	8	10	12
SiO_2	44·1	50·2	50·3	46·8	42·6	41·7	38·3	34·3	32·3	32·2
TiO_2	0·20	0·34	0·36	0·86	1·0	0·96	0·21	0·81	0·48	0·17
Al_2O_3	2·5	3·8	3·9	7·9	16·2	18·6	20·3	20·9	20·4	20·0
Fe_2O_3	5·0	2·4	2·1	2·1	3·6	2·9	5·4	5·3	7·7	10·2
FeO	4·1	6·4	6·1	5·3	7·3	10·2	11·6	11·9	15·7	14·7
MnO	0·15	0·16	0·17	0·18	0·28	0·35	0·46	0·38	0·49	0·53
MgO	32·8	27·4	24·2	15·1	16·1	14·4	14·4	15·1	13·6	13·0
CaO	2·3	5·5	9·3	18·0	9·7	7·4	5·4	5·2	4·6	4·2
Na_2O	0·92	0·36	0·87	0·23	0·12	0·61	0·32	1·2	0·32	0·15
K_2O	0·70	<0·05	0·35	0·33	<0·05	0·31	<0·10	0·76	0·17	<0·10
P_2O_5	0·029	0·013	0·008	0·025	0·044	0·050	0·061	0·071	0·11	0·12
H_2O^+	6·6	2·2	0·76	1·6	0·70	0·68	0·35	0·86	1·4	2·3
S	0·12	0·32	0·28	0·34	0·13	0·09	0·19	0·67	1·54	1·19
CO_2	0·16	0·41	0·65	0·70	1·1	1·4	2·2	1·9	1·6	1·4
TOTAL *less* O for S	99·62	99·39	99·21	99·19	98·84	99·61	99·19	99·02	99·64	99·62
Atomic per cent; H_2O-and CO_2-free										
Si	16·8	18·5	18·5	17·7	16·0	15·7	14·7	12·9	12·9	12·9
Ti	0·06	0·09	0·10	0·24	0·28	0·28	0·06	0·24	0·14	0·05
Al	1·1	1·6	1·7	3·5	7·1	8·2	9·2	9·7	9·5	9·5
Fe^{2+}	1·4	0·7	0·6	0·6	1·0	0·8	1·5	1·6	2·3	3·1
Fe^{3+}	1·3	2·0	1·9	1·7	2·3	3·2	3·7	3·9	5·2	4·9
Mn	0·05	0·05	0·05	0·06	0·09	0·11	0·15	0·12	0·16	0·18
Mg	18·5	15·0	13·2	8·5	9·0	8·0	8·2	8·9	8·0	7·8
Ca	0·9	2·2	3·7	7·3	3·9	3·0	2·2	2·2	2·0	1·8
Na	0·7	0·2	0·6	0·2	0·1	0·4	0·2	0·9	0·2	0·1
K	0·3	tr.	0·2	0·2	tr.	0·2	tr.	0·4	0·1	0·1
P	0·01	tr.	tr.	0·01	0·01	0·02	0·02	0·02	0·03	0·03
S	0·08	0·22	0·19	0·24	0·09	0·06	0·14	0·48	1·1	0·90
O	58·8	59·6	59·4	59·7	60·1	60·0	59·9	58·6	58·3	58·7
$Fe^{\circ}+Mg+Mn$ atomic per cent	21·2	17·7	15·7	10·8	12·4	12·1	13·5	14·5	15·7	16·0
$\frac{(Fe^{\circ}+Mn)\times 100}{Fe^{\circ}+Mn+Mg}$	13·0	15·1	15·9	21·4	27·3	33·9	39·8	38·8	48·8	51·3
Ca	4	11	19	40	24	20	14	13	11	10
Mg	38	75	68	47	55	53	52	53	46	44
$Fe^{\circ}+Mn+Mg$	13	14	13	13	21	27	34	34	43	46
Al	1	7	4	15	30	34	36	33	35	34
Ca	4	10	18	34	17	13	9	9	7	7
$Fe^{\circ}+Mn+Mg$	95	83	78	51	53	53	55	58	58	59

Fe° = total iron. Analyses made in the Geochemical Laboratory, Department of Geology, Edinburgh University.

The rocks contain serpentine, scapolite, prehnite, dolomite, and a second amphibole as alteration products of the primary minerals.

A different type of contact is represented by specimen (Z 116) from Camas an Lochain. It comes from the margin of a layer of ultrabasic rock a few feet thick which does not contain olivine-rich material internally. A transition from pyroxenite to garnet–augite gneiss is shown within 4 cm.

The sequence of rock types in this transition is:

(1) Pyroxenite gneiss; augite-rich matrix with clusters of amphibole, hypersthene, and spinel.

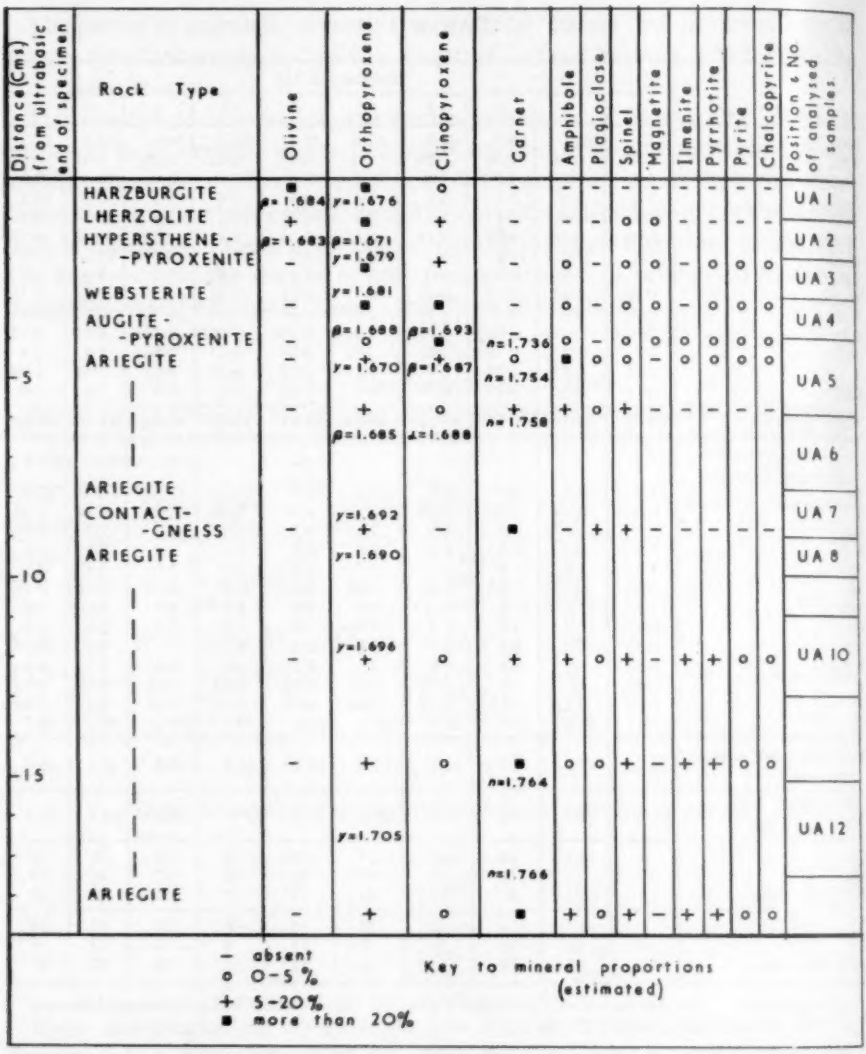

FIG. 3. Tabular representation of the petrography of the zoned ultrabasic contact from Loch an Daimh Mhor, (specimen UA).

(2) Pyroxenite gneiss; augite-rich matrix with clusters of amphibole, hypersthene, and spinel rimming aggregates of plagioclase grains.

(3) Contact gneiss; augite-rich matrix with large patches of garnet margined by complex plagioclase–garnet–spinel–hypersthene intergrowths, and with some amphibole.

(4) Garnet–augite–gneiss, with accessory plagioclase, similar to (X 646) described below.

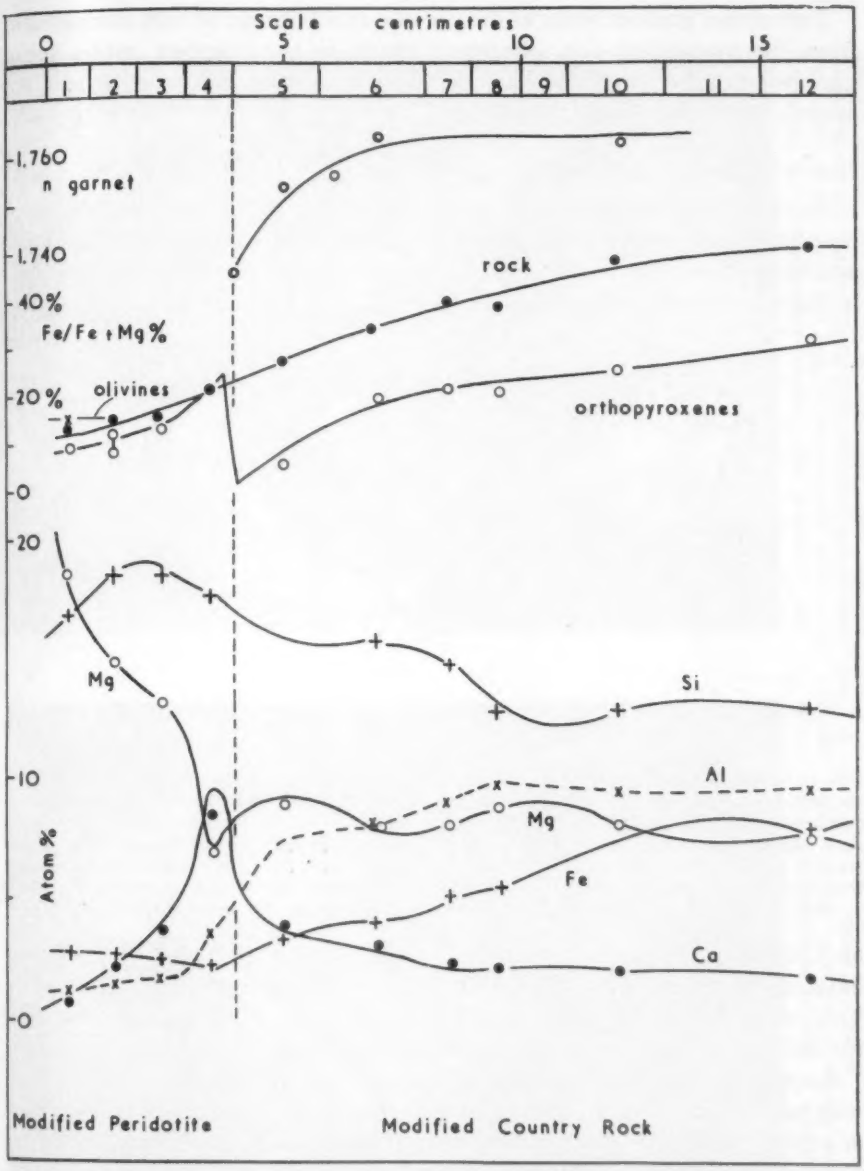

FIG. 4. Distribution curves of elements with position in the specimen UA Centimetre scale and sample-number divisions shown at top. Analytical results plotted at middle of sample zone to which they refer. Optical results for garnet, olivine, and pyroxene shown in the appropriate positions. In the case of olivine and orthopyroxene the refractive index measurements have been converted to Fe/Fe+Mg ratio via charts given by Tröger (1956) and Hess (1952). The objections to the latter procedure have been discussed elsewhere, but the present data are believed to show the form of variation in the ferromagnesian parageneses, even if their precision is low.

The contact gneisses occur at the site of a rapid change of rock composition, from the magnesium-rich, ultrabasic gneiss to the iron-rich garnet–augite gneisses (cf. Table 7). The unusual petrographic features can be ascribed to the presence of strong chemical gradients.

Garnet–augite gneiss (*X 646*), *Geodh' Eanruig*

The rock is coarse-grained, with a matrix of granular augite enclosing large porphyroblasts of garnet which are rimmed by granular plagioclase, iron ore, and hypersthene. The chemical analysis, norm, and mode of this rock are given in Table 7, column 3, and the same data for (Z 125), a similar gneiss from Camas

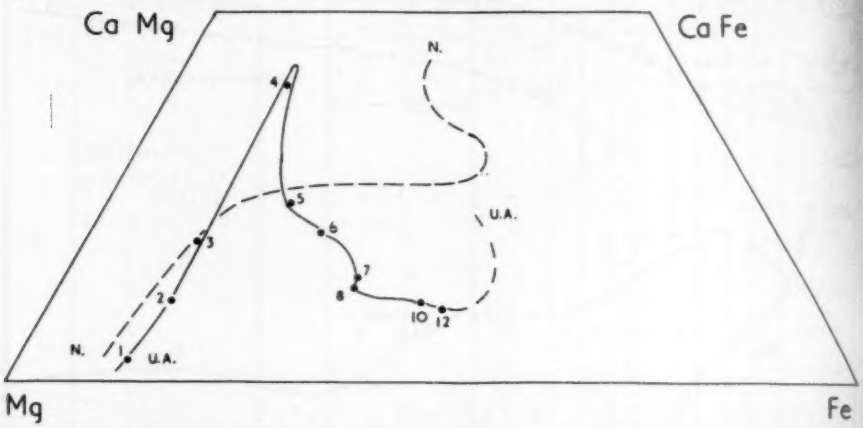

FIG. 5. Mutual variation in Ca, Mg, and total Fe+Mn in the zones of specimen UA is shown by the solid curve, which is compared with the broken curve *N* representing the inferred variation between ultrabasic rock and basic gneiss in circumstances where reaction has taken place on a larger scale than in specimen UA The latter must be envisaged as a condensed representation of the reaction process. On the basis of petrographic observations only, it may be suggested that about the thin layers of pyroxenite which do not contain olivine internally, the variation is more nearly linear than either of the curves drawn. The broken curve is based on the rock analyses of Table 7.

an Lochain, in Table 7, column 4. The augite and hypersthene from (X 646) have been analysed (Table 4, VIII and IX), and also the garnet (Table 5, VII). Trace-element data for the plagioclase are given (Table 5, VIII), and optical data for the minerals of (X 646) and (Z 125) in Table 6.

Large rounded porphyroblasts of isotropic pink garnet occur in (X 646), with narrow rims of granular plagioclase. The garnet encloses rounded grains of augite, plagioclase, iron ore, and hypersthene as single crystals. Between the plagioclase rim and the granular augite matrix of the rock there is a zone of granular hypersthene which may show good crystal terminations towards the plagioclase. Iron ore and an anhedral olive-green amphibole with marked pleochroism are present in these rims about garnet.

The margins of the garnet porphyroblasts are irregular, the garnet extending as cuspate or lobate protrusions along the boundaries of the plagioclase grains,

FIG. 6. Large grain of iron ore in garnet–augite gneiss, X 646, showing coarse lamellae of magnetite. Reflected light, crossed nicols, × 50 approx.

FIG. 7. Grain of augite in garnet–augite gneiss, X 646. The grain is cut nearly perpendicular to [001] and shows well-developed thin lamellae of hypersthene (pale) parallel to [100]. A few of the coarser lamellae contain plagioclase and iron ore, and terminate in larger, lozenge-shaped grains of hypersthene, as at the mid-top left boundary. Crossed nicols, × 50 approx.

and particularly along the boundaries between plagioclase and grains of hypersthene which occur close to the garnet. The plagioclase is twinned on the albite and pericline laws, and is unzoned, but all the grains have a mantle of more sodic plagioclase except where they are in contact with the garnet. The compositions of these plagioclases have been estimated from refractive index determinations as An_{71} (cores), and An_{60} (rims) (Table 6). Plagioclase is also present as small, irregular grains associated with iron ore, and hypersthene as coarse lamellae in the augite. The composition of this plagioclase has been estimated as An_{55} (Table 6).

The hypersthene is strongly pleochroic, and contains numerous small brown plates which may be very thin lamellae of iron ore, and are oriented roughly parallel to (101). There are other fine but continuous lamellae oriented parallel to (100) of the hypersthene, which have the relative refractive indices appropriate to augite intergrown with the hypersthene in such a way that (100) and [001] are common to both structures. An X-ray single-crystal study of this hypersthene (method of Bown & Gay, 1959) confirms the orientation and identification of the augite lamellae, and also reveals the disorientation of the [001] axis of hypersthene through about 8° in the plane (010) which has been recorded from other metamorphic hypersthenes (Henry, 1942). The disoriented units appear to be present on a submicroscopic scale since the coarse lamellar structure described by Henry is not visible in these hypersthenes. Material of the two orientations appear to be present in approximately equal proportions.

The iron ore occurs as three types, the greater part of it forming large anhedral grains enclosed within, or marginal to, the garnet porphyroblasts. By reflected light these appear as coarse bar-like intergrowths of isotropic magnetite and anisotropic ilmenite (Fig. 6). The magnetite lamellae are parallel to one direction only, probably (0001), of the ilmenite, and there are no further fine lamellae of magnetite in the ilmenite, or vice versa. Ulvöspinel and spinel have not been detected. Iron ore also occurs as fine vermicular intergrowths with the garnet, where it appears to be magnetite alone. The small granules of iron ore which occur with plagioclase, and with hypersthene in the coarse lamellae in augite, also appear to be magnetite.

Augite occurs as a coarse granular aggregate forming the matrix of the rock, in which are set the garnet porphyroblasts and their rims. The mineral is pale green and feebly pleochroic in thin section. Much smaller grains of plagioclase, hypersthene, and ore occur among the augite-rich areas, generally as clusters at the junction of three augite grains, and occasionally as components of coarse lamellae in the augite (Fig. 7). The lamellae and the trains of blebs are parallel to the trace of (100) in the section, which in certain cases may lie at up to 40° from the prominent {110} cleavage. The hypersthene component of these lamellae can sometimes be seen to extend to the margin of the augite grain, where it expands into a lozenge-shaped grain, sometimes with good crystal terminations externally. The augite also contains many fine lamellae parallel to (100) which

are continuous across the grains, and appear to be hypersthene. An X-ray single-crystal study was made of a large augite grain cut from thin section, which contained both coarse and fine lamellae of hypersthene, iron ore of the coarse lamellae, and plagioclase. The reflections due to plagioclase have not been identified. The hypersthene and augite are intergrown with (100) and [001] of the two structures in common. The spinel phase has the cell dimensions of magnetite, and is present as an oriented intergrowth similar to that produced by exsolution (Bown & Gay, 1959). The analysis of augite from this rock includes the fine hypersthene lamellae, but does not include the material of the coarse lamellae.

Apatite is present in small amounts as an accessory constituent. It occurs in the plagioclase rims about the garnet.

Small amounts of sericite and carbonate are present as alteration products of the plagioclase, and a little blue-green amphibole has formed by alteration of the augite. The hypersthene has altered slightly to a dark-brown, fibrous material which may be another variety of amphibole.

Garnetiferous basic gneisses

The garnetiferous basic gneisses are represented by analyses of two rocks, (X 195) from Loch an Daimh Mhor and (Z 117) from Camas an Lochain (Table 7, columns 5 and 6 respectively). Mineralogical data for these rocks are given in Table 6, chemical analyses of both garnets in Table 5, IX and X, and trace-element data for the plagioclase of (Z 117) in Table 5, XI. Mineralogical data for (Z 127), a gneiss more garnetiferous than either of the analysed specimens, are also given in Table 6.

In the more garnetiferous basic gneisses the garnet forms moderate to large porphyroblasts with plagioclase rims, as in the garnet–augite gneisses to which they are transitional. In some of these rocks there is a zone about the garnet in which plate-like crystals of hypersthene, tabular approximately parallel to (001), are set radially to the garnet margin and within the rim of granular plagioclase. The garnet has long extensions from the main mass along both boundaries of these hypersthene strips.

In those garnetiferous basic gneisses with more than 5 per cent of modal garnet this mineral occurs as rounded grains, the size of which increases as the amount of garnet increases. In those gneisses with less than 5 per cent of garnet the mineral occurs largely as mantles about iron ore, and occasionally about apatite. A gneiss of this type from Geodh' nam Cliabh, with common garnet rims about iron ore (X 260), has been analysed (Table 7, column 7). Mineralogical data for this rock and for (X 245) from Geodh Eanruig are given in Table 6.

The garnet mantles of (X 245) are formed along iron ore–plagioclase boundaries, and sometimes extend a short way along adjacent pyroxene–plagioclase boundaries. The garnet is pink, isotropic, and contains fine vermicular or dendritic inclusions of iron ore. In this specimen the amount of garnet is observed

to increase towards a thin vein along which quartz and feldspar appear to have been introduced. In (X 260) the texture appears to be uniform, and not associated with the formation of acid veins.

Specimen (X 245) is unique among the examined material in containing bulbous overgrowths of an isotropic or cryptocrystalline material which have formed on the surfaces of garnet towards plagioclase, and also about dendritic growths of pyrite in the plagioclase. The pyrite occurs as chains of small cubes, and is probably of secondary origin as are, presumably, the overgrowths.

Basic gneiss (X 291), Geodh' nam Cliabh

This is a medium-grained, granular gneiss containing abundant plagioclase, augite, and hypersthene, with accessory iron ore, apatite, potash feldspar, and garnet. The chemical analysis, norm, and mode of the rock are given (Table 7, column 8), as are analyses of the augite and hypersthene (Table 4, X and XI). Trace-element data for the plagioclase (Table 5, XII) and other mineralogical data (Table 6) are also given.

The grain size is about 1 mm, and the ferromagnesians tend to be aggregated into small clusters or chains. In parts there are clusters of larger grains of augite, up to 4 mm across.

The plagioclase occurs as anhedral grains twinned on the albite and pericline laws. The twin lamellae pinch out towards the grain centres, and most of the grains are slightly bent. There are abundant very fine, rod-like inclusions of potash feldspar with $2V$ about 60° (−), suggesting orthoclase, and also small, irregular marginal patches of orthoclase which are greatly subordinate in volume to the plagioclase. The marginal patches of potash feldspar are observed in contact with unaltered hypersthene.

The augite is pale green and feebly pleochroic. Most of the grains are slightly bent. Small granules of iron ore are common along boundaries between augite grains, and there are occasional included blebs of plagioclase. Fine lamellae of hypersthene parallel to (100) are common, as in the augite of the garnet–augite gneiss (X 646). Coarse lamellae containing hypersthene, plagioclase, and iron ore have been observed in the coarser clusters of augite, and also trains of blebs of these materials, in all cases lying parallel to the trace of (100). An X-ray single-crystal study of a coarse lamellar intergrowth showed the augite and hypersthene to be arranged with (100) and [001] in common, as in the pyroxene of (X 646).

The hypersthene is strongly pleochroic, and forms smaller grains than the augite. Some of it occurs as poorly formed grains inset at the margins of the augite. In some cases these inset grains are continuous with the material of the coarse lamellae in the augite. Fine lamellae of augite occur parallel to (100) and there are small plate-like inclusions of brown material parallel to (101) approximately, as in the hypersthene of (X 646).

The iron ores have been examined by reflected light. The larger grains are

rounded and composed of ilmenite and magnetite, frequently in a coarse bar-like intergrowth. The ilmenite is anisotropic, and extinguishes parallel to the magnetite lamellae. There are no fine lamellae of either oxide in the other, nor is there spinel or ulvöspinel in the magnetite. The latter mineral, however, contains frequent small inclusions of silicate. Very small amounts of pyrite occur, as clusters of small cubes, and may be of secondary origin.

Garnet is scarce, and occurs as small, rounded grains without crystal form. It is pale pink and isotropic. Apatite is a frequent accessory, and the prism zone faces are developed in some of the grains. Sericite and carbonate are present as a patchy alteration of the plagioclase, and there is some iron oxide staining along the cracks. The hypersthene is altered partly to small flakes of biotite, which also occur about iron ore, and sometimes to chlorite.

A basic gneiss (37,099) with more hypersthene than (X 291) has been described by Muir & Tilley (1958). Analyses of the pyroxenes of (37,099) are quoted (Table 4, XII and XIII) and optical data given in Table 6. Types with less hypersthene than (X 291) have also been noted, e.g. (X 290) from the same locality, which contain 5·3 per cent hypersthene and only 1·5 per cent iron ore. (X 276), again from Geodh' nam Cliabh, contains 14·1 per cent hypersthene, 5·6 per cent iron ore, and 1·7 per cent garnet as rims about the iron ore. The amount of hypersthene and iron ore is greatest in those basic gneisses which contain a small amount of garnet.

CHEMISTRY AND MINERAL PARAGENESES

The chemistry of the rocks and minerals of the ultrabasic association has been illustrated by the analyses and other data in Tables 2–7. The analyses of the basic series have been converted to atomic percentages, calculated water-free, and are plotted in the diagram (Fig. 8).

The calcium content of the basic and garnetiferous basic gneisses (Table 7, columns 3–8) is higher than usual in basic igneous rocks, and as a group the calcium content is higher than that of any igneous rock series of comparable silica content.

The distribution of magnesium, iron, aluminium, and silicon shows culminations and depressions.

Chromium, nickel, and, to a lesser extent, cobalt, are relatively abundant in the ultrabasic group, but fall to uniformly low values in the garnetiferous basic gneisses.

Potassium is low throughout. The sodium/calcium ratio is highest in the basic gneiss and lowest in the ultrabasic other than the dunite gneiss. The composition of the plagioclase in the rock does not appear to be directly influenced by the sodium/calcium ratio.

Among the minerals, titanium is contained largely in ilmenite, and is present in decreasing concentration in augite, hypersthene, and garnet respectively. Manganese, like iron, shows an inverse distribution to titanium in the last three

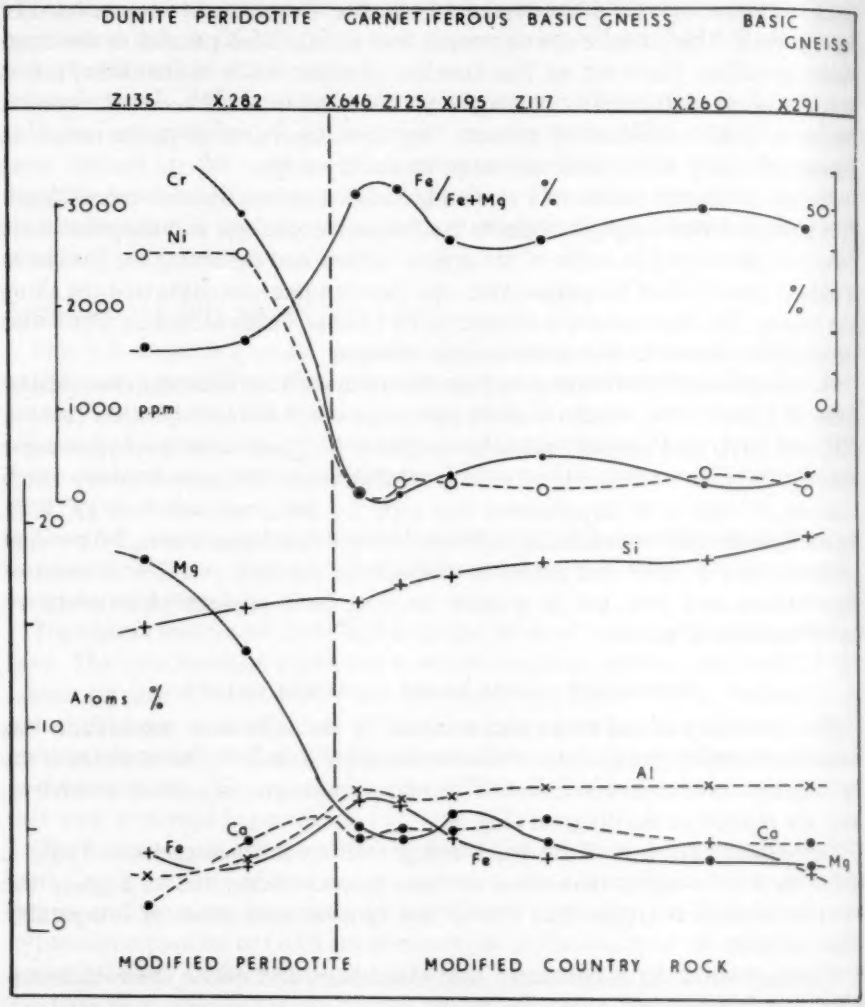

FIG. 8. Distribution curves of elements in the samples whose analyses are presented in Table 7. These samples were collected from various basic/ultrabasic masses, without regard to position, before the significance of the variation was appreciated. The abscissa in this diagram is therefore an arbitrary linear scale giving prominence to the various rock types in proportion to their distribution in the outcrops. Vertical dashed line marks the estimated position of the contact gneisses.

minerals. The iron/magnesium ratio decreases on passing from garnet to hypersthene to augite in any one rock, but the distribution in olivine and spinel presents anomalous features (discussed below). Trivalent cations are concentrated in augite relative to hypersthene, e.g. chromium, vanadium, aluminium, and ferric iron, while divalent cations such as nickel, cobalt, manganese, and ferrous iron are concentrated in the hypersthene. None of the augites is notably rich in titanium or sodium, and they do not resemble the clinopyroxenes of tholeiitic or

alkali igneous rocks, nor of eclogites. They are comparable with the pyroxenes from the Madras charnockite series and metamorphosed pyroxene-bearing rocks (Brown, 1957; Murray, 1954; Wilkinson, 1956, 1957; Alderman, 1936; Howie, 1955; Muir & Tilley, 1958).

Yttrium is concentrated in the garnets (cf. Keith & Roy, 1954; Jaffe, 1951), and strontium and barium in the plagioclases.

The parageneses in the ferromagnesian minerals are represented in Fig. 9, which also contains a curve representing the apparent variation of rock composition in the zoned series.

In Fig. 9, points shown with solid ornament were obtained by analysis and all others were estimated from optical data. Compositions were obtained from the diagrams of Hess (1949, 1952) and Tröger (1956). The compositions of olivines and spinels are indicated on parallel scales below that for orthopyroxene. Rock compositions are shown by crosses, orthopyroxenes by squares, and the remaining minerals by circles. The nature of the mineral to which each circle refers is indicated by the label attached to the curve or scale close to which the mineral plots. The curves shown for clinopyroxene and garnet are believed to represent the probable composition ranges of these minerals in the rocks described in this paper. The same numeral is used for a rock and for the points representing its constituent minerals. In the case of the contact gneiss specimens designated 3 and 3′, the mineral compositions are known to vary within one hand-specimen. Each of the six linked optical estimates for orthopyroxene, clinopyroxene, and garnet from 3 and 3′ refer to coexisting minerals from the same part of a thin section (data of Table 1) and it has been necessary to assume the calcium content of one clinopyroxene and all the garnets of 3 and 3′ as lying on the curves drawn to represent the composition range of these minerals. Positions on these curves were obtained by interpolation using the determined refractive indices and the refractive indices of analysed minerals. The points for orthopyroxene, clinopyroxene, and garnet from 3, shown in solid ornament, refer to analysed or partially analysed material. The two garnets of lowest Fe:Mg ratio are those analysed in full (Table 5, II and III). All tie lines for coexisting minerals of the contact gneisses are shown dashed. For the assemblage 9, two points are shown near the orthopyroxene composition range. The upper (circle) is that found by analysis of material containing some clinopyroxene; the lower (square) is the composition corrected after a grain count.

Points numbered 1, 2, and 4–9 refer to rocks, the analyses of which are given in Table 7, columns 1–8 respectively. Other points are numbered thus: 1′ olivine–orthopyroxene from (X 191), an olivine-rich peridotite from Loch an Daimh Mhor. 2′ hypersthene from pyroxenite (anal. R. A. Howie). 2″ pyroxenes and olivine from peridotite (37310) (Muir & Tilley, 1958). 3 data from specimens (X 192) and (X 819), identical with parts of specimen (UA). 3′ data from specimen (Z 116). 9′ pyroxenes from basic gneiss without garnet (37,099) (Muir & Tilley, 1958).

TABLE 4

Analyses of pyroxenes

	Peridotites				*Pyroxenite*	*Contact gneiss*		*Garnetiferous basic gneiss*		*Basic gneisses*			
	I	II	III	IV	V	VI	VII	VIII	IX	X	XI	XII	XIII
SiO_2	51·38	53·08	50·35	53·95	52·44	49·01	50·50	49·17	48·50	50·04	49·99	50·01	50·34
TiO_2	0·38	0·21	0·43	0·11	0·09	0·84	0·25	0·55	0·06	0·56	0·13	0·58	0·13
Al_2O_3	4·52	4·45	5·17	4·24	4·45	5·58	7·16	5·51	4·66	4·89	2·89	4·55	3·14
Fe_2O_3	1·85	1·59	1·69	2·24	1·27	2·75	1·85	2·31	3·56	1·79	1·69	2·61	2·97
FeO	3·34	10·62	3·28	8·40	13·85	4·55	9·28	8·32	19·57	9·99	24·86	8·07	22·53
MnO	0·15	0·21	0·13	0·25	0·26	0·30	0·21	0·19	0·30	0·23	0·56	0·29	0·70
MgO	15·21	28·98	15·41	30·17	26·72	13·77	28·70	12·52	23·32	11·74	17·60	12·40	19·52
CaO	22·96	0·50	22·80	0·57	0·35	22·29	1·58	20·82	0·12	19·89	1·84	20·82	0·60
Na_2O	0·54	0·06	0·44	0·03	tr.	0·64	—	0·35	—	0·68	—	0·70	0·05
K_2O	0·03	0·03	0·01	0·01	nil	0·12	—	0·03	—	0·06	—	0·04	0·03
H_2O^+	—	—	—	—	—	—	—	0·11	—	—	—	—	—
H_2O^-	—	—	nil	nil	0·03	—	—	0·05	—	—	—	0·02	0·03
TOTAL	99·73	100·36	99·83‡	100·02†	99·96	99·83	99·53	99·93	100·09	99·87	99·56	100·09	100·04
	Trace elements, parts per million												
Cr	2,500	1,000	2,000	1,000		300 180	1,000 650	55		1,000	220	250	
Ni	250	250	200	1,500		130 110	700 1,000	80		60	30	80	
Co	30	100	22	85		20 25	60 60	65		60	70	45	
V	220	50	140	55		180 220	100 100	320		800	100	270	
Li	10	*	16	1		22 8	3 2	30		*	3	40	
Sr	45	*	25	*		30 30	20 *	10		20	*	*	
Ba	35	*	*	*		* *	45 *	20		20	*	*	
Rb	*	*	*	*		* *	* *	*		*	*	*	
Ga	*	5	*	*		5 5	5 5	5		10	5	*	
Sc	100	*	65	*		100 100	22 *	220		220	35	120	
Zr	22	22	20	20		220 220	30 22	100		220	45	120	
Yt	10	*	10	*		65 100	20 10	35		100	20	25	

Atomic proportions to 6 oxygen atoms

Si	1·877	1·877	1·848	1·898	1·899	1·837	1·804	1·854	1·811	1·885	1·917	1·872	1·899
A^{iv}	0·123	0·123	0·152	0·102	0·101	0·163	0·196	0·146	0·189	0·115	0·083	0·128	0·101
A^{vi}	0·061	0·065	0·075	0·071	0·087	0·083	0·104	—	0·053	0·101	0·047	0·070	0·035
Ti	0·011	0·006	0·011	0·002	0·002	0·025	0·006	0·015	0·004	0·016	0·004	0·018	0·002
Fe^{3+}	0·050	0·042	0·048	0·058	0·034	0·077	0·049	0·063	0·100	0·051	0·049	0·072	0·086
Fe^{2+}	0·102	0·317	0·101	0·296	0·416	0·142	0·276	0·258	0·609	0·314	0·794	0·252	0·709
Mn	0·005	0·006	0·004	0·006	0·008	0·009	0·006	0·006	0·009	0·007	0·018	0·009	0·023
Mg	0·827	1·539	0·848	1·587	1·428	0·768	1·520	0·691	1·293	0·657	1·001	0·697	1·105
Ca	0·898	0·019	0·899	0·021	0·014	0·895	0·060	0·829	0·005	0·802	0·076	0·836	0·025
Na	0·038	0·002	0·031	—	—	0·046	—	0·025	—	0·049	—	0·049	0·004
K	—	—	—	—	—	0·006	—	—	—	—	—	—	—
ΣX	1·99	2·00	2·02	1·99	1·99	2·07	2·02	1·98	2·01	2·00	1·99	2·00	1·99
C	47·7	1·0	47·3	1·1	0·7	47·4	3·1	44·4	0·3	43·8	3·9	44·8	1·3
M	43·9	80·0	44·6	82·7	75·2	40·6	79·5	37·6	64·2	35·9	51·7	37·4	56·8
F	8·4	19·0	8·1	16·2	24·1	12·0	17·4	18·0	35·5	20·3	44·4	17·8	41·9

‡ Includes 0·12 per cent Cr_2O_3.
† Includes 0·05 per cent Cr_2O_3.
• Indicates trace-element concentration below limit of sensitivity.

I, II = augite and hypersthene from peridotite (X 282).
III, IV = augite and hypersthene from peridotite (37,310) (Muir & Tilley, 1958).
V = hypersthene from pyroxenite (H 66) (anal. R. A. Howie, personal communication).
VI, VII = augite and hypersthene from contact gneiss (X 819); the two columns of trace-element data beneath each are for light and heavy fractions respectively, the analysed augite being the heavy fraction, and the analysed hypersthene the light fraction.
VIII, IX = augite and hypersthene from garnet–augite gneiss (X 646).
X, XI = augite and hypersthene from basic gneiss (X 291).
XII, XIII = augite and hypersthene from basic gneiss (37,099) (Muir & Tilley, 1958).

Spectrographic determinations of trace elements in Tables 4, 5, and 7 are by Mr. R. Allen, Department of Mineralogy and Petrology, Cambridge. Limits of sensitivity given by Nockolds & Allen (1956).

TABLE 5

Analytical data for amphibole, garnets, and plagioclases

Rock type	*Peridotite*	*Contact gneiss*						*Garnetiferous basic gneiss*					*Basic gneiss*
	I	II	III	IV	V	VI	VII	VIII	IX	X	XI	XII
Specimen:	X 282	X 819	X 192	X 819	X 819	X 819	X 646	X 646	X 195	Z 117	Z 117	X 291
Mineral:	Amphibole	Garnet L_1	Garnet	Garnet L_2	Garnet H_1	Garnet H_2	Garnet	Plagioclase	Garnet	Garnet	Plagioclase	Plagioclase
SiO_2	45·87	39·45	39·15				37·37		38·80	38·31		
TiO_2	0·63	0·09	0·09				0·81		0·37	0·15		
Al_2O_3	8·43	23·46	22·57				21·55		22·58	22·34		
Fe_2O_3	1·94	5·05	4·34	Partial analyses for CaO,			0·93		2·55	3·16		
FeO	5·87	12·37	15·60	MgO, MnO and total			24·60		19·70	21·84	ca.	ca.
MnO	0·07	0·54	0·36	iron made on portions			1·04	ca.	0·53	0·86		
MgO	21·79	15·15	12·31	variably contaminated			6·81	$Ab_{25}An_{75}$	8·58	7·25	$Ab_{44}An_{56}$	$Ab_{46}An_{54}$
CaO	12·22	6·33	5·24	by spinel			6·81		6·49	6·71		
Na_2O	1·04	n.d.	n.d.				n.d.		n.d.	n.d.		
K_2O	0·34	n.d.	n.d.				n.d.		n.d.	n.d.		
H_2O^+	1·79	n.d.	n.d.				n.d.		n.d.	n.d.		
H_2O^-	0·14	n.d.	n.d.				n.d.		n.d.	n.d.		
TOTAL	100·13	100·44	99·73				99·92		99·60	100·62		
	Trace elements, parts per million											
Cr	2,500	180	40		80		45	5		220	5	5
Ni	600	90	30		30		•	15		5	10	•
Co	35	60	20		30		45	10		30	•	•
V	220	50	32		32		80	•		100	•	•
Li	2	•	3		•		•	16		2	3	3
Sr	160	•	•	n.d.	•	n.d.	•	1,000		•	450	700
Ba	45	•	10		•		•	550	n.d.	•	100	350
Rb	•	•	•		•		•	30		•	•	•
Ga	5	10	5		5		5	15		5	22	15
Sc	45	22	100		30		100	•		100	•	•
Zr	22	45	22		30		45	•		22	•	•
Yt	10	15	20		20		200	•		100	•	•
	Atomic proportions†											
Si	6·599	2·899	2·929				2·916		2·957	2·933		
Al	{1·401 / 0·016}	2·030	1·897				1·978		2·024	2·006		
Ti	0·068	0·005	0·005				0·048		0·021	0·009		
Fe^{3+}	0·209	0·279	0·249				0·093		0·145	0·181		
Fe^{2+}	0·705	0·758	0·973				1·610		1·252	1·393		
Mn	0·009	0·033	0·023				0·069		0·035	0·056		
Mg	4·649	1·434	1·368				0·789		0·971	0·824		
Ca	1·805	0·499	0·420				0·569		0·530	0·550		
Na	0·289	—	—				—		—	—		
K	0·062	—	—				—		—	—		
H	1·715	—	—				—		—	—		
X	2·16	3·00	2·93				3·11		2·95	3·01		
Y	5·62	2·03	1·90				1·98		2·02	2·01		
Z	8·00	2·90	3·02				2·92		2·96	2·93		
OH	1·72	—	—				—		—	—		
Ca	25·2	16·6	13·9	16·0	11·5	14·7	18·5		18·0	18·2		
Mg	62·3	47·8	45·1	50·5	47·6	43·2	25·6		33·0	27·6		
Fe^c	12·4	35·6	41·0	35·5	40·9	42·1	55·8		49·0	54·2		

Plagioclase compositions estimated from refractive index (data in Table 6).

Fe^c = total iron + manganese.

• Indicates trace-element concentration below limit of sensitivity.

† Structure formulae calculated on basis of 24 oxygen atoms (amphibole, column I) or of 12 oxygen atoms (garnets, columns II, III, VII, IX, and X).

Optical data for the minerals is given in Table 6.

Garnets (X 819) L_2, H_1, H_2 are heavily contaminated by spinel, with R.I. ranging from 1·740 to 1·800, and cell size ranging from 8·11Å to 8·12 Å. The refractive indices quoted in Table 2 for these samples are values for the best match with the liquids.

Analyst: M. J. O'Hara.

TABLE 6

Properties of minerals

Rock type	*Specimen*	*Olivine*	*Clinopyroxene*	*Orthopyroxene*	*Garnet*	*Plagioclase*
Dunites	Z 135	$\beta = 1{\cdot}695$	none	$\beta = 1{\cdot}676$, $2V = 78°$ (−)	none	none
	X 191	$\beta = 1{\cdot}675$	none	$\gamma = 1{\cdot}676$, $\beta = 1{\cdot}672$		
	X 593	$\beta = 1{\cdot}668$	n.d.	$\gamma = 1{\cdot}675$		
	Z 140	$\alpha = 1{\cdot}675$	n.d.	$\gamma = 1{\cdot}687$		
Peridotites	Z 111	$\gamma = 1{\cdot}696$	n.d.	$\gamma = 1{\cdot}691$		
	37,310	$\beta = 1{\cdot}674$	$\gamma = 1{\cdot}714$, $2V = 55°$ (+)	$\beta = 1{\cdot}683$, $2V = 84°$ (−)		
	X 282*	$\beta = 1{\cdot}675$	$\beta = 1{\cdot}683$, $2V = 54°$ (+)	$\gamma = 1{\cdot}688$, $2V = 77°$ (−)		
Pyroxenite	X 284		$\beta = 1{\cdot}692$, $2V = 54°$ (+)	$\gamma = 1{\cdot}691$, $2V = 76°$ (−)		
Garnet-augite gneisses	X 646†		$\beta = 1{\cdot}699$, $2V = 55°$ (+)	$\gamma = 1{\cdot}711$, $\beta = 1{\cdot}702$, $2V = 62°$ (−)	$n = 1{\cdot}787$, $a_0 = 11{\cdot}575$	$\alpha = 1{\cdot}568$
	Z 125		$\beta = 1{\cdot}696$, $2V = 53\frac{1}{2}°$ (+)	$\gamma = 1{\cdot}720$, $\beta = 1{\cdot}718$, $2V = 52°$ (−)	$n = 1{\cdot}782$	$\alpha = 1{\cdot}566$
Garnetiferous basic gneisses	Z 127	none	$\beta = 1{\cdot}693$, $2V = 55°$ (+)	$\beta = 1{\cdot}718$, $2V = 63°$ (−)	n.d.	$\alpha = 1{\cdot}564$
	X 195		$\beta = 1{\cdot}696$, $2V = 55°$ (+)	$\beta = 1{\cdot}705$, $2V = 62°$ (−)	$n = 1{\cdot}782$, $a^\circ = 11{\cdot}565$	$\beta = 1{\cdot}562$
	Z 117		$\beta = 1{\cdot}696$, $2V = 53\frac{1}{2}°$ (+)	$\gamma = 1{\cdot}710$, $2V = 57°$ (−)	$n = 1{\cdot}780$, $a^\circ = 11{\cdot}511$	$\beta = 1{\cdot}563$
	X 245		n.d.	n.d.	$n = 1{\cdot}792$	n.d.
	X 260		$\beta = 1{\cdot}694$, $2V = 51°$ (+)	$\gamma = 1{\cdot}721$, $2V = 54\frac{1}{2}°$ (−)	$n = 1{\cdot}810$	$\beta = 1{\cdot}561$
Basic gneisses	37,099		$\beta = 1{\cdot}702$, $2V = 56°$ (+)	$\alpha = 1{\cdot}701$, $\gamma = 1{\cdot}717$, $2V = 59°$ (−)	none	n.d.
	X 291‡		$\beta = 1{\cdot}703$, $2V = 49°$ (+)	$\gamma = 1{\cdot}721$, $\beta = 1{\cdot}717$, $2V = 57°$ (−)		$\beta = 1{\cdot}560$

* Contains spinel, $n = 1{\cdot}823$; amphibole, $\beta = 1{\cdot}655$; and hypersthene, $\alpha = 1{\cdot}677$ $\beta = 1{\cdot}682$, as rims about olivine.
† Contains plagioclase as inclusions in augite, when $\alpha = 1{\cdot}557$, and as mantles about calcic plagioclase when $\beta = 1{\cdot}560$.
‡ Contains plagioclase as inclusions in augite, when $\beta = 1{\cdot}560$.

From the diagram it appears that:

(i) Orthopyroxene has a greater Fe:Mg ratio than the associated clinopyroxene, but the contrast is greater in garnet-poor assemblages (8, 9, 9′) than in garnet-rich assemblages (4, 6, 7).

(ii) Garnet, where present in small amounts mantling iron ore (8), has a high Fe:Mg ratio.

(iii) All the ferromagnesian minerals have an increasing Fe:Mg ratio on passing from the richly garnetiferous to the garnet-free basic gneisses, which is not reflected in the Fe:Mg ratio of the rocks concerned. This arises through the varying proportion of the garnet relative to the other phases.

(iv) The pyroxene assemblages with lowest Fe:Mg ratio come from certain contact gneisses, not from the ultrabasic gneisses which have the lowest Fe:Mg ratios in the rocks as a whole.

(v) The olivine in 2, 2″ appears to have a lower Fe:Mg ratio than the associated orthopyroxene, which is a relationship not expected at equilibrium (Bowen & Schairer, 1935; Ramberg & De Vore, 1951). These are rocks with relatively low amounts of olivine. Peridotites rich in olivine, and poor in clinopyroxene, amphibole, and spinel (e.g. 1, 1′, and part of sample UA, (Figs. 3, 4)) appear to contain olivine with higher Fe:Mg ratio than the associated ortho-

TABLE 7. *Rock analyses*

	1	2	3	4	5	6	7	8
Specimen No.:	Z 135	X 282	X 646	Z 125	X 195	Z 117	X 260	X 291
SiO_2	37·66	42·09	41·38	43·80	45·52	47·56	47·42	52·27
TiO_2	0·26	0·37	0·76	1·97	0·91	0·88	1·43	1·53
Al_2O_3	5·93	7·34	15·24	13·45	14·67	15·64	15·58	15·96
Fe_2O_3	6·46	3·06	3·68	2·78	2·30	1·77	4·51	1·27
FeO	5·88	7·12	16·25	16·35	11·99	9·30	8·89	7·71
MnO	0·12	0·31	0·44	0·32	0·38	0·21	0·27	0·16
MgO	30·53	24·44	8·67	7·70	9·90	7·55	5·97	5·83
CaO	2·76	10·73	10·67	11·59	11·46	13·54	12·46	10·47
Na_2O	0·45	0·76	1·12	1·32	0·76	1·98	2·74	3·51
K_2O	0·13	0·18	0·91	0·15	0·88	0·20	0·25	0·55
P_2O_5	0·04	0·03	0·03	0·12	0·04	0·14	0·16	0·14
H_2O^+	0·68	0·12	0·07	0·11	0·32	0·30	0·37	0·04
H_2O^-	8·84	3·17	0·65	0·43	1·20	0·52	0·38	0·47
TOTAL	99·74	99·72	99·87	100·19	100·33	99·59	100·43	99·91
	Atomic per cent calculated from above							
Si	14·9	15·8	16·0	16·8	17·2	17·8	18·0	19·1
Ti	0·1	0·1	0·2	0·6	0·3	0·2	0·4	0·4
Al	2·8	3·3	6·9	6·1	6·5	6·9	7·0	6·8
Fe^{2+}	1·9	0·9	1·1	0·8	0·6	0·5	1·3	0·3
Fe^{3+}	1·9	2·2	5·2	5·2	3·8	2·9	2·8	2·3
Mn	tr.	0·1	0·1	0·1	0·1	0·1	0·1	0·1
Mg	18·1	13·7	5·0	4·4	5·6	4·2	3·4	3·2
Ca	1·2	4·3	4·4	4·8	4·6	5·4	4·0	4·1
Na	0·4	0·6	0·8	1·0	0·5	1·4	2·0	2·5
K	0·1	0·1	0·4	0·1	0·4	0·1	0·1	0·3
P	tr.	tr.	tr.	tr.	tr.	tr.	tr.	tr.
O	58·6	58·8	59·9	60·1	60·3	60·5	60·7	60·9
	Trace elements, parts per million							
Cr	3,000+	3,000	65	45	220	400	120	220
Ni	2,500	2,500	55	180	180	100	250	80
Co	220	220	100	100	55	50	100	55
V	7	220	220	650	450	320	450	220
Li	•	3	10	8	5	15	10	5
Sr	•	50	125	50	350	150	125	1,200
Ba	20	50	100	50	220	30	100	300
Rb	•	•	•	•	•	•	•	•
Ga	•	•	•	15	10	15	15	15
Sc	•	35	100	100	45	50	45	45
Zr	45	45	55	70	45	22	100	100
Yt	•	•	100	45	20	15	45	45
	C.I.P.W. Norms							
Or	0·8	1·1	5·4	0·9	5·2	1·2	1·5	3·3
Ab	3·8	0·5	6·0	11·1	6·5	16·8	23·2	29·6
An	13·7	16·0	33·8	30·2	34·2	33·1	29·4	26·1
Ne	—	3·3	1·8	—	—	—	—	—
Cor	tr.	—	—	—	—	—	—	—
Di	—	29·5	25·1	22·1	18·6	28·1	26·2	20·4
Hy	15·3	—	—	9·8	13·1	3·5	2·3	13·7
Ol	46·7	41·1	29·8	17·3	16·0	11·7	7·3	1·1
Mt	9·4	4·4	5·6	4·1	3·4	2·5	6·5	2·8
Ilm	0·5	0·7	1·4	3·7	1·7	1·7	2·7	2·9
Rest	9·6	3·2	0·8	0·8	1·6	1·0	1·2	0·8
	Modes, vol. per cent							
Olivine	X	27·7	—	—	—	—	—	—
Amphibole	O	22·2	1·8	—	—	—	—	—
Spinel	O	1·7	—	—	—	—	—	—
Augite	—	19·9	16·9	38·0	X	X	27·8	20·2
Hypersthene	X	25·1	11·0	9·7	X	X	6·4	11·6
Garnet	—	—	56·5	33·9	X	X	5·0	0·2
Plagioclase	—	—	10·4	13·4	X	X	53·0	63·9
Ore	O	2·1	3·3	4·6	O	O	7·5	2·9
Apatite	—	—	tr.	0·4	O	O	0·3	1·2
Biotite	—	—	0·1	—	—	—	—	—
Calcite	tr.	tr.	tr.	tr.	tr.	tr.	tr.	tr.
S.G.	n.d.	3·11	3·63	n.d.	3·34	n.d.	3·08	2·87

* Below limit of sensitivity.
Analyst: M. J. O'Hara.

X = more than 5 per cent.
O = less than 5 per cent.

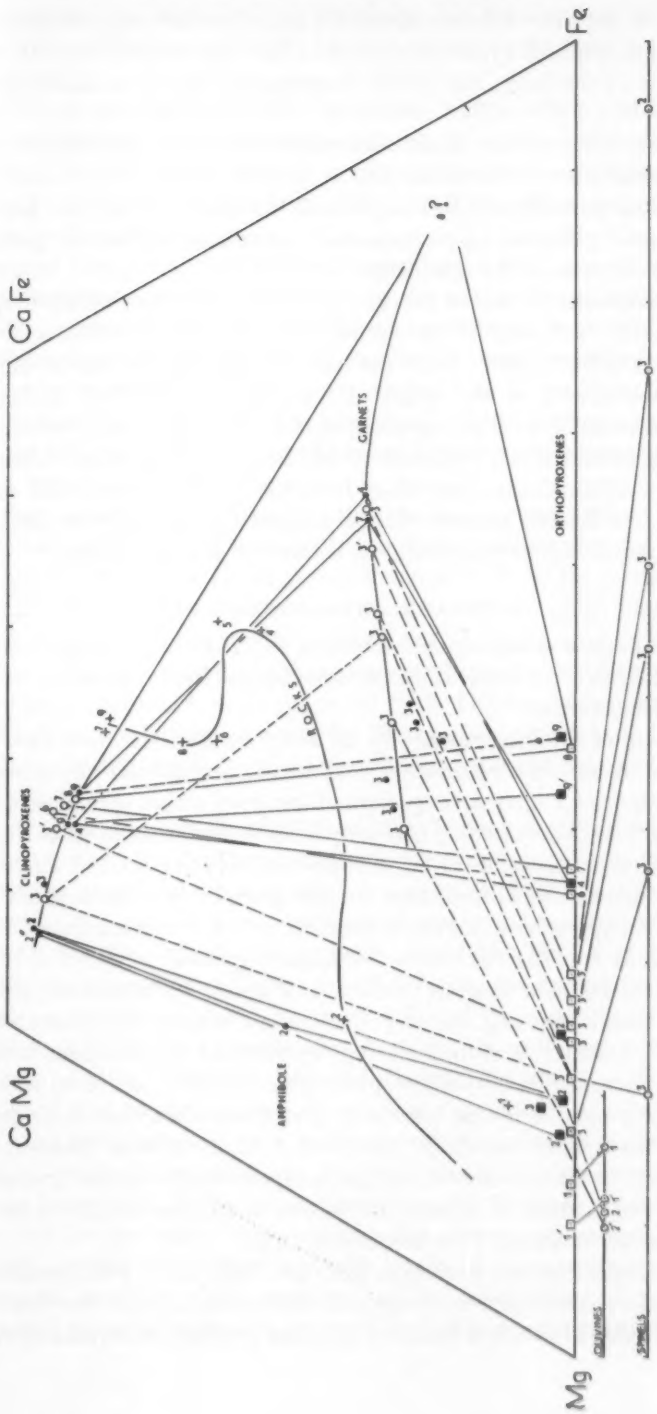

FIG. 9. Plots of Ca–Mg–Fe° + Mn for the minerals and rocks of Tables 4–7.

pyroxene. In the case of the peridotite (X 282) there are rims of orthopyroxene about olivine, and this pyroxene appears to have a lower Fe:Mg ratio than that in the mass of the rock, but it is still apparently not in equilibrium with the olivine.

(vi) Spinel compositions have been estimated on the assumption that only Fe:Mg substitution is involved, and that they are pure aluminium spinels. These assumptions are probably unjustified, but it is likely that the general form of paragenesis indicated (most magnesian spinels in the contact gneisses, and hercynite-rich types in the ultrabasics) is valid.

(vii) The calcium content of the clinopyroxenes coexisting with orthopyroxene is comparable with that of pyroxenes from the Madras charnockite series (Howie, 1955), but slightly lower calcium content is found, particularly at the magnesium-rich end of the range. If the presence of coarse orthopyroxene lamellae in some of these clinopyroxenes is considered, it may be inferred that the clinopyroxenes which originally crystallized contained more orthopyroxene molecule in solid solution than those from the Madras charnockite series, and hence that the Scourie gneisses were crystallized under different physical conditions (possibly higher temperatures) within the granulite facies.

SUMMARY AND CONCLUSIONS

The ultrabasic and basic gneisses belong to the granulite-mineral facies, and are quite distinct from rocks of the eclogite facies (Fyfe, Turner, & Verhoogen, 1958; O'Hara, 1960).

Some form of genetic relationship between the ultrabasic and basic gneisses is indicated by the close association of extreme types in relatively small masses, by the presence of a zonal arrangement of the types within the masses (although this zoning is complex), and by the rarity of individual rock units of the association as isolated components of the gneiss complex. The only unit which is found commonly among the surrounding banded gneisses is a basic gneiss which is never rich in hypersthene and never contains garnet. Small masses of ultramafic rock occur as rounded inclusions in banded gneisses adjacent to ultrabasic and basic masses near Badcall (Sutton & Watson, 1951) and adjacent to the masses at Geodh' Eanruig and west of Pairc a Cladaich. Such occurrences are exceptional, however, and the rock type in those which have been investigated is a relatively iron-rich amphibole–pyroxenite (unpublished data) which is not similar to any member of the ultrabasic group described here. It is improbable that such relationships would be observed if the association represented accidental xenoliths of an earlier rock series incorporated in a banded gneiss magma, or represented a series of separate intrusions, of sill-like form, into the banded gneisses before or during their metamorphism.

The Geological Survey geologists (Clough, Teall, *et al.*, 1907) suggested that the ultrabasic rocks might represent early differentiates from the banded gneiss 'magma'. Watson (Sutton & Watson, 1951) has pointed out structural difficulties

in envisaging such an origin and suggested that the basic and ultrabasic rocks might have been sills in a rock series later converted to the banded gneisses by migmatization.

The ultrabasic gneisses have a high chromium, nickel, cobalt, and magnesium content, and show a strong chemical similarity to typical ultrabasic intrusive rocks, either of the type interpreted as early differentiates in magmatic series (Nockolds & Allen, 1953, 1956; Hess 1960), or of the alpine serpentinite type (Turner & Verhoogen, 1951).

The mineral parageneses of the basic, garnetiferous basic, garnet–augite, and contact gneisses are adequately explained by the assumption that the rocks are thoroughly metamorphosed, the mineral paragenesis being controlled by the local rock composition and the physical conditions, and uninfluenced by the composition of minerals in neighbouring rocks. This is particularly apparent when comparing the magnesian pyroxene pair, which coexists with garnet in some of the contact gneisses, with the more ferriferous pyroxene pair of the peridotites and pyroxenites where garnet is absent.

From their chemistry it can be seen that the basic series gneisses cannot be related to each other by any igneous differentiation mechanism yet proposed. Primary igneous crystallization of garnet is denied both by the textural and by the mineral relationships noted above. Reasons will be given elsewhere for believing that the adjacent banded gneisses do not bear an igneous differentiation relationship to the ultrabasic association, and are themselves unlike any common igneous rocks. The mode of origin suggested by the Geological Survey geologists is abandoned, as also is that suggested by Watson, since neither of these offers an explanation of the chemistry of the basic series or the close association of the different rock types.

The basic series may owe its origin to reaction between an ultrabasic intrusive mass and its country rock under granulite facies conditions. There is, however, no precedent in geological literature for this suggestion. Previous descriptions of assemblages produced by reaction between ultrabasic masses and their country rock under greenschist or amphibolite facies conditions (Hess & Phillips, 1936) or granulite facies conditions (Sørensen, 1954) record the formation of sharply defined zones of monomineralic nature. Studies of the assemblages produced where materials of different composition have reacted with each other at high temperatures (Adams, 1930; Cockbain & Johnson, 1958; Berry, Allen, & Snow, 1950) indicate that where the reaction involves the transfer of components in response to an initial concentration gradient, with precipitation of the migrating components in crystalline phases in a matrix which remains essentially solid throughout the process, the resultant chemical profile between the original end-members will not be linear. The concentration of any component may show maxima and minima which may lie outside the limits of concentration in either of the original reactants. The chemistry of the basic series at Scourie has features which are consistent with an origin by diffusion of materials across the

boundary of an ultrabasic intrusive mass at high temperatures, in rocks which were solid throughout the process. Water-vapour was present, and the textures of these rocks suggest that the transfer of material might have been largely along grain boundaries.

The original contact of the ultrabasic mass appears to have been within the rocks termed 'contact gneisses', since it is within these that the chromium, nickel, and cobalt content characteristic of the original ultrabasic material falls off most rapidly. Silicon, aluminium, calcium, and iron appear to have been added to the dunite gneiss to produce peridotite and pyroxenite gneiss, leading to the reaction:

$$(\text{olivine} + \text{hypersthene}_1) + \textit{introduced components} \rightarrow (\text{hypersthene}_2 + \text{augite} + \text{spinel} + \text{amphibole})$$

dunite gneiss — *peridotite, pyroxenite gneiss*

Hypersthene_1 is crystallized in metamorphic equilibrium with the olivine, and has a lower iron/magnesium ratio than the latter, as is observed in the olivine-rich gneisses poor in augite, spinel, and amphibole. Hypersthene_2 is crystallized in equilibrium with the introduced components and the augite, spinel, and amphibole produced by reaction. It is generally of a higher iron/magnesium ratio than hypersthene_1. In the peridotites it is possible that the main part of the rock represents the products of this reaction, while the olivine is a residual part of the original reactant which did not recrystallize in equilibrium with the new phases because diffusion of material continued after the period in which rapid recrystallization of the phases was produced. Such an interpretation explains the rims of hypersthene about the olivine and the apparently igneous mineral relationships found in the peridotite gneisses, e.g. (X 282), and can be extended to account for the abundance of textures which appear to be due to reactions proceeding after the end of general recrystallization in the garnetiferous basic gneisses.

In the case of the garnetiferous basic gneisses, which probably represent modified country rock, it is not certain what has been added since the country rock may have undergone simultaneous or subsequent migmatization and, if so, there is no means of telling what was the composition of the original country rock. A description of the country rocks will be given elsewhere. It seems probable that magnesium and iron were derived in part from ultrabasic material. The source of the high calcium content of these rocks is unknown, but calcium enrichment adjacent to intrusive ultrabasic masses has been previously recorded (Turner, 1948).

Two conclusions which have a bearing on the origin of leucocratic gneisses associated with these ultrabasic and basic gneisses are:

(1) The distribution of elements in the zoned association does not represent

final equilibrium. A chemical potential gradient tending to drive ferromagnesian elements from the ultrabasic into the adjacent rocks was still in existence at the close of metamorphism.

(2) The ultrabasic masses vary in size, and some smaller ones have been completely modified to pyroxenite. It cannot be assumed that each layer of ultrabasic material began to react at the same time nor that the speed of reaction was the same in each case. For these reasons differences in the chemical distribution amongst the final products, between one occurrence and another in the same province, are to be expected.

An account of these leucocratic gneisses will be published elsewhere.

ACKNOWLEDGEMENTS

I wish to thank Professor C. E. Tilley for suggesting the subject for study, and for his interest and advice in the progress of the work. I also wish to thank Professor F. H. Stewart, Dr. S. O. Agrell, Dr. S. R. Nockolds, and Dr. J. Phemister for reading this paper, Dr. Nockolds for permission to publish trace-element data, and Dr. P. Gay and Dr. M. G. Bown for assistance with the X-ray studies. I would also like to thank K. Rixon, M. Haslop, R. Lee, and Miss J. Tarrant for their assistance and Miss C. G. M. Berry for typing the final draft.

REFERENCES

Adams, F. D., 1930. The transfusion of matter from one solid to another under the influence of heat—a new factor in the process of metamorphism. *Canad. J. Res.* **2**, 153.

Alderman, A. R., 1936. Eclogites from the neighbourhood of Glenelg, Inverness-shire. *Quart. J. geol. Soc. Lond.* **92**, 488–530.

Berry, T. F., Allen, W. C., & Snow, R. B., 1950. Chemical changes in basic brick during service. *J. Amer. ceram. Soc.* **33**, 121–32.

Bowen, N. L., & Schairer, J. F., 1935. The system MgO–FeO–SiO_2. *Amer. J. Sci.*, 5th ser., **29**, 151–217.

Bown, M. G., & Gay, P., 1959. Identification of oriented inclusions in pyroxene crystals. *Amer. Min.* **44**, 592–602.

Brown, G. M., 1957. Pyroxenes from the early and middle stages of fractionation of the Skaergaard intrusion, East Greenland. *Miner. Mag.* **31**, 511–43.

Clough, C. T., Teall, J. J. H., *et al.*, 1907. The geological structure of the North-West Highlands of Scotland. *Mem. geol. Surv. Scotland.*

Cockbain, A. G., & Johnson, W., 1958. Examination of used chrome-magnesite refractories by petrological and X-ray techniques. *Trans. Brit. Ceram. Soc.* **57**, 511–25.

Davidson, C. F., 1943. The Archaean rocks of the Rodil district, South Harris. *Trans. roy. Soc. Edin.* **61**, 71–112.

Fyfe, W. S., Turner, F. J., & Verhoogen, J., 1958. Metamorphic reactions and metamorphic facies. *Mem. geol. Soc. Amer.* **73**.

Henry, N. F. M., 1942. Lamellar structure in orthopyroxenes. *Miner. Mag.* **26**, 179–89.

Hess, H. H., 1949. Chemical composition and optical properties of common clinopyroxenes. *Amer. Min.* **36**, 621–66.

—— 1952. Orthopyroxenes of the Bushveld type, &c. *Amer. J. Sci.*, Bowen vol., 173–88.

—— 1960. Stillwater Igneous Complex, Montana. *Mem. geol. Soc. Amer.* **80**.

—— & Phillips, A. H., 1936. Metamorphic differentiation at contacts between serpentinite and siliceous country rocks. *Amer. Min.* **21**, 333–62.

Howie, R. A., 1955. The geochemistry of the charnockite series of Madras, India. *Trans. roy. Soc. Edin.* **62**, 725–68.

JAFFE, H. W., 1951. Role of Yttrium and other minor elements in the garnet group. *Amer. Min.* **36**, 133–55.

JOHANNSEN, A., 1938. *A descriptive petrography of the igneous rocks*. Chicago: Chicago University Press.

KEITH, M. L., & ROY, R., 1954. Structural relations among double oxides of trivalent elements. *Amer. Min.* **39**, 1–23.

MUIR, I. D., & TILLEY, C. E., 1958. The composition of coexisting pyroxenes in metamorphic assemblages. *Geol. Mag. Lond.* **95**, 403–9.

MURRAY, R. J., 1954. The clinopyroxenes of the Garbh Eilean sill, Shiant Isles. Ibid. **91**, 17–31.

NOCKOLDS, S. R., & ALLEN, R., 1953. The geochemistry of some igneous rock series. Part I. *Geochim. et cosmoch. Acta*, **4**, 105–42.

—— —— 1956. The geochemistry of some igneous rock series. Part III. Ibid. **7**, 34–77.

O'HARA, M. J., 1960. A garnet–hornblende–pyroxene rock from Glenelg, Inverness-shire. *Geol. Mag. Lond.* **97**, 145–56.

RAMBERG, H., & DE VORE, G., 1951. The distribution of Fe^{++} and Mg^{++} in coexisting olivines and pyroxenes. *J. Geol.* **59**, 193–210.

SØRENSEN, H., 1954. The border relations of the dunite at Sorassuit, Sukkertoppen District, West Greenland. *Medd. Grønland*, **135**, No. 4.

SUTTON, J., & WATSON, J., 1951. The pre-Torridonian metamorphic history of the Loch Torridon and Scourie areas in the North-West Highlands and its bearing on the chronological classification of the Lewisian. *Quart. J. geol. Soc. Lond.* **106**, 241–308.

TEALL, J. J. H., 1885. The metamorphosis of dolerite into hornblende schist. Ibid. **41**, 132–45.

TRÖGER, W. E., 1956. *Optische bestimmung der gesteinsbildenden minerale*. Stuttgart.

TURNER, F. J., 1948. Mineralogical and structural evolution of the metamorphic rocks. *Mem. geol. Soc. Amer.* **30**.

—— & VERHOOGEN, J., 1951. *Igneous and metamorphic petrology*. New York: McGraw-Hill.

WILKINSON, J. F. G., 1956. Clinopyroxenes of alkali olivine basalt magma. *Amer. Min.* **41**, 724–43.

—— 1957. The clinopyroxenes of a differentiated teschenite sill near Gunnedah, New South Wales. *Geol. Mag. Lond.* **94**, 123–34.